The System Silver - Iron - Sulfur: Phase Equilibria And Geologic Applications.

68-15,921

TAYLOR, Lawrence A., 1938-

THE SYSTEM Ag-Fe-S: PHASE EQUILIBRIA AND GEOLOGIC APPLICATIONS.

Lehigh University, Ph.D., 1968
Geology

University Microfilms, Inc., Ann Arbor, Michigan

THE SYSTEM Ag-Fe-S: PHASE EQUILIBRIA AND GEOLOGIC APPLICATIONS

by

Lawrence A. Taylor

A DISSERTATION

Presented to the Graduate Committee

of Lehigh University

in Candidacy for the Degree of

Doctor of Philosophy

in Geological Sciences

Lehigh University

1968

Approved and recommended for acceptance as a dissertation in partial fulfillment of the requirements for the degree of Doctor of Philosophy.

May 20, 1968
(date)

Emmar Kullerud
Professor in Charge

Accepted, May 20, 1968
(date)

Special committee directing the doctoral work of Mr. Lawrence A. Taylor

Emmar Kullerud, Chairman

Dale Simpson

R. M. Kraft

A. J. Gallagher, Jr.

J. Harold Ryan

ACKNOWLEDGMENTS

The writer is indebted to the many people who have provided the assistance necessary for the completion of this study. Dr. Gunnar Kullerud, Senior Staff Member of the Geophysical Laboratory and Adjunct Professor at Lehigh University, has been most generous with his laboratory facilities, his time spent in stimulating discussion and criticism, and his continual guidance, as Thesis Advisor, through all "phases" of this investigation. The writer also wishes to express his gratitude to Dr. G. W. Roland, Research Associate at Lehigh, whose suggestions, discussions, and encouragements formed an integral part of this study. Thanks are due to Dr. James R. Craig for his assistance in the laboratory and his helpful discussions of experimental results. Mr. J. Kocmaneck of the Geophysical Laboratory kindly aided in the preparation of certain polished sections and photographs. Significant improvements in the manuscript resulted from the reviews of Drs. G. Kullerud, G. W. Roland, and J. D. Ryan; these efforts are gratefully acknowledged.

Samples have been generously provided for the writer by The Czechoslovakian National Museum, Mr. P. E. Desautels of the United States National Museum, Mr. A. R. Geyne, Director of Compania de Real del Monte y Pachuca, Hidalgo, Mexico, Drs. E. Nickel and W. Petruk of the Geological Society of Canada, Mr. W. Quellmalz, Dresden, East Germany, and Dr. M. Stemprok, Prague, Czechoslovakia. Dr. R. W. Hutchinson,

University of Western Ontario, was instrumental in providing information and suggestions concerning the obtaining of natural specimens. The operators of the R. L. 407, Glen Lake, Hi Ho, and Silverfields silver mines at Cobalt, Ontario, and the Kidd Creek Deposit, Texas Gulf Sulfur Company, Timmons, Ontario, kindly permitted the writer to obtain samples from their mines during the summer of 1966.

Above all, the author is particularly indebted to his wife, Pat, for her patience, understanding, and encouragement throughout the years of study. For much of the preliminary typing and the meticulous final copy of this manuscript, the author also wishes to express gratitude to his wife.

TABLE OF CONTENTS

LIST OF FIGURES

LIST OF TABLES

LIST OF PLATES

ABSTRACT

Quench-type and DTA experiments conducted in silica tubes were used to investigate the Ag-Fe-S system from liquidus temperatures to below 200°C under the vapor pressures of the system. Several hydrothermal experiments, also conducted in silica tubes, were performed at temperatures below 300°C.

Ternary liquid-immiscibility fields dominate the phase relations at high temperatures (>1000°C). A sulfur-rich two-liquid field, which spans from the Ag-S to the Fe-S joins above 1083±2°C, is present above 607±2°C in the ternary system. Metal-rich immiscible liquids, which probably originate on the Ag-Fe join above 1533±2°C, are present in the ternary system above 906±2°C. The assemblage Ag + pyrrhotite becomes stable at 955±3°C (a pseudobinary eutectic). With decreasing temperature, the assemblages argentite + pyrrhotite and argentite + pyrite become stable at 622±2° and 607±2°C, respectively; the reactions involve ternary invariant conditions (neither join is pseudobinary). The assemblage argentite + pyrrhotite + pyrite becomes stable at 532±2°C (ternary eutectic near Ag_2S in composition). A subsolidus invariant reaction at 248±8°C results in the formation of the silver + pyrite assemblage. No ternary solid phases were encountered in dry experiments above 150°C.

Less than 0.2 at.% Ag is soluble in pyrite and pyrrhotite at 600°C and less than 0.8 at.% Fe in argentite at

500°C. Silver has no measurable effect on $\underline{d}_{(10.2)}$ values of pyrrhotite or the cell dimension of pyrite ($\underline{a}_{25°}$ = 5.4175±0.0002Å). The presence of iron lowers the fcc ⇌ bcc inversion temperature of Ag_2S from 52° to >100°C, depending on the associated Ag-Fe-S phases; however, the bcc ⇌ mono. inversion temperature is not measurably affected.

Heating of sternbergite and argentopyrite (both $AgFe_2S_3$) samples has demonstrated instability at 152°C (e.g., partial breakdown of sternbergite in 405 days); rate studies have shown that a 10°C temperature increase results in approximately a 5-fold increase in breakdown rate.

Fugacities of sulfur over binary and ternary univariant assemblages were investigated through use of the electrum-tarnish and pyrrhotite-indicator methods. This study has demonstrated that binary fugacity data are applicable to ternary assemblages.

Several significant points of geologic interest from the experimentally determined phase equilibria are discussed. The silver deposits of Cobalt, Ontario, are used to demonstrate the combinedusage of various types of thermodynamic data to delineate ore-forming conditions. In addition to geologic applications, a section is devoted to a brief discussion of microtextures, in the Ag-Fe-S system, of possible metallurgical importance.

INTRODUCTION

The most common sulfide minerals —— the iron sulfides, pyrite (FeS_2) and several species of pyrrhotite ($Fe_{1-x}S$) —— occur as major or minor constituents of all silver deposits. Commonly associated with these iron sulfides, are the economically important silver minerals —— argentite and acanthite (Ag_2S) and native silver —— which provide the bulk of the silver content in the Ni-Co-native silver ore type. Physico-chemical data on coexisting iron- and silver-sulfide minerals are important to an interpretation of the environment of the geologic processes pertaining to the formation of these deposits. Phase equilibria in the Ag-Fe-S system provide new and valuable information on silver-mineral deposition.

The iron-sulfide minerals, in addition to being associated with the silver minerals, commonly contain small, but economic, quantities of silver. Several recent investigators, notably Sutherland (1967), have been concerned with the effect of silver upon the phases and phase relations in the Fe-S system. In this respect, the solubility of silver in pyrite ("argentiferous pyrite") and pyrrhotite, as well as the effect of silver present in solid solution on the cell dimensions of pyrite and pyrrhotite, are important.

The reported Ag-Fe-S ternary minerals, sternbergite,

argentopyrite (both $AgFe_2S_3$), frieseite ($Ag_2Fe_5S_8$), and argyropyrite ($Ag_3Fe_7S_{11}$), are not commonly found in ore deposits containing iron- and silver-sulfide minerals. They have been described in ores believed to have been subjected to high temperatures and pressures of metamorphism (e.g., Broken Hill, Australia), as well as in oxidized and supergene-enriched ores (e.g., Joachimsthal, Czechoslovakia). No thermodynamic data, which could explain the limited, however, diverse geologic occurrences of these various phases, are present in the literature.

Phase equilibria in the system Ag-Fe-S have many immediate applications; however, when these data are used collectively with other pertinent systems such as Ag-As-S, Fe-As-S, Cu-Fe-S, Ag-Bi-S, etc., valuable knowledge can be obtained relating to the physical and chemical nature of the fluids responsible for the deposition of the ore minerals.

This investigation was undertaken as part of the sulfide experimental research program, in the Department of Geological Sciences at Lehigh University, under the direction of Dr. Gunnar Kullerud, Senior Staff Member, Geophysical Laboratory, Carnegie Institution of Washington, and Adjunct Professor of Geochemistry at Lehigh University. This study was preceded at Lehigh by investigations in the Co-As-S and Co-Fe-S systems, Ph.D. theses on the Ag-Bi-S and Ag-Bi-Pb-S systems (Craig, 1965) and the Ag-As-S system (Roland, 1966), and recently, by post-doctoral research in the Ag-Pb-As-S and Ag-Pb-Sb-S systems (Roland, 1968, personal communication).

MINERALS IN THE Ag-Fe-S SYSTEM

The chemical compositions of 17 minerals can be plotted on a composition diagram of the Ag-Fe-S system (Figure 1). Pertinent crystallographic data are reported in Table 1.

The compound Ag_2S has been described as two distinct mineral species: cubic argentite and monoclinic acanthite. Cubic Ag_2S is stable only above 177±1°C —— where a phase transition takes place. Below this temperature, the cubic morphology of the nonquenchable argentite phase is often preserved but, according to Ramsdell (1943), all room-temperature Ag_2S X-ray powder-diffraction patterns reflect the monoclinic structure of acanthite. Therefore, usage of argentite as a mineral name refers to a paramorph of acanthite after argentite.

Evidence for the bcc ⇌ mono. phase transition of Ag_2S at 177±1°C has been used extensively as an indicator of the minimum temperature of mineral deposition in ore deposits. Ramdohr (1955) stated that the frequent twinning observed in natural Ag_2S results from this inversion, and thus, the presence of twinning indicates initial deposition above 177±1°C; he considered Ag_2S which is free of twinning as having formed below this temperature.

Although pyrite is commonly believed to be stoichiometric FeS_2, many authors have reported slight variations in the cell dimensions which Kullerud and Yoder (1959) believed are more likely due to presence of impurities (e.g.,

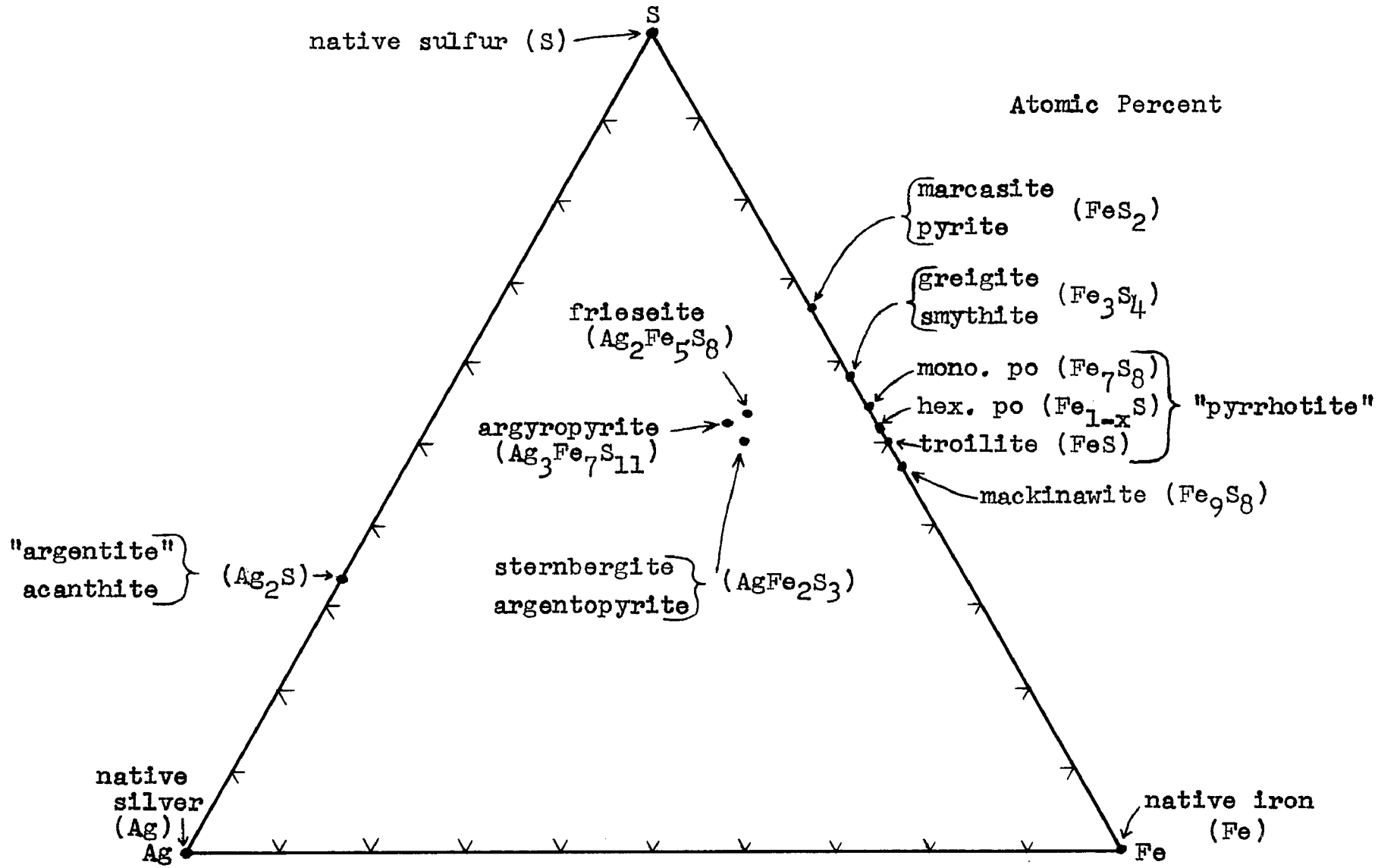

Figure 1. The compositions of reported minerals within the Ag-Fe-S system.

Table 1. Natural and synthetic phases in the Ag-Fe-S system.

Phase and Composition	Crystallography and Reference	Reference to X-ray Powder Data
Ag	cubic (Vegard, 1916)	Swanson et al. (1953)
Fe	cubic (Palache et al., 1944)	Swanson et al. (1955a)
S	orthorhombic (Abrahams, 1955) monoclinic (Tuller, 1954)	Swanson et al. (1960)
acanthite, Ag_2S (III)	monoclinic (Ramsdell, 1943)	Djurle (1958)
argentite, Ag_2S (II)	bcc (Djurle, 1958)	Djurle (1958)
Ag_2S (I)	fcc (Djurle, 1958)	Djurle (1958)
marcasite, FeS_2 (?)	orthorhombic (Buerger, 1931)	Berry and Thompson (1962)
pyrite, FeS_2	cubic (Palache et al., 1944)	Swanson et al. (1955b)
smythite, Fe_3S_4	hexagonal (Erd et al., 1957)	Erd et al. (1957)
greigite, Fe_3S_4	cubic (Skinner et al., 1964)	Skinner et al. (1964)
mackinawite, Fe_9S_8	tetragonal (Evans et al., 1962)	Kouvo et al. (1963)
troilite, FeS	hexagonal (Alsén, 1925)	Grønvold and Haraldsen (1952)
intermediate, $Fe_{1-x}S$ pyrrhotite	hexagonal (Alsén, 1925)	Carpenter and Desborough (1964)
monoclinic, Fe_7S_8 pyrrhotite	monoclinic (Byström, 1945)	Carpenter and Desborough (1964)
sternbergite, $AgFe_2S_3$	orthorhombic (Haidinger, 1828)	Berry and Thompson (1962)
argentopyrite, $AgFe_2S_3$	orthorhombic (Murdock & Berry, 1954)	Berry and Thompson (1962)
frieseite, $Ag_2Fe_5S_8$	orthorhombic (Peacock, 1942)	
argyropyrite, $Ag_3Fe_7S_{11}$	orthorhombic (Weisbach, 1877)	

Ni, Co, Cu, As, etc.) rather than variations in the metal to S ratio. The composition of maracasite is also reported as FeS_2 and has therefore been considered a polymorph of pyrite. Kullerud (1967a; 1967b) stated that marcasite was not formed in experiments in the Fe-S and Fe-S-O systems but commonly formed in experiments in the Fe-S-O-H system. He concluded, supporting Buerger's (1934) contention, that marcasite is slightly sulfur deficient, with the structure possibly containing SH^- bonds. These results suggest that marcasite is not an FeS_2 polymorph and is, also, not a phase in the Fe-S system.

Two minerals, smythite (Erd et al., 1957) and greigite (Skinner et al., 1964), are reported as having the composition Fe_3S_4. Little is known concerning their stability relations except that they are both probably unstable above 200°C.

Independently, Evans et al. (1962, 1964) and Kouvo et al. (1963) described natural occurrences of a tetragonal compound near FeS composition for which the name mackinawite has subsequently been accepted; this mineral is identical to the previously described cubic "kansite" (Meyer et al., 1957). Several specimens of mackanawite analysed by Clark (1966b) gave a composition $(Fe,Ni,Co)_{1+x}S$ with $x \leq .07$. Berner (1962b) has synthesized this tetragonal phase in aqueous Fe-S solutions demonstrating that Ni and Co are not essential components of the mackinawite structure.

Pyrrhotite, $Fe_{1-x}S$, exists in nature as at least three distinct mineral species. Carpenter and Desborough (1964) and Arnold (1967) reported that all naturally occurring pyrrhotites possess supercell modifications of the simple hexagonal NiAs-type cell originally ascribed to pyrrhotite (Alsén, 1925). Troilite, FeS, has a supercell with $\underline{a} = \sqrt{3}\underline{A}$, $\underline{c} = 2\underline{C}$ (Grønvold and Haraldsen, 1952),* intermediate pyrrhotite (hexagonal $Fe_{1-x}S$) with $\underline{a} = 2\underline{A}$, $\underline{c} = 5\underline{C}$ (Carpenter and Desborough, 1964), and monoclinic pyrrhotite, about Fe_7S_8, a cell with $\underline{a} = 2\underline{B}$, $\underline{b} = 2\underline{A}$, and $\underline{c} = 4\underline{C}$ (Bertaut, 1953).

Four minerals containing Ag, Fe, and S as major components —— the "Silberkiesgruppe" of Ramdohr (1960) —— have been described in the literature since 1828.** Based on the close similarity between the cell dimensions of argentopyrite and sternbergite and a cell content of $4(AgFe_2S_3)$ for argentopyrite versus $8(AgFe_2S_3)$ for sternbergite, Murdock and Berry (1954) suggested that these minerals are dimorphs. The X-ray diffraction data and physical properties of these two minerals are fairly well established; however, for frieseite and argyropyrite, X-ray data are lacking, reported compositions are at variance, and the physical and optical

---

* Normal lower case symbols are used to denote the crystallographic axes of the superstructure based on the NiAs arrangement; upper case symbols are used to denote the NiAs-type substructure (Wuensch, 1963, p. 157).

** Palache, et al. (1944) also report a mineral "silberkies" originally described by Streng (1878), not as a new mineral species, but as a possible variation of a mineral in the "silberkiesgruppe".

properties are not distinctly different from sternbergite or argentopyrite.

Argyropyrite was originally described as a mineral with composition $Ag_3Fe_7S_{11}$ (Weisbach, 1877). Most physical properties are similar to those of sternbergite, but this mineral has a prismatic habit similar to argentopyrite. Frieseite was originally described as a mineral with composition $Ag_2Fe_5S_8$, with all its physical properties identical to sternbergite, except that it has a thick-tabular habit versus thin-platey for sternbergite. Samples of frieseite and sternbergite upon X-ray examination by Peacock (1942) gave exactly the same patterns and cell dimensions. If the differences in composition of argyropyrite and frieseite from $AgFe_2S_3$ are due to contamination or poor analysis, these minerals may be paramorphs of sternbergite after argentopyrite.

The X-ray powder-diffraction tracings of sternbergite and argentopyrite are in good agreement with those of Berry and Thompson (1962) and Murdock and Berry (1954), respectively. No new information concerning their structures was determined during the present study.

EXPERIMENTAL METHODS

The various experimental methods employed during this investigation to study particular aspects of phase relations in the Ag-Fe-S system are discussed below.

Quench-Type Experimentation

The majority of experiments involved the use of sealed, evacuated, silica-glass tubes with minimum vapor volume as described by Kullerud and Yoder (1959). Such experiments are commonly referred to as "quench-type" or "silica-tube" experiments. The equipment necessary for such experimentation is available at Lehigh University, Department of Geological Sciences, and has previously been described in detail by Craig (1965) and Roland (1966).

One of the basic assumptions concerning the use of quench-type experiments is that the nature (e.g., composition and interrelationships) of the phases present at the annealing temperature can be inferred from the products as examined at room temperature. In order to help preserve evidence of the high-temperature phase relations, the silica tubes, at the termination of the heating period, are rapidly chilled to room temperature by immersion in cold water; the temperature of the tubes reaches 25°C in an estimated 3-5 seconds. Therefore, in the context of this study, the term "quench" is not used to mean an "instantaneous freezing" but is applied to the technique of rapid chilling.

The attainment of equilibrium in quench-type experiments is commonly hindered by inhomogeneity of the charge and/or slow reaction rates. To help alleviate these difficulties, two practices were adopted during the present study; 1) many charges were homogenized by partial or complete melting in sealed, evacuated, silica tubes in an oxygen-natural gas flame prior to annealing at the desired temperature, 2) frequently, the silica tube of an experiment was rapidly chilled to room temperature, the tube opened, the material carefully ground under toluene* (to prevent oxidation), the charge resealed in a clean tube, and the tube again placed at the annealing temperature. This procedure considerably hastened otherwise sluggish reactions, because the grinding provided an enormous increase in reaction surfaces; however, as explained in a later section, this grinding may have certain deleterious effects as well. Extreme care was taken with grinding with consequent loss of less than 1.0 mg of a 100 mg charge. The material lost was assumed to have the composition of the bulk charge.

DTA Experimentation

Certain phases in the Ag-Fe-S system are nonquenchable and cannot be studied by quench-type experiments. Noteable examples in the Ag-Fe-S system are the bcc ⇄ fcc and bcc ⇄

* The charges of early experiments were ground under acetone. However, it was found that acetone readily picks up moisture from the atmosphere thus making it unsuitable for this use.

mono. transformations of Ag_2S. However, the thermal energy associated with a nonquenchable phase transformation can often be detected by differential thermal analysis. For this reason, numerous DTA experiments were conducted in the laboratory of Dr. Gunnar Kullerud of the Geophysical Laboratory of the Carnegie Institution of Washington, D. C., according to the procedure described by Kullerud (1963b). A detailed description of this DTA apparatus and technique was given by Craig (1965).

High-Temperature X-Ray Experimentation

A Unicam high-temperature X-ray camera was used during this study for the examination of the nonquenchable bcc and fcc forms of Ag_2S. These experiments were conducted in the Kullerud Laboratory at the Geophysical Laboratory; technical details concerning this apparatus were discussed by Craig (1965).

Aqueous Experimentation

The reaction rates of many quench-type experiments conducted in the Ag-Fe-S system below about 300°C were extremely slow i.e., they would require years to attain equilibrium. Therefore, other methods of experimentation were conducted in an attempt to overcome this kinetic factor. Berner (1962a, 1964) and Clark and Kullerud (1963) have reported excellent results with the aqueous precipitation of sulfide phases at elevated temperatures. Barnard and Christopher

(1966a, 1966b) have reported the presence of various salts (i.e., NaCl, NH_4Cl) in solution to be very effective in transporting and recrystallizing sulfide phases. Although the exact mechanisms of formation and effects of the additional components (e.g., H_2O, various salts) are not completely known, these methods of aqueous experimentation can result in feasible reaction periods. If the presence of H_2O does not cause a change in the number or composition of the solid phases under consideration, it may be regarded as only a reaction medium or catalyst for the experiment.

Precipitation Experiments

Several aqueous experiments involved the mixing of solutions at elevated temperatures. No attempt was made to exclude air from the experiments. The components for the reaction were present as dissolved salts and, upon mixing of the solutions of the respective salts, a black precipitate usually formed which was identified by X-ray powder-diffraction analysis. The Teflon-bomb technique (Kullerud, 1962) was also used where it was desirable to mix the solutions at temperatures above 100°C. In this technique, very limited amounts of air were enclosed in the reaction vessel because the bomb was not evacuated before sealing.

Recrystallization Experiments

Aqueous experiments were also conducted using a 2M NH_4Cl solution as the reaction medium. Solid phase reactants

(100 mg charges) —— the same reactants as used in the anhydrous experiments —— and the salt solution (1.5-2.0 ml) were placed in sealed, evacuated, silica tubes and annealed at temperatures below 300°C. The solid products of such experiments were not analysed for chlorine; however, several experiments in the Fe-S system duplicated by both the dry and aqueous recrystallization techniques gave exactly the same phase relations and $d_{(10\cdot2)}$ values for the pyrrhotites involved. This suggests that either chloride ions do not enter the pyrrhotite structure, or the effect of chloride ion contained in the pyrrhotite structure is not of sufficient magnitude to be detected by the X-ray technique used. The former suggestion is more plausible.

Fugacity Determinations

Kullerud and Yoder (1959) reviewed the various methods of determining fugacities (non-ideal pressures) of sulfur over sulfide-phase assemblages. An electrum-tarnish method (Barton and Toulmin, 1964) for measurement of sulfur fugacities has since been developed and applied to sulfides. This method has been used to calibrate yet another method for sulfur-fugacity determinations —— the pyrrhotite-indicator method (Toulmin and Barton, 1964).

Both the electrum-tarnish and pyrrhotite-indicator methods for determining the fugacities of sulfur in laboratory sulfide systems were used in the course of this investigation and are described in much more detail in a later section (page 89).

PREPARATION OF REACTANTS

Reactants used in the preparation of experiments consisted of either the elements or the binary compounds, Ag_2S, FeS_2, and $Fe_{1-x}S$, previously synthesized from the elements. Elements of the highest available purity were used in this study. Iron was obtained from the Battelle Memorial Institute, Columbus, Ohio. The silver and sulfur were obtained from the American Smelting and Refining Company, South Plainfield, New Jersey.

The iron, bar 83 of 99.995+wt.% purity, was obtained as a 1 lb. cylinder 1 1/2 inches in diameter. The supplier's analyses report S, B, Si, Na, V, Zn, and Zr, as well as 40 other metallic impurities, as not detected; elements detected (in ppm) are: O_2- 1.8, C- 4, Cr- 3, Co- 10, Ni- 4, P- 5; all others total <10 ppm.

Grade A-59 silver, of 99.999+wt.% purity, was obtained as 2 ounce bars. The supplier's spectrographic analyses report Au, Bi, Ca, Cd, Cr, In, Mn, Ni, Pb, Sb, Te, and Zn as not detected; maximum impurities of other elements (in ppm) are: Mg- 4, Si- 2, Fe- 3, Cu- 4, and Al- 1.

"Special High Purity" sulfur, of 99.999+wt.% purity, was obtained as fragments. The supplier's spectrographic analyses report Ag, Al, Bi, Ca, Cd, Cr, Cu, Fe, In, Mg, Ni, Pb, Sb, Si, Sn, Te, and Zn as not detected; Na and Cl are each listed as 1 ppm on the basis of chemical analyses.

Silver and iron were separately treated in a hydrogen-

reduction furnace at 800°C for 3-4 hours and 850°C for 6-8 hours, respectively, before use. The reduced materials were stored in sealed, evacuated, pyrex or silica-glass tubes to avoid oxidation.

Silver and sulfur were mixed in an atomic ratio of 2:1 in order to prepare 1 gm charges of Ag_2S. The charges were heated in a sealed, evacuated, silica tube at 600±10°C for a period of 3-5 days to insure complete reaction. Upon completion of the heating, the Ag_2S was carefully filed and any file teeth associated with the Ag_2S were removed with a magnet. The Ag_2S was examined in polished section for purity.

Pyrrhotite (of desired composition) was prepared by weighing into a silica tube, correct proportions of Fe and S for a 500 mg. charge*. The sealed, evacuated tube was placed in a furnace at a temperature of 600±10°C for 24 hours, then the tube was quenched, the charge carefully ground under toluene, reloaded into a clean tube, and heated for an additional 72 hours. At the end of the time, the pyrrhotite was again ground, reloaded, and placed in the furnace for an additional 24 hours. A representative portion of this fresh pyrrhotite was taken from the tube for examination of composition and purity. A sharp 10·2** X-ray

---

* Difficulty with inhomogeneity was encountered if the charge weighed more than about 500 mg.

**Abbreviated Miller-Bravais indices.

reflection and optical purity in polished section were used as indications of homogeneity. Because pyrrhotite oxidizes in a few days if exposed to air, this starting material was stored in sealed, evacuated tubes or, as in earlier experiments, kept in a vacuum desiccator (pressure approximately 10 mm Hg) until ready for use.

For the synthesis of pyrite, previously prepared pyrrhotite of known composition was mixed with an amount of sulfur calculated to give 600-800 mg total, with a bulk composition of FeS_2 + 0.2-0.3 wt % S (to compensate for sulfur loss to the vapor phase). This charge was heated in a sealed, evacuated, silica tube at 600±10°C for 48 hours, the tube quenched, the charge carefully ground under toluene (to prevent oxidation), reloaded into a clean tube with an excess of 0.1 wt.% S, and heated for an additional 24 hours. Another careful grinding preceeded a final 24 hours of heating. The excess sulfur present was removed by placing the tube in a thermal gradient, causing the sulfur to migrate to the cooler end of the tube. After quenching, the tube was carefully opened, the visible sulfur removed, and the FeS_2 was ground under CS_2 to dissolve sulfur and then under alcohol to dissolve CS_2. The pyrite was stored in a vacuum desiccator to prevent moisture contamination and oxidation.

IDENTIFICATION OF PHASES

The phases encountered during this study were identified by 1) visual examination, 2) low-power binocular microscope, 3) magnet, 4) reflecting microscope, and 5) X-ray powder-diffraction methods.

1) Visual examination of the charge was used extensively when a liquid phase was suspected at the temperature of the experiment. The tube was taken out of the vertical furnace and immediately examined at temperature prior to chilling. This technique was very useful in detecting the presence of small amounts of a sulfur-rich liquid which might otherwise go undetected in the room temperature products.

2) The unopened silica tubes were examined after quenching with a low-power (0.7-3X objective) binocular microscope to ascertain as far as possible if reaction had taken place, if separation of the charge into two or more discrete portions had occurred (suggesting inhomogeneity), or if sulfur-rich liquid, as shown by small droplets of sulfur on the tube walls, was possibly present at the annealing temperature of the experiment.

3) Monoclinic pyrrhotite has a higher magnetic susceptibly than the associated phases in Ag-Fe-S and Fe-S experiments. A magnet was used to determine if one of the products in an unopened tube consisted of monoclinic pyrrhotite, and, in experiments on the Fe-S join, this effect could even be

used to estimate relative proportions of hexagonal and monoclinic pyrrhotite phases.

4) Representative portions (about 50 mg) of charges were cast in a clear, cold-setting, mounting medium. Bakelite epoxy resin which hardens in approximately 4 hours at 25°C and Geomount plastic which hardens in approximately 20-30 minutes at 25°C were the mounting media used. The mounted charges were polished with various abrasives on a series of cloth-covered steel laps using a Sampson-Patmore polishing machine. The polished sections were then examined with a Leitz Dialux reflecting microscope. Oil-immersion objectives, because of their much higher resolution, as compared to air objectives, were used almost exclusively.

The optical properties of the synthetic solid phases in the Ag-Fe-S system are identical to the properties of their natural analoges. Examination of polished sections of experimental charges commonly revealed "liquid textures" -- evidence of the presence of liquid at the annealing temperature. These textures consist of fine-grained intergrowths of the appropriate unary and binary solid phases.

Powder smear-mounts for X-ray powder-diffraction study were made by grinding the material under toluene and smearing this powder on a glass slide with an acetone-Duco Cement solution. Malleable phases were finely filed before smearing on the glass slide. Diffractometer tracings were obtained using a North American Philips X-ray diffraction unit. The radiation used was either nickel-filtered copper ($\lambda K_{\alpha} = 1.5418$Å)

or manganese-filtered iron (λK_{α} = 1.9373Å). When it was necessary to determine exact interplanar spacings of a phase, an internal standard, silicon ($\underline{a}$ = 5.4306Å, Parrish, 1953) or fluorite ($\underline{a}$ = 5.4638±0.0003Å, Roland, 1966), was incorporated with the sample during the grinding for the powder smear mount. At least 8 sets of reflections of the peaks of interest were obtained by oscillation from both low to high and high to low angles with a reversal of the slide after the fourth oscillation. The goniometer speed was 1/2 degree 2θ per minute with a chart speed of 1/2 inch per minute. Computations of cell dimensions were made using the G.E. 225 computer and a least-squares program, written by Dr. G. W. Roland*, which operates on the 2θ values of previously indexed lines. Each line is accorded a weighing factor using the method described by Burnham (1962).

The iron content of the pyrrhotite made in this study, as well as the metal content of the natural pyrrhotites examined, were determined according to the method of Arnold (1962) using a graph of $\underline{d}_{(10\cdot2)}$ versus atomic percent iron in the pyrrhotite based on the data of Toulmin and Barton (1964). The standard deviation of the measurements of the 2θ value of the 10·2 reflections of the pyrrhotites was ±0.12°, which corresponds to ±0.10 at.% iron.

---

*Research Associate, Department of Geological Sciences, Lehigh University.

DATA CONCERNING THE UNARY AND BINARY SYSTEMS

A systematic study of ternary phase relations necessitates a thorough knowledge of the binary systems which in turn requires a complete understanding of the respective unary systems (the elements). The unary and binary systems are well known at temperatures above approximately 300°C. However, a number of experiments in the present study were conducted in the binary systems at temperatures both above and below 300°C and are reported at the end of the discussion of each system.

The Elements

Ag

Kracek (1946) reported the melting point of pure silver, in the presence of vapor, as 960.5°C. Solid silver occurs in only one crystalline modification which possesses a face-centered cubic structure, space group Fm3m (Swanson, et al., 1953).

Fe

The melting point of pure iron in the presence of vapor is reported as 1534°C (Hansen and Anderko, 1958). Iron possesses three structural modifications at one atmosphere pressure (α stable below 910°C, γ stable between 910° and 1390°C, and δ stable from 1390°C to the melting point) which are all cubic; the γ phase is face-centered cubic (fcc) whereas the α and δ phases are body-centered cubic (bcc).

S

Meyer (1965) and Tuller (1954) compiled data pertaining to the phase relations and thermodynamics of pure sulfur. Bell *et al.* (1967) determined that low-temperature sulfur (orthorhombic) inverts to a higher-temperature form (monoclinic), in the presence of vapor, at 102±1°C and that the triple point of sulfur is at 114±1°C. At all temperatures of experimentation in the present study (above 114°C), the assemblage liquid S + vapor occurs in the sulfur corner of the ternary system.

The Binary Systems

Ag-S System

The condensed phase diagram of the Ag-S system is shown in Figure 2 based on the data of Kracek (1946) and Hansen and Anderko (1958). Silver sulfide (Ag_2S) is the only compound in the system. The maximum limits of solid solution from Ag_2S composition are less than 2.7± 0.2 at.% toward sulfur at 804±2°C and less than 1.3±0.3 at.% toward silver at 740±3°C —— the compositions of the sulfur-rich monotectic and silver-rich eutectic points, respectively (see Figure 2). Wagner (1953) reported a maximum variation in composition of the low-temperature form from $Ag_{2.000}S$ to $Ag_{2.002}S$.

Two nonquenchable phase transitions in Ag_2S are reported. The low-temperature polymorph (acanthite) has a monoclinic structure (Ramsdell, 1943). The intermediate-

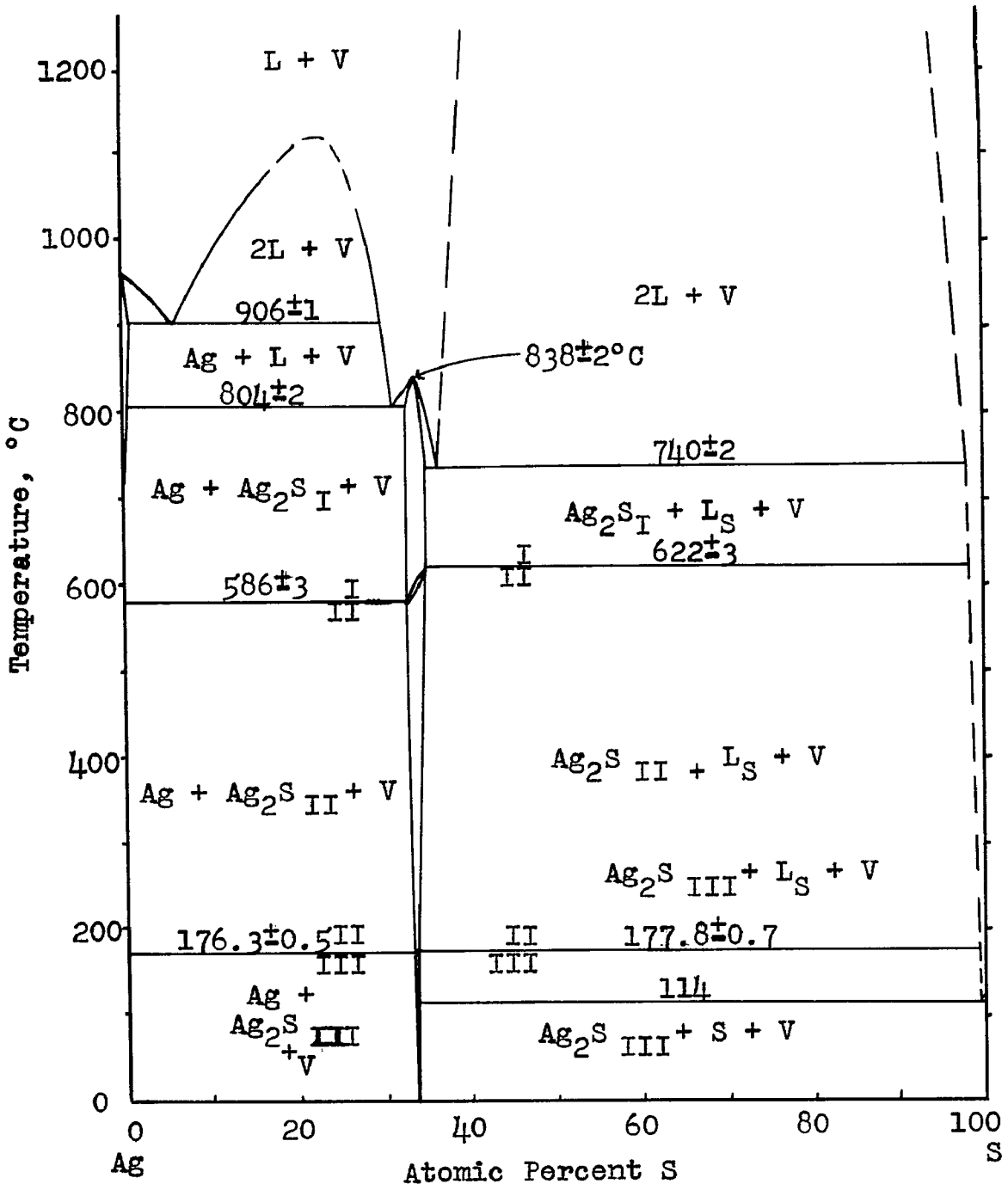

Figure 2. Condensed phase relations in the system Ag-S. This diagram is based on the compilation by Hansen and Anderko (1958).

temperature polymorph (argentite) is body-centered cubic (bcc) (Rahlfs, 1936; Djurle, 1958) and the high-temperature form is face-centered cubic (fcc) (Djurle, 1958).

A recent study was conducted by Sadanaga and Sueno (1967) on the 177°C inversion in Ag_2S. They heated Ag_2S by means of a small furnace attached to the goniometer head of a Weissenberg camera and observed twin formation in Ag_2S at all temperatures above 152°C. The intensity and number of twin reflections became greater as the 177°C inversion temperature was approached. Therefore, Ag_2S shows a progression of twin formation with increasing temperature premonitory to the inversion at 177°C.

Present Study.

Experiments were conducted to investigate the hypothesis that twinning is not present in Ag_2S formed below the 177°C structural transition. Ag_2S was made by direct reaction of Ag and S at 156±2°C for 6 days and also at 166±3°C for 37 days. The temperature of one experiment at 158°C was closely monitored and the heat of reaction was not observed to raise the temperature of the charge measurably. Examination of polished sections of the charges at room temperature revealed numerous inversion-like twins; the appearance of Ag_2S formed at 166±3°C and at 185±2°C for 63 days but quenched to room temperature before examination was very similar.

The experiments conducted by Sadanaga and Sueno (1967) showed that twinning exists in Ag_2S formed and examined at

temperatures above 152°C but below 177°C. Experiments conducted during the present study showed that this twinning is preserved upon rapid chilling to room temperature and is similar to the twinning formed in Ag_2S synthesized above the inversion temperature. A lower-temperature limit for twin formation was not determined during the present study. However, because Sadanaga and Sueno (1967) used annealing times on the order of 24 hours and observed twinning at 152°C, it is suspected that longer reaction times will produce twinning at temperatures below 152°C. These observations present serious doubt concerning the criterion of twinning in Ag_2S as evidence for initial deposition as argentite above 177°C as stated by Ramdohr (1960).

Experiments listed in Table 2 show maximum solid solution of Ag_2S toward Ag of <0.3 at.% Ag at 750±5°C and toward S of <2.2 at.% S at 700±3°C. Experiments conducted to determine this latter figure were based on the presence of liquid sulfur as observed in the experiments at the annealing temperature.

Table 2. Experiments conducted on the Ag_2S solid solution.

Reactants	At.% Comp.	Temp., °C	Time, hrs.	Products at Temp.
Ag + S	66.7-33.3	750±5	72	Ag_2S + V
Ag + S	66.8-33.2	750±5	72	Ag_2S + V
Ag + S	67.0-33.0	750±5	72	Ag_2S + Ag + V
Ag + S	67.2-32.8	750±5	72	Ag_2S + Ag + V
Ag + S	64.0-36.0	700±3	93	Ag_2S + L_s
Ag + S	64.3-35.7	700±3	93	Ag_2S + L_s
Ag + S	64.5-35.5	700±3	93	Ag_2S + L_s
Ag + S	66.7-33.3	700±3	93	Ag_2S + V

Fe-S System

The condensed equilibrium diagram of the Fe-S system above approximately 320°C is shown in Figure 3, as reproduced from Kullerud and Yoder (1959) and Kullerud (1961).

The solid solution of $Fe_{1-x}S$ (pyrrhotite) was shown by Hägg and Sucksdorff (1933) to be due to the omission of Fe from the FeS structure; the cell dimensions are dependent on the Fe deficiency of the pyrrhotite*. The beta transformation of $Fe_{1-x}S$, characterized by a break in magnetic susceptibility, cell dimensions, and thermal properties, is variously reported as occurring at 315-318°C (Roberts, 1935), 320°C (Kullerud, 1967a), and 325°C (Haraldsen, 1941). Above this transition temperature, taken as 320±5°C in this study, $Fe_{1-x}S$ is reported to possess simple hexagonal NiAs structure (Grønvold and Haraldsen, 1952). However, Corlett (1968) believes that pyrrhotites possess this simple hexagonal structure above 225±25°C.

Desborough and Carpenter (1965) found that both natural and synthetic pyrrhotite annealed at temperatures above 315±10°C but chilled to room temperature before examination, exhibit a hexagonal supercell based on the NiAs structure with $\underline{a} = 2\underline{A}$ and $\underline{c} = 7\underline{C}$**. Below 320±5°C, $Fe_{1-x}S$ is reported

* The solvus curve that forms the sulfur-rich limit of hexagonal pyrrhotite was determined throughout the temperature range 325°C (52.71 at.% S) to 743°C, where the sulfur content reached a maximum of 55.1 at.% S (Arnold, 1962).

** This supercell is probably a "quench product" and not stable at the annealing temperature.

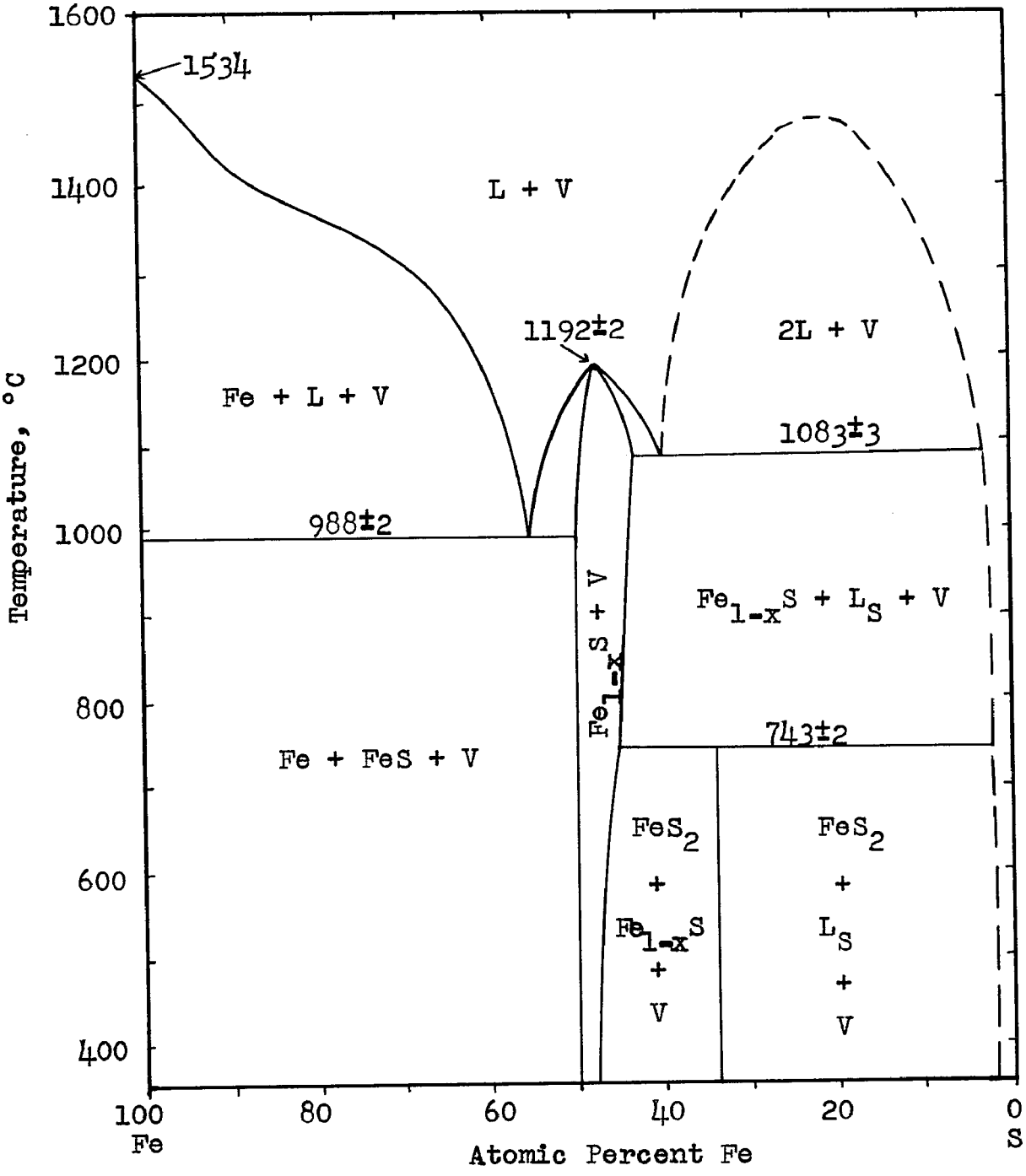

Figure 3. Condensed phase relations in the Fe-S system at high temperatures, after Kullerud and Yoder (1959) and Kullerud (1961).

to possess several superstructures, all based on the NiAs structure. Desborough and Carpenter (1965) found that certain pyrrhotite samples chilled from annealing temperatures below 315±10°C possess a hexagonal supercell with $\underline{a} = 2\underline{A}$ and $\underline{c} = 5\underline{C}$. Byström (1945) found that there also exists a pyrrhotite with monoclinic structure. This compound, with or near Fe_7S_8 composition, has a supercell with $\underline{a} = 2\underline{B}$, $\underline{b} = 2\underline{A}$, and $\underline{c} = 4\underline{C}$ (Bertaut, 1953; Wuensch, 1963). The upper-stability temperature of monoclinic $Fe_{1-x}S$ is variously reported as 315°C (Desborough and Carpenter, 1965), 308±5°C (Clark, 1966a), 305±5°C (Arnold, 1967), and less than 265°C (Buseck, 1962; Kullerud et al., 1963). Hall and Yund (1966) believe that it is always a metastable phase. Corlett (1968), based on high-temperature precession photographs, stated the upper-stability temperature of the monoclinic structure in air as 225±25°C; above this temperature all pyrrhotite is hexagonal. She reported that rapid cooling of samples with compositions between Fe_9S_{10} and Fe_7S_8 which were annealed above 225±25°C produced a metastable phase with a hexagonal supercell, $\underline{a} = 2\underline{A}$ and $\underline{c} = 3\underline{C}$. Slower cooling (minutes versus seconds) allowed the simple hexagonal structure to invert to the monoclinic.

Troilite, FeS, stable below 139°C, is also hexagonal but with a supercell with $\underline{a} = \sqrt{3}\underline{A}$ and $\underline{c} = 2\underline{C}$ (Grønvold and Haraldsen, 1952; Bertaut, 1956).

The phases Fe_9S_8 (mackinawite) and Fe_3S_4 (smythite and

greigite) -- discussed in a previous section -- were not encountered during the experimental portion of this study and are not pertinent to this discussion.

Phase relations in the FeS-FeS_2 portion of the Fe-S system below 320°C are not clearly defined at present; however, the most recent interpretation is shown in Figure 4.

Present Study.

A common way to speed up otherwise slow reactions is to regrind the charge to create more fresh surface areas for reaction. Because duplication of some experiments concerning monoclinic pyrrhotite (abbrev. = m-po) as a phase gave ambiguous results, the possible effects of grinding were evaluated.

Figure 5 shows the effect of grinding on the X-ray powder-diffraction pattern of m-po. A m-po of Fe_7S_8 composition, synthesized at 300°C in 3 weeks, was subjected to various durations of regular hand grinding under toluene. At the end of each grinding interval, a representative portion of the ground material was X-rayed. Examination of the X-ray tracings reveals that the 408 and $\bar{4}08$ reflections of m-po, with increased grinding time, become diffuse and are gradually replaced by a single reflection which has a $d_{(10\cdot2)}$ value corresponding to a composition of 46.7 ± 0.1 at.% Fe. However, the intensity (visual estimate) of this reflection is approximately 2/3 of that obtained from the

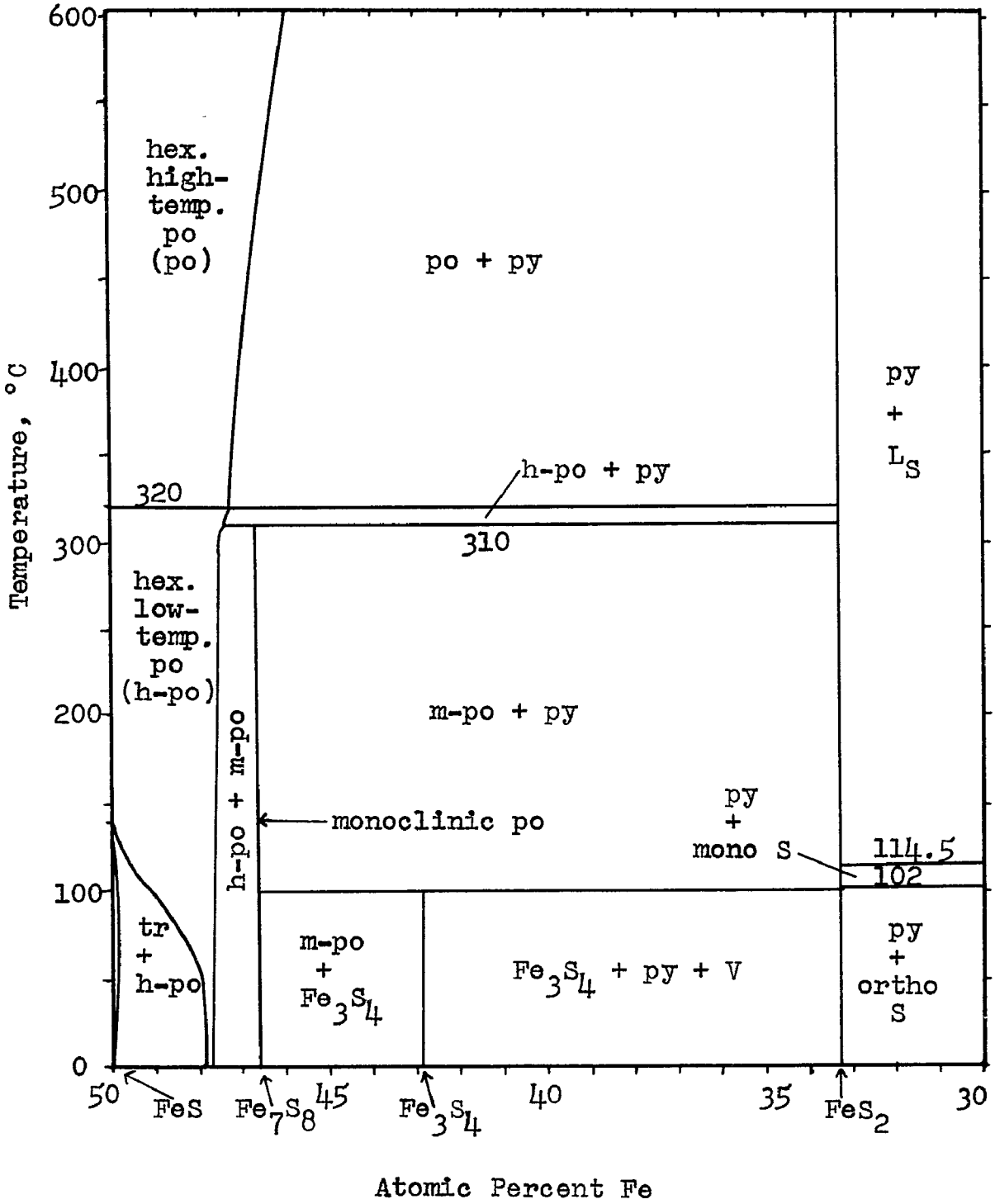

Figure 4. Condensed phase relations in the FeS-FeS_2 portion of the Fe-S system at low temperatures, after Kullerud (1967a).

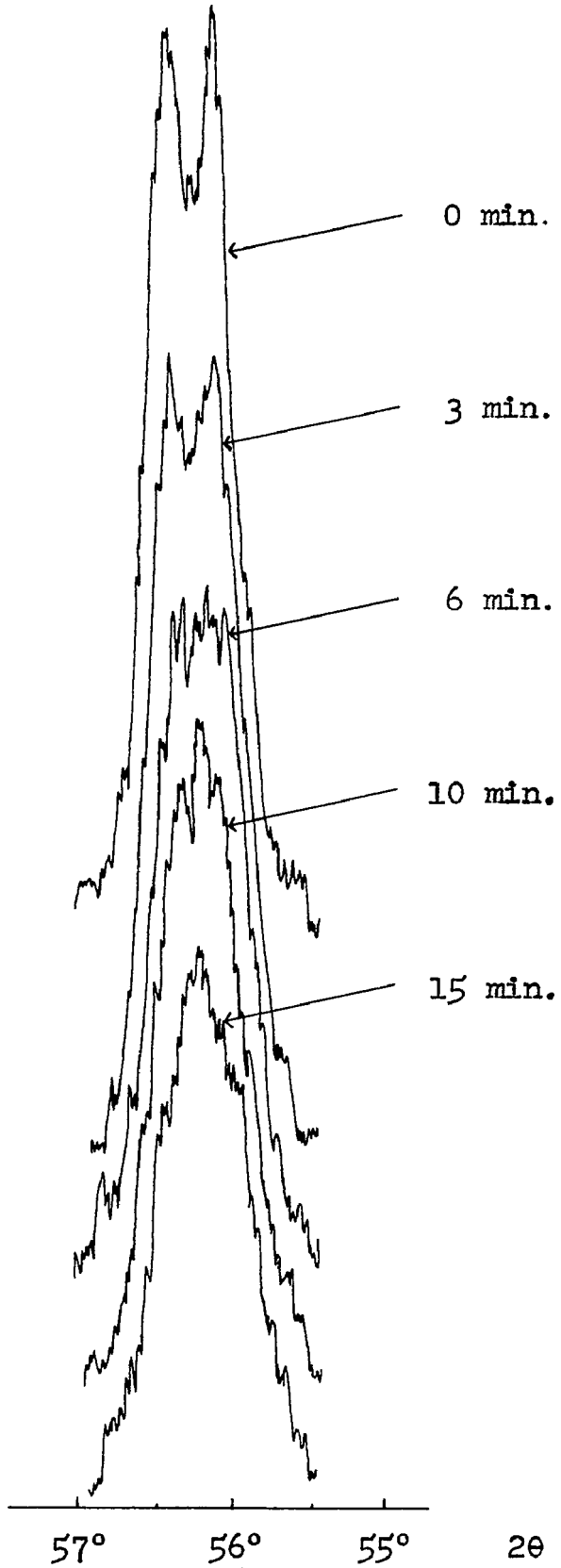

Figure 5. The effect of grinding on the X-ray powder-diffraction pattern of the 408-408 reflections of monoclinic pyrrhotite. The times represent the duration of the grinding, by hand, under toluene prior to the X-ray tracing. X-ray conditions used were Fe unfiltered radiation at 50kV and 10 mA with a chart rate of 1 inch/minute.

unground m-po. Supercell reflections, although present, could not be positively identified because of poor resolution. The presence of reflections in addition to those mentioned by Desborough and Carpenter (1965) were also observed. It is therefore highly suggestive, although not conclusive, that the grinding transformed the monoclinic phase into a hexagonal phase; however, the change may have been one of "crystallinity", resulting in a loss of resolution of the 408 and $\bar{4}08$ reflections.

The thermal effects of grinding are not large. A thermocouple placed in the toluene during grinding showed a temperature increase of 1/2 to 3/4°C. The exact nature of the energy that is put into the system by grinding is not known.

Hall and Yund (1966) believe that m-po is unstable and that the stable phase is low-temperature hexagonal po (abbrev. h-po). The change from m-po to h-po during grinding, as noted above, could be interpreted as evidence that this is true. Grinding might add enough activation energy to drive the reaction into the stable state (h-po), however, the converse could also be true -- the h-po is metastable. The m-po might be the stable phase in the condensed system whereas pressures introduced during grinding might transform m-po into a stable high-pressure modification of h-po.

The implications regarding all experimental work which incorporates regrinding techniques into the procedure are noteworthy. The transformation of a phase or assemblage to

another may be greatly influenced by the P-T conditions introduced during grinding.

The low-temperature hexagonal pyrrhotite-troilite solvus was investigated by both dry and aqueous experimental techniques. Both types of experiments were based on the exsolution of a previously synthesized homogeneous po into a mixture of troilite and h-po. In the aqueous experiments, the charge was placed in approximately 2cc of 2m NH_4Cl solution and sealed under a partial vacuum in a 1 cm I.D. silica or pyrex glass tube. The dry experiments consisted of normal "quench-type" experiments. Figure 6 shows a plot of the experimental results listed in Appendix 5a. These data are in good agreement with the results of Hall and Yund (1966). The aqueous and dry experiments are also in close agreement.

Several experiments (Appendix 5b) were conducted on the m-po—py solvus. The charges consisted of high-temperature po containing 46.0 at.% Fe. This po, upon annealing, exsolved py and became monoclinic. The composition of the monoclinic phase was determined by heating it at 330-350°C for 5-10 minutes according to the method of Kullerud *et al.* (1963); this transformed the m-po into a hexagonal po of the same composition whose $d_{(10.2)}$ was determined. Longer annealing periods allow the hexagonal po time to equilibrate to the py-po solvus. Hall and Yund (1966) and Clark (1966a), based on dry experiments, have also found indications that

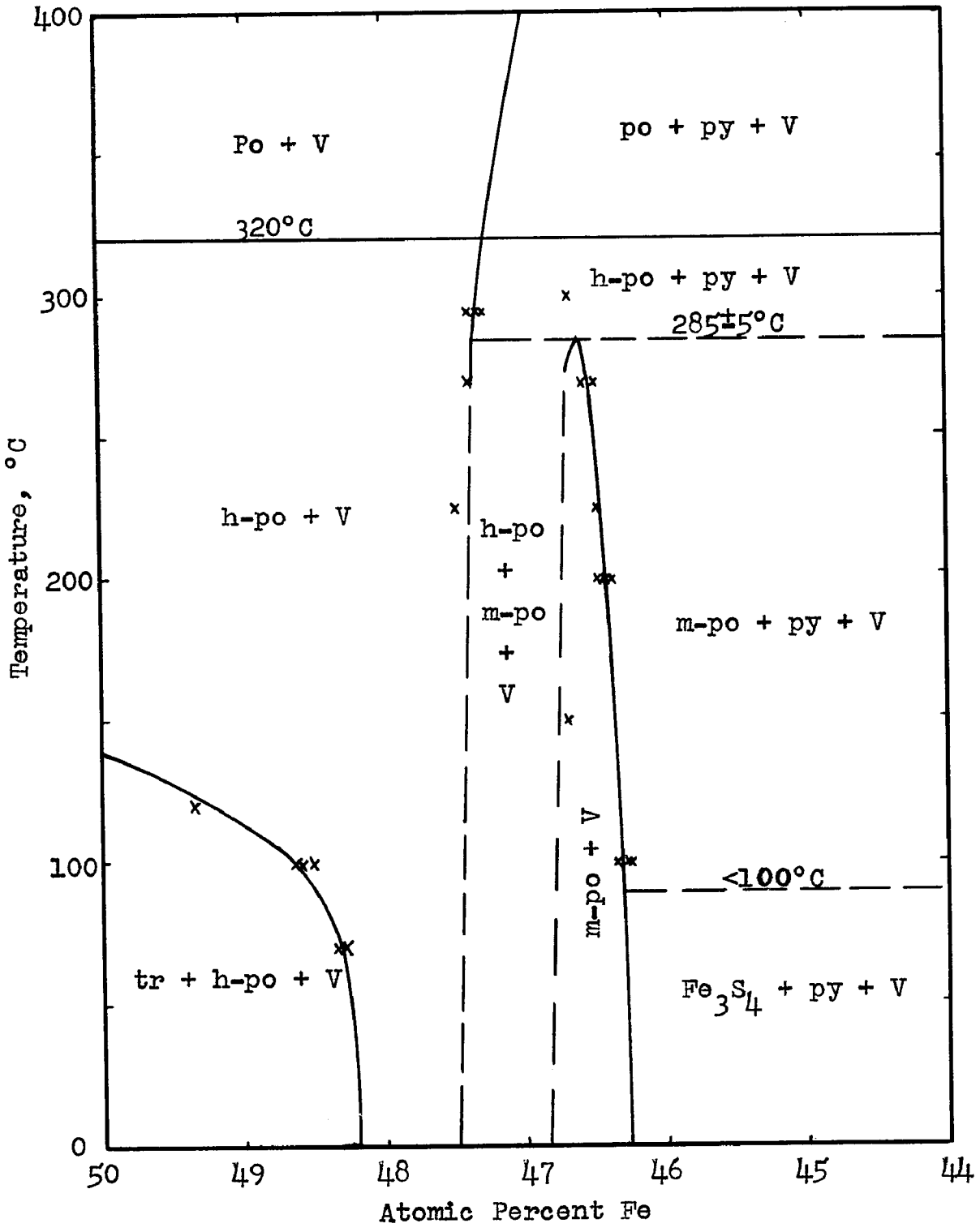

Figure 6. Condensed phase relations in a portion of the Fe-S system at low temperatures based on experiments conducted during the present study. Crosses represent the compositions of the pyrrhotites in the experiments (Appendix 5).

m-po does have appreciable solid solution from Fe_7S_8 composition toward py as shown in Figure 6. Because no Fe_3S_4 phases (i.e., greigite or smythite) were among the products of the experiments at 100±10°C, it is suggested that the upper stabilities of these phases are below this temperature and both are shown as <100°C in Figure 6.

Heating experiments with m-po (Appendix 5c) gave a breakdown temperature of 310±5°C, because m-po above this temperature quickly (i.e., in minutes) inverts to a hexagonal po having Fe_7S_8 composition. This h-po must be metastable for, if annealing is continued, it slowly equilibrates to a py + po + V assemblage. The initial h-po formed by the reaction m-po (Fe_7S_8) → h-po (Fe_7S_8) is nearly nonquenchable, for if this h-po is allowed to cool 30 seconds in air before rapid chilling to room temperature, the product was found to be m-po. The activation energy associated with the breakdown must be very small; these kinetics emphasize the improbability of ever finding a high-temperature po in nature. The reaction associated with the m-po upper-stability temperature was not shown to be reversible at 310±5°C. If the po + py + V assemblage, stable above 310°C, is annealed at temperatures below 310°C, but above 285±5°C, m-po does not reform but the h-po of the py + h-po + V assemblage has equilibrated to a composition which lies on an extension of the high-temperature po solvus. At 270±10°C the h-po + py reacts to m-po; because of the "inertness" of py however,

the reaction does not go to completion. Based on the above data, the upper-stability temperature of m-po is shown as 285±5°C on Figure 6.

With experiments on the m-po—h-po solvus which were believed to contain h-po and m-po, the charges were annealed at 330-350°C for 5-10 minutes as discussed before. These mixtures reequilibrated to a one-phase h-po in this short time. Therefore, no data were obtained on m-po compositions in equilibrium with h-po during this study.

X-ray powder-diffraction tracings of natural h-po and m-po show intense 10·2 and 408 - $\bar{4}08$ reflections, respectively; mixtures of these two minerals show two reflections, 10·2 and 408 superposed and the $\bar{4}08$. The intensity of this first peak is a function of percentage of h-po present. During the present study, m-po with much larger $\bar{4}08$ than 408 reflections was commonly encountered in experiments above about 200°C. This intensity distribution may be a function of the m-po monoclinicity (i.e., the β angle may change with temperature). At 152±5°C the m-po was "normal" (i.e., $I_{408} = I_{\bar{4}08}$). A natural specimen of m-po which gave a larger $\bar{4}08$ reflection was found at Cobalt, Ontario and is further discussed on pages 118-119.

The supercell reflections indicated by Carpenter and Desborough (1964) and Desborough and Carpenter (1965) are not wholly consistent with the number and position of extra reflections observed during the present study. The super-

structures of pyrrhotite will require further investigation.

Based on quench-type experiments, Kullerud and Yoder (1959) were not able to determine any measurable solid solution of pyrite from stoichiometric FeS_2. However, on the premise that a small amount of solid solution may affect the cell dimension of pyrite, several experiments were conducted during the present study. The two extremes of pyrite solution were formed by experiments with charge compositions in the univariant fields flanking the py + V field (Table 3). The cell dimension of synthetic pyrite at 25°C have been variously reported:

5.4165±? Swanson et al. (1955b)
5.4175±0.0003 Lepp (1956)
5.419 ±0.002 Kullerud and Yoder (1959)
5.4189±0.0004 Straumanis et al. (1964)

Table 3 shows the cell dimension of synthetic pyrite based on X-ray measurements at 25°C and refinement by a least-squares computer program. No measurable differences in cell dimensions of pyrite in equilibrium with sulfur or with po were observed and $a_{25°} = 5.4175 \pm .0002$Å was determined for $FeS_{2\pm x}$.

Table 3. Cell dimensions of synthetic pyrites.

Charge Composition	Temp., °C	Time, Days	$a_{25°}$ Å
py + po	662±3	10	5.4176±0.0001
py + arg	662±3	51	5.4175±0.0002
py + S	662±3	10	5.4175±0.0002
py	662±3	51	5.4175±0.0001
py + po	665±3	41	5.4176±0.0002
py + S	665±3	41	5.4175±0.0002
py + po	500±3	167	5.4175±0.0002
py + S	500±3	167	5.4178±0.0003
py + arg	500±3	167	5.4177±0.0002
po + S	500±3	167	5.4175±0.0001
py	500±3	167	5.4175±0.0001

Anisotropic pyrite is commonly observed in many natural specimens (Ramdohr, 1955) and many causes of the anisotropy have been postulated in the literature: a) internal strain, b) oriented inclusions, c) trace-element substitution, d) directional hardness as it may give rise to submicroscopic, oriented pits, scratches, etc. in polished section surfaces, and e) crystal-lattice distortion at the crystal surface, partly controlled by the orientation of the underlying lattice, as a result of polishing technique (Gibbons, 1967).

During an investigation of the equilibrium relations between pyrrhotite and pyrite, Arnold (1962) found that his synthetic pyrites were, in general, anisotropic. Stanton (1957) reports that pyrites are intrinsically anisotropic. Anisotropy in pyrite, with polarization colors from pink to light-grey, was encountered in the present investigation. Experiments conducted during the early part of this study commonly contained anisotropic pyrite, whereas later experiments to duplicate previous results failed to produce this feature of the pyrite. The pyrite starting material of the early experiments was finely ground and kept in a vial under atmospheric conditions until ready for use. In the later experiments, the pyrite was kept in sealed, evacuated pyrex tubes or in a vacuum desiccator (<10 mm Hg) until ready for use. Finely ground material has deliquescent properties and if allowed to set in air will pick up a certain amount of moisture. If this material is then used in an experiment, a small quantity of H_2O is introduced into the charge. It

is suggested that the anisotropism of the pyrite may have been caused by this presence of H_2O. This water present at the annealing temperature may have slightly, but not measurably, entered the pyrite structure and modified it to a non-cubic symmetry. Kullerud (personal communication, 1968) arrived at a similar conclusion concerning synthetic anisotropic pyrite.

Ag-Fe System

The phase relations in the Ag-Fe system based on data compiled by Hansen and Anderko (1958) and Elliot (1965) are shown in Figure 7. Tammann and Oelsen (1930) reported a solid solubility of Fe in Ag of less than 0.001 wt.% at 1000°C. Fink and deMarchi (1938) indicated a solubility of Ag in Fe of less than 0.13 at.% at 950°C.

Present Study.

In the present study it was determined that the presence of Fe does not measurably (i.e., ±3°C) lower the freezing point of Ag on the Ag-Fe join. Therefore, the Ag-Fe eutectic temperature is given as 958±3°C as compared with the melting point of 960.5°C for pure Ag. The liquid (i.e., the eutectic composition) at this temperature contains more than 99.5 at.% based on appearance of phase experiments listed in Table 4.

Table 4. Experiments conducted on the Ag-Fe join.

Reactants	Comp., at.%	Temp., °C	Time, min.	Products at Temp.
Ag - Fe	99.0-1.0	956±2	450	Fe + Ag + V
Ag - Fe	99.0-1.0	960±2	420	Fe + L_{Ag} + V
Ag - Fe	99.5-0.5	960±2	4560	Fe + L_{Ag} + V
Ag - Fe	95.0-5.0	955±3	20	Fe + Ag + V

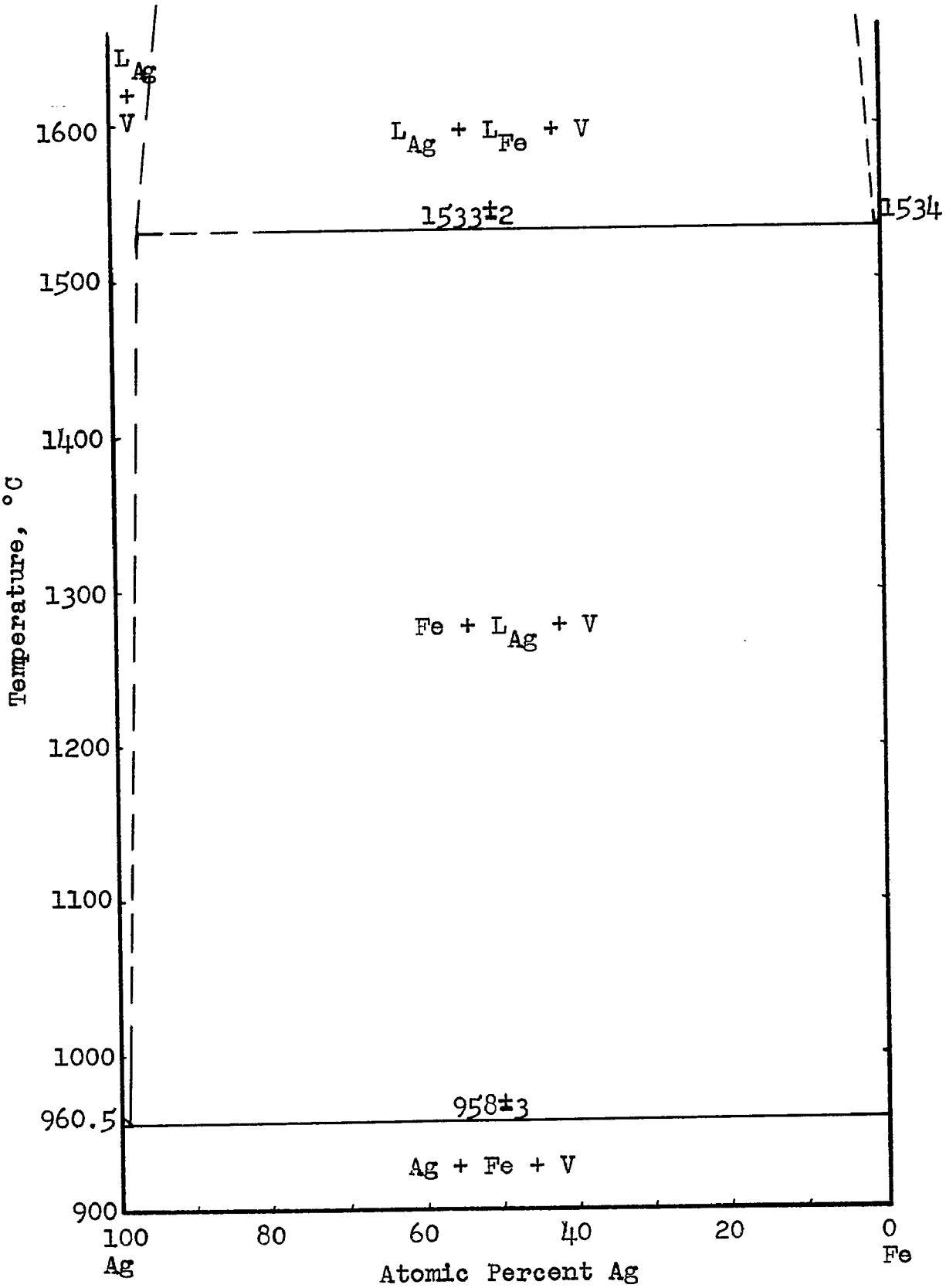

Figure 7. Condensed phase relations in the Ag-Fe system. This diagram is based on the compilations of Hansen and Anderko (1958) and Elliot (1965) and the experiments listed in Table 4.

THE TERNARY SYSTEM

Previous Data

The Ag-Fe-S system had received little attention prior to this study. Lüder (1924) confirmed the eutectic melting of Ag_2S and FeS at 610°C and 89 wt.% Ag_2S that had previously been reported by Friedrich (cited in Lüder). Lüder presented new cooling-curve data showing that a liquid-immiscibility field recedes from the Ag-Fe join into the ternary system with decreasing temperature and occupies a large region of the metal-rich portion of the system above 910°C. The only stable tielines observed during his study were those from Ag to FeS (reported stable above at least 910°C) and those from Ag_2S to FeS (stable below 610°C). These are shown in Figure 8.

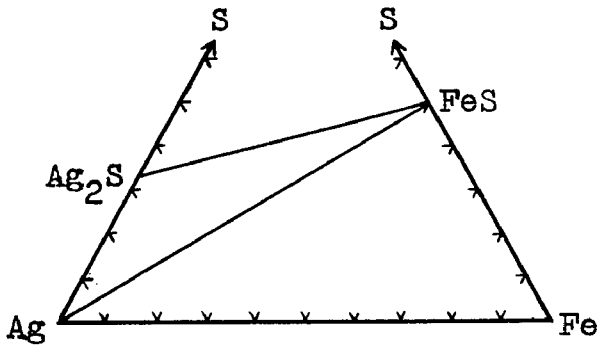

Figure 8. Schematic diagram showing tielines between Ag_2S and FeS (below 610°C) and between Ag and FeS (stable to above at least 910°C) as determined by Lüder (1924).

Results of This Study

Quenching experimentation in this study was initiated at high temperatures where reaction rates are rapid (hours) relative to those at low temperatures where many months may be required to attain equilibrium. Although of limited geologic significance, the high-temperature relations will be described in detail because they contribute to an understanding of the low-temperature relations and because they may have important metallurgical applications. The scheme of presentation is as follows: first the 1200°C isotherm is considered and next, the developments in relations with decreasing temperature are derived. Experimental data from this study are discussed in appropriate sections.

The 1200° Isotherm.

Qualitative data on the extent of liquid immiscibility at 1200°C (Figure 9) can be gained from consideration of the binary phase relations and the DTA data reported by Lüder (1924). Immiscible metal- and sulfur-rich liquids occur in the Ag-S system above 740±2°C (Kracek, 1946) and in the Fe-S system above 1083±3°C (Kullerud, 1961). A continuous two-liquid field has been shown in Figure 9 crossing the ternary system from the Ag-S join to the Fe-S join at 1200°C. Although no experiments were conducted on this liquid immiscibility in the present study, it is known that such relations occur in many other sulfide-type systems, e.g., Ag-Bi-S

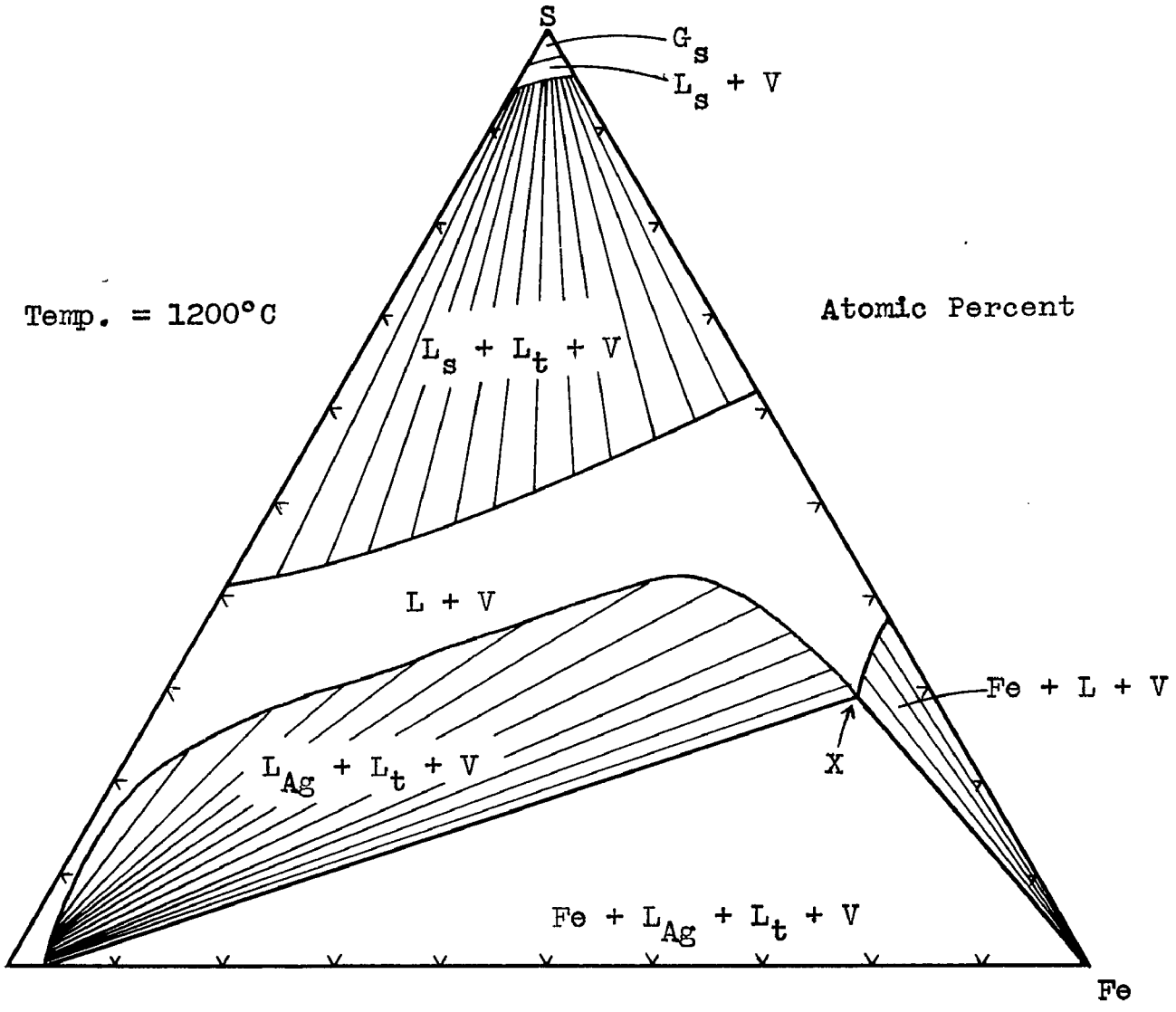

Figure 9. Schematic 1200°C isotherm of the Ag-Fe-S system. The presence of the $L_S + L_t + V$ field is based on hypothetical considerations (see text). The shape of the $L_{Ag\text{-rich}} + L_t + V$ field and the position of Point X are from Lüder (1924).

(Craig, 1965), Cu-Fe-S (Kullerud, 1964), Fe-Pb-S (Brett and Kullerud, 1967). The shape of the boundaries of this two-liquid field are shown as convex outward as based on the theoretical considerations of divariant field shapes discussed by Williamson and Morey (1918). Tielines in the metal-rich two-liquid field are drawn schematically, although some data on their relative orientations are reported by Lüder (1924). The critical point of sulfur is at 1040±5°C and 118 bars (Rassow, 1920), and therefore, a supercritical gas phase has been shown as the stable phase in the sulfur-corner of Figure 9. The addition of Ag and Fe to sulfur liquid will have a large effect on the critical points of ternary liquids because the critical points of Ag (>>1900°C) and Fe (>>3200°C) are so much higher in temperature than the critical point of sulfur. For this reason, a vapor phase (subcritical) has been shown in equilibrium with most of the ternary phase assemblages in Figure 9.

Initial modifications with decreasing temperature of the phase relations at 1200°C are caused by reactions occurring in the Fe-S system. The developments involved are shown in Figure 10 as depicted on a liquidus-surface diagram and accompanying isothermal sections. At 1192±2°C, pyrrhotite crystallizes from a homogeneous liquid on the Fe-S join (Point A of Figure 10) and the divariant field po + $L_{po\text{-}rich}$* + V

---

*Subscripts are used to differentiate liquids of various compositions, e. g., $L_{po\text{-}rich}$ refers to a pyrrhotite-rich liquid, L_t refers to a ternary liquid phase.

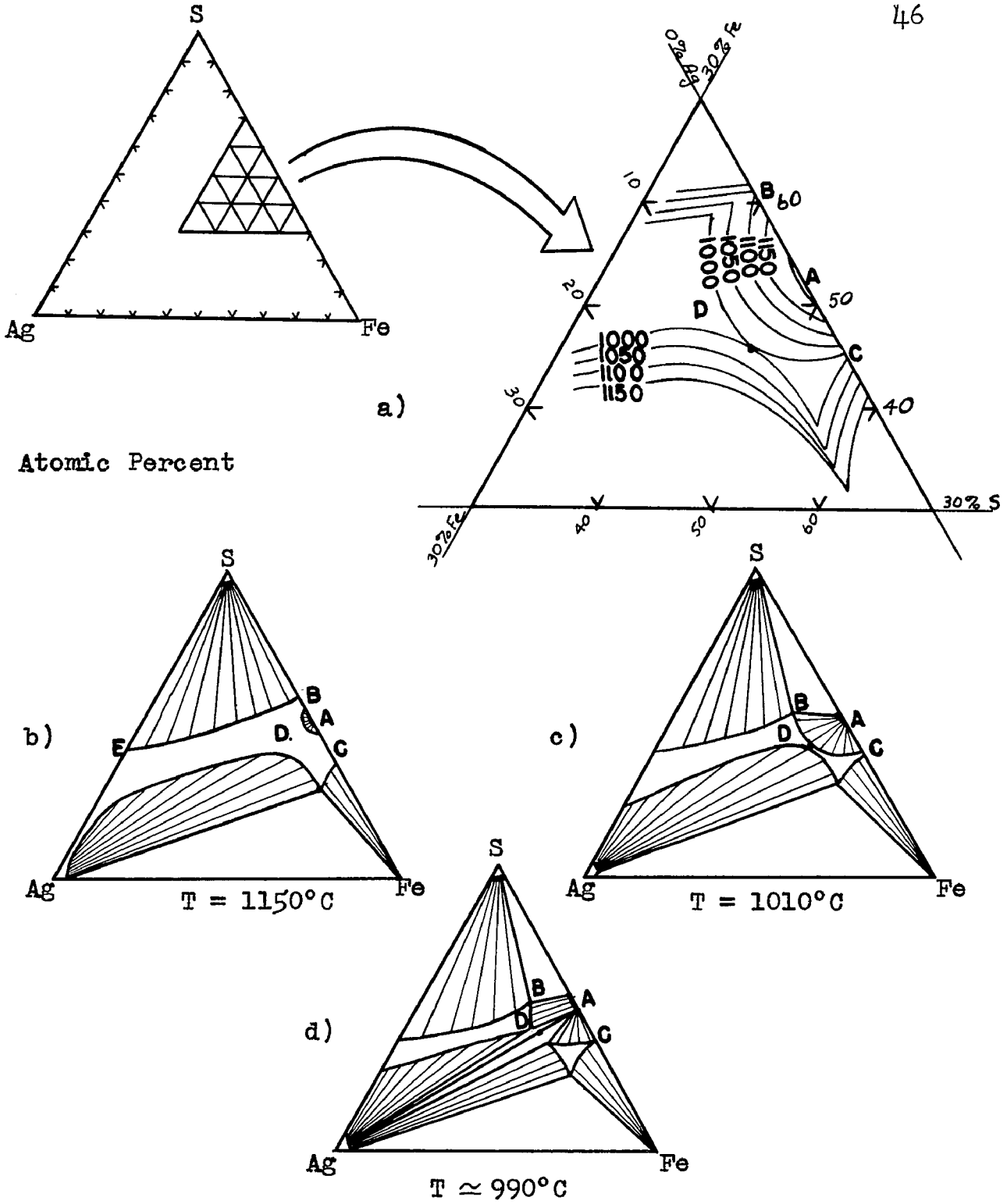

Figure 10. a) Schematic liquidus-surface diagram of a portion of the Ag-Fe-S system. The points designated by letters are explained in the text. b-d) Schematic isotherms of the Ag-Fe-S system at 1150°, 1010°, and 990°C.

expands into the ternary system. Immiscible liquids are absent below 1083±3°C on the Fe-S join, disappearing by crystallization of the pyrrhotite-rich liquid ($L_{po\text{-}rich}$) to pyrrhotite and sulfur-rich liquid (L_S) in the presence of vapor. The four phase assemblage po + $L_{po\text{-}rich}$ + L_S + V is invariant in the binary system but extends as a univariant assemblage from the invariant point to lower temperatures in the ternary system (since the addition of Ag as a third component adds a degree of freedom).

Figure 10 shows a schematic plot of liquidus relations resulting in the development of Point D. This point is a ternary singular point* and the reaction involved can be written $L_t \rightleftharpoons L_{Ag\text{-}rich}$ + po** in the presence of vapor. Two experiments (Table 5) were conducted at 990±10°C, one with a composition on the Ag-FeS join, and the other with a composition within the Ag + Fe + FeS field. These experiments show that at this temperature the join po + $L_{Ag\text{-}rich}$ is stable. The temperature of the singular reaction at Point D is 1004±3°C, as determined by quench-type and DTA experiments (listed in Table 5 and Appendix 1).

---

* Singular points are distinguished by singular, particular, or critical values of the Phase Rule variables P, T, and X but are not truly invariant in a ternary system. A detailed discussion of this concept is provided by Ricci (1951, p. 26).

** Throughout the text, all reactions are written with the high-temperature assemblage on the left-hand side of the equation.

Table 5. Experiments to determine the temperature of the singular reaction: $L_t \rightleftarrows L_{Ag\text{-}rich} + po$ in the presence of vapor.

Reactants	At.% Comp.	Temp., °C	Time, Min.	Products at Temp.
Fe-FeS + Ag	95-5	990±5	70	$L_{Ag\text{-}rich} + L_t + V$
FeS + Ag	80-20	990±5	70	$L_{Ag\text{-}rich} + po + V$
FeS + Ag	50-50	1065±5	10	$L_{Ag\text{-}rich} + L_{po} + V$
FeS + Ag	50-50	1040±5	10	$L_{Ag\text{-}rich} + L_{po} + V$
FeS + Ag	50-50	1010±5	10	$L_{Ag\text{-}rich} + L_{po} + V$
FeS + Ag	50-50	990±5	10	$L_{Ag\text{-}rich} + po + V$

Point C in Figure 10 represents the composition where Fe and FeS crystallize eutectically at 988±2°C. Below this temperature, the binary metal-rich liquid recedes into the ternary system generating the univariant field Fe + FeS + L_t + V. The ternary liquid field in this assemblage decreases in size with decreasing temperature (see Figure 11) and disappears through ternary monotectic crystallization, $L_t \rightleftarrows Fe + FeS + L_{Ag\text{-}rich}$, in the presence of vapor, which occurs at 965±3°C. DTA and quench-type experiments used to determine this temperature are described in Appendixes 1 and 4a.

Silver solidifies at 960.5°C and the eutectic on the Ag-Fe join at 958±3°C results in the withdrawal of the silver-rich liquid ($L_{Ag\text{-}rich}$) into the ternary system as shown in Figure 12. It is anticipated that the univariant field Ag + Fe + FeS + V probably develops with decreasing temperature by a singular reaction: $L_{Ag\text{-}rich} \rightleftarrows Ag + FeS$, in the

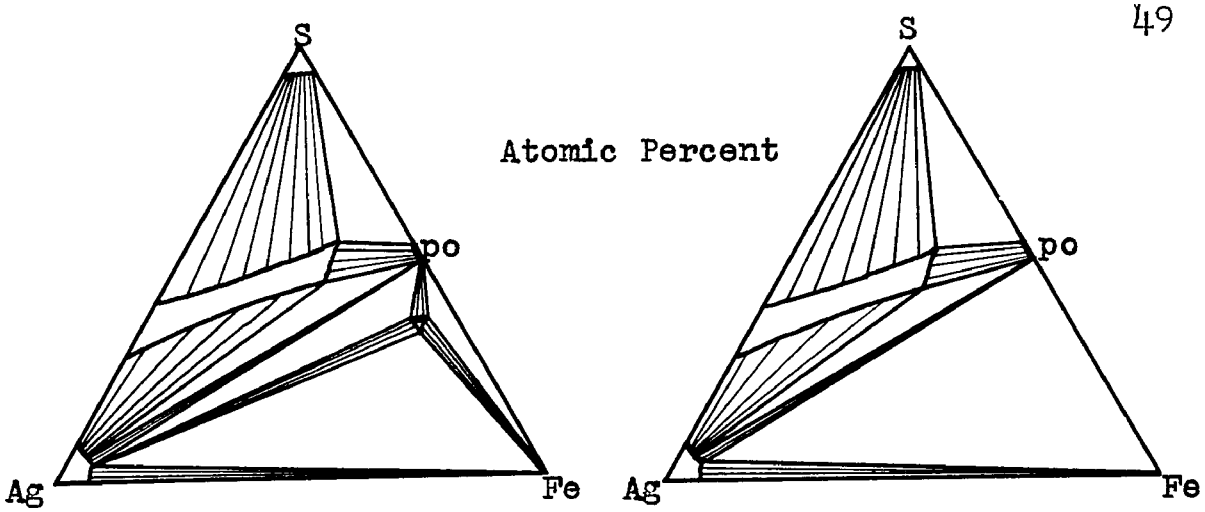

Figure 11. Schematic representation of the monotectic reaction: $L_t \rightleftarrows Fe + FeS + L_{Ag\text{-}rich}$, in the presence of vapor, at $965 \pm 3°C$.

presence of vapor, followed by ternary eutectic crystallization of Ag-rich liquid to Fe + Ag + FeS. These crystallization events are shown in a series of isotherms in Figure 12. Both reaction points must lie very near to pure Ag in composition. The temperature of the singular reaction of the Ag-FeS join was determined, both by DTA (Appendix 1) and quench-type experiments (Table 6), as $955 \pm 3°C$ and, although not investigated thoroughly, the ternary eutectic temperature is at most only a few degrees below 955°C.

Table 6. Experiments conducted on the upper stability of the Ag-FeS assemblage.

Reactants	Comp., at.%	Temp. °C	Time	Products at Temp.
Ag+FeS	26-74	960 ± 3	1h	po + $L_{Ag\text{-}rich}$ + V
Ag+FeS	26-74	956 ± 2	1h	po + $L_{Ag\text{-}rich}$ + V
Ag+FeS	26-74	952 ± 3	2h	po + Ag + V
Ag+FeS+Fe	80-10-10	957 ± 2	2h	Fe + FeS + $L_{Ag\text{-}rich}$ + V
Ag+FeS+Fe	80-10-10	948 ± 2	2h	Fe + FeS + Ag + V

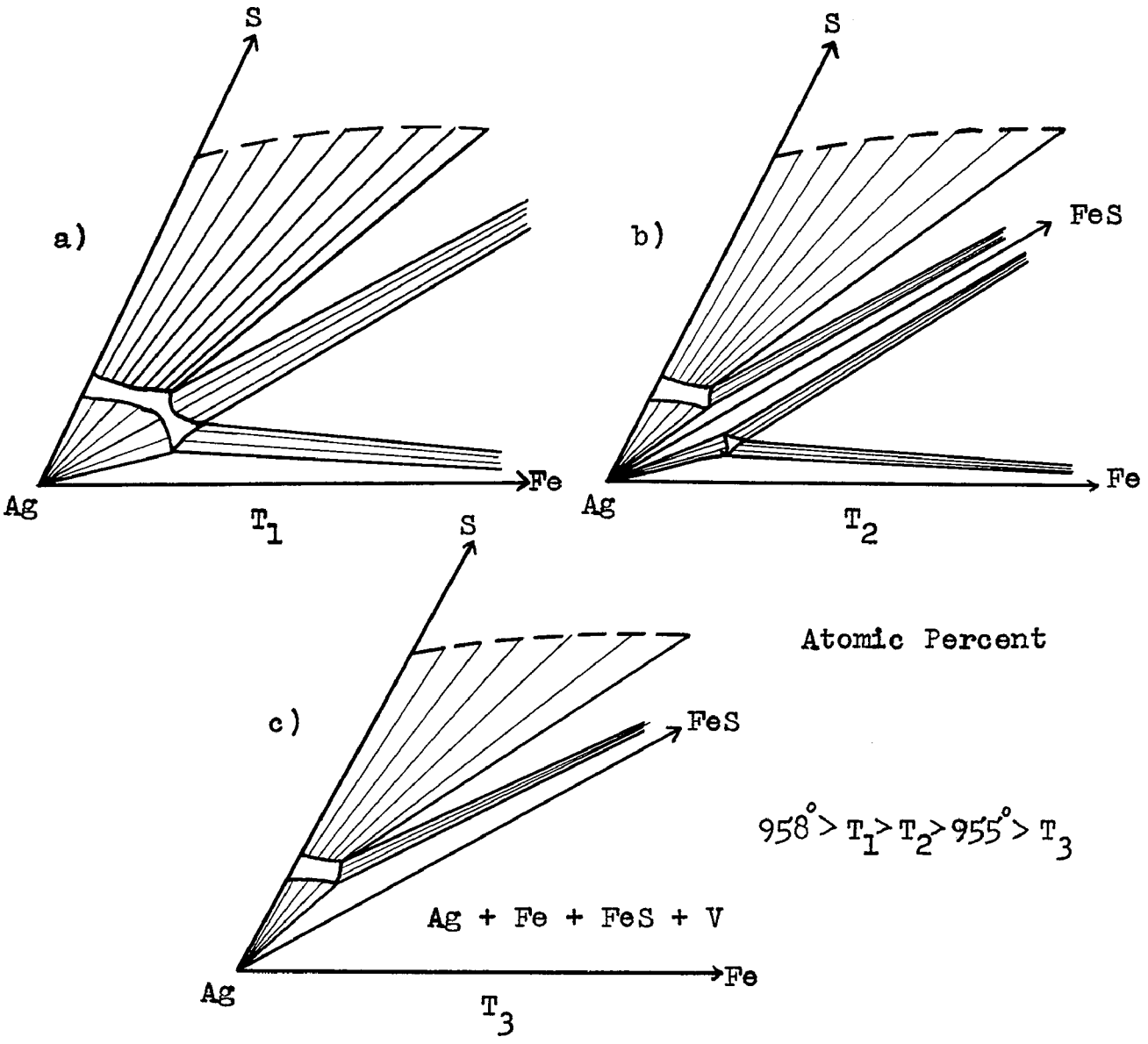

Figure 12. Schematic isotherms of a portion of the Ag-Fe-S system depicting developments involved in formation of the Ag + Fe + FeS + V field. Sections a, b, and c are at succeedingly lower temperatures designated as T_1, T_2, and T_3.

Development of the Ag + arg + po + V Field

With the establishment of Ag-FeS tielines, the metal-rich 2L + V assemblage is confined to the Ag-Ag_2S-FeS compositional field as shown in Figure 13a.

Several DTA experiments, listed in Table 7, were conducted during the investigation of the Ag + arg + po + V field. The thermal effects recorded at high temperatures depend upon the heating cycle (i.e., 1st or 2nd). During the 1st heating, Ag-rich liquid segregated to the bottom of the tube. Therefore, on the 2nd heating, the charge was not homogeneous and the different portions of the charge gave thermal effects which were not indicative of the total bulk composition. For this reason, only the data obtained during the 1st heating cycle pertains to the bulk composition of the experiments.

Table 7. DTA experiments to investigate the development of the Ag + arg + po + V field.

Composition, at.%			Thermal Effect, °C*		
Ag	Fe	S	heating	cooling	Interpretation
65.0	5.0	30.0**	519	518	Ag_2S - bcc ⇌ fcc
			623	619	Ag^2+ L_t ⇌ arg + po
			910	893***	see text
			520	518	
			622	619	
			905	898***	
55.0	15.0	30.0**	518	518	Ag_2S - bcc ⇌ fcc
			622	624	Ag^2+ L_t ⇌ arg + po
			935	---	see text
45.0	25.0	30.0**	no data	<800°C	
			942	---	$L_{Ag\text{-}rich}$ + po⇌Ag + L_t
			905	---	
			937	---	see text

*The thermal effect of quartz is omitted.
**Starting materials: Ag, Fe, and S.
***Supercooling of liquid.

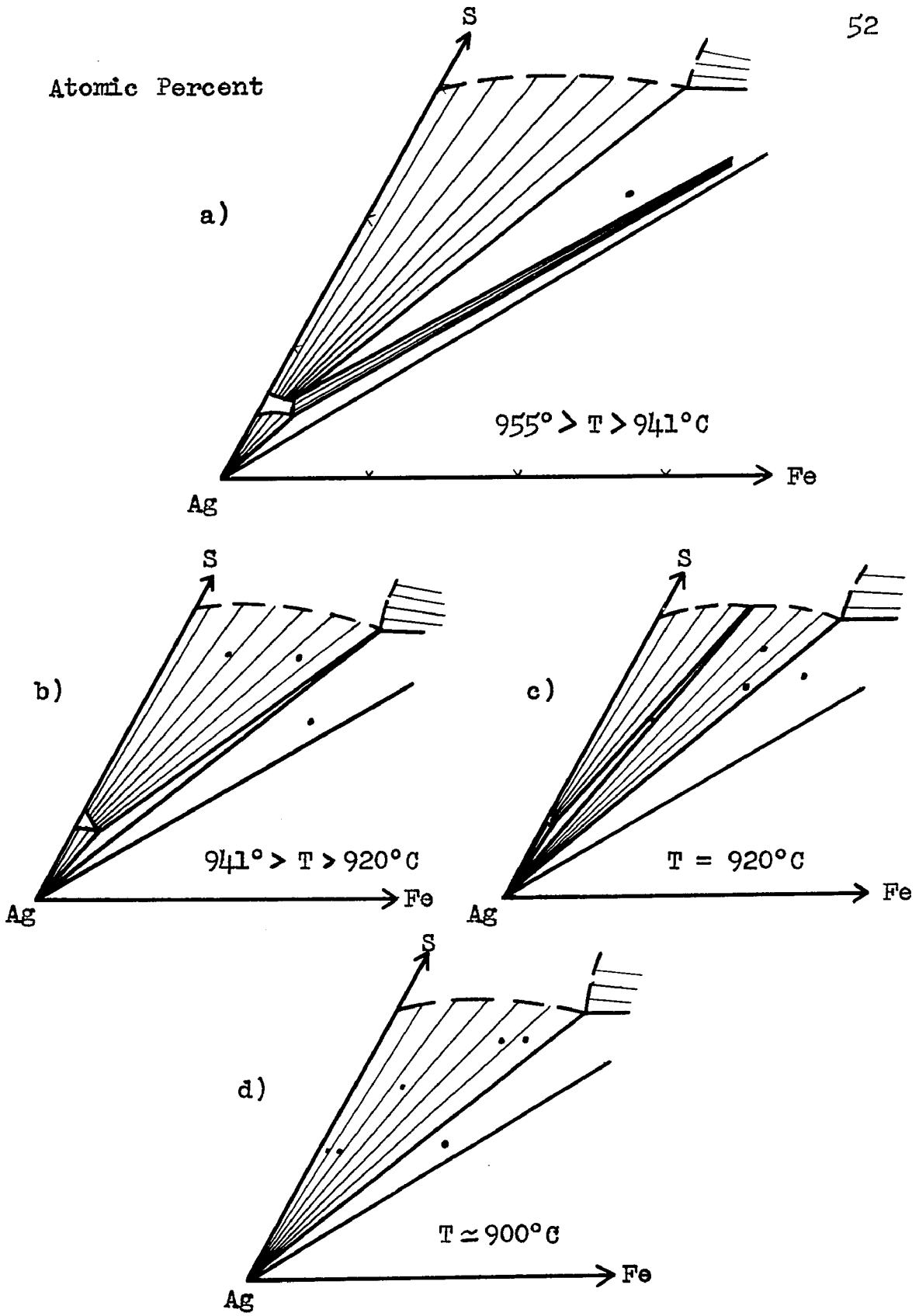

Figure 13. Schematic phase relations associated with development of the Ag + arg + po + V field. Points represent compositions of experiments listed in Table 8.

Quench-type experiments, listed in Table 8 were conducted to determine the nature of the reactions which were recorded in the DTA experiments. The thermal effect at 942°C was investigated by experiments conducted above and below this temperature. The results are interpreted as evidence for an invariant point, $L_{Ag\text{-}rich} + po \rightleftharpoons Ag + L_t$, in the presence of vapor, at 941±3°C as shown schematically in Figure 13a-b. In addition, the compositions of several experiments conducted at approximately 920°C (Table 9) are plotted in Figure 13c. At this temperature the tieline from Ag to ternary liquid of the Ag + L_t + po + V field passes through a point of approximately Ag_{50} Fe_{20} S_{30} at.% (see Figure 13c). Experiments, also listed in Table 8 and plotted in Figure 13d, demonstrate that this immiscible liquid field is not present in the system at 903±2°C.

Table 8. High-temperature experiments conducted in the $Ag\text{-}Ag_2S\text{-}FeS$ composition field.

Composition, at.%					
Ag	Fe	S	Temp., °C	Time	Products at Temp.
50.0	22.5	27.5	952±2	1h	$L_{Ag\text{-}rich}$ + L_t + po + V
50.0	22.5	27.5	948±2	18h	$L_{Ag\text{-}rich}$ + L_t + po + V
50.0	22.5	27.5	939±2	19h	Ag + L_t + po + V
50.0	22.5	27.5	938±2	1d18h	Ag + L_t + po + V
50.0	22.5	27.5	930±2	1h	Ag + L_t + po + V
55.0	15.0	30.0	918±2	1h	Ag + L_t + V
60.0	15.0	25.0	920±2	1h10m	Ag + L_t + V
50.0	22.5	27.5	921±2	3d3h	Ag + L_t + po + V
70.0	5.0	25.0	920±2	7h10m	Ag + L_t + $L_{Ag\text{-}rich}$ + V
79.0	1.0	20.0	903±2	1h	Ag + L_t + V
78.0	2.0	20.0	903±1	1h	Ag + L_t + V
70.0	5.0	25.0	903±1	1h10m	Ag + L_t + V
57.0	13.0	30.0	903±2	1h	Ag + L_t + V
53.0	17.0	30.0	903±2	1h	Ag + L_t + V
65.0	15.0	20.0	900±5	1h	Ag + L_t + po + V

The sequence of events shown in Figure 13 is: a ternary reaction, po + $L_{Ag\text{-}rich} \rightleftarrows Ag + L_t$, in the presence of vapor, with the formation of $Ag + L_{Ag\text{-}rich} + L_t + V$ field, subsequent change in composition of the ternary liquid of this assemblage with the resultant expansion of the $Ag + L_t + V$ field, and the disappearance of the 2L + V field at 906±2°C on the $Ag\text{-}Ag_2S$ join.

The 935°C thermal effect on heating (Table 7) is explained as due to passage of the charge from the $Ag + L_t + V$ to the $Ag + L_t + L_{Ag\text{-}rich} + V$ field. The 910°C effect represents the same development at a composition closer to the $Ag\text{-}Ag_2S$ join. No unexplained thermal effects below 906±2°C were detected in the DTA experiments. The Ag-rich liquid withdraws to the $Ag\text{-}Ag_2S$ join and is last present at the binary monotectic temperature of 906±2°C. This development is apparently unusual for sulfide systems; however, a similar feature occurs in the Fe-Ni-S system (Kullerud, 1963a).

Below 906±2°C, the phase relations in the $Ag\text{-}Ag_2S\text{-}Fe_{1-x}S$ portion of the system remain unchanged to 838±2°C, except for a small composition change of the ternary liquid of the $Ag + L_t + V$ field toward the Ag-S join. The phase argentite (Ag_2S*) crystallizes from a homogeneous liquid in

*It is realized that this phase should be labeled $Ag_{2\pm x}S$ because of the solid solution field of Ag_2S. However, for brevity, $Ag_{2\pm x}S$ in synthetic phase assemblages will be written as arg or Ag_2S.

the Ag-S system at 838±2°C (Kracek, 1946), and the divariant field, arg + L_t + V, forms. Below the binary eutectic temperature of 804±2°C, liquid is not present on the Ag-Ag_2S join but has receded into the ternary system with the resultant formation of the Ag + arg + L_t + V field. These developments are illustrated by the liquidus-surface diagram and the schematic isotherms of Figure 15. The ternary liquids of the univariant fields flanking the Ag + L_t + V divariant field change composition, with decreasing temperature, as schematically shown in Figure 14.

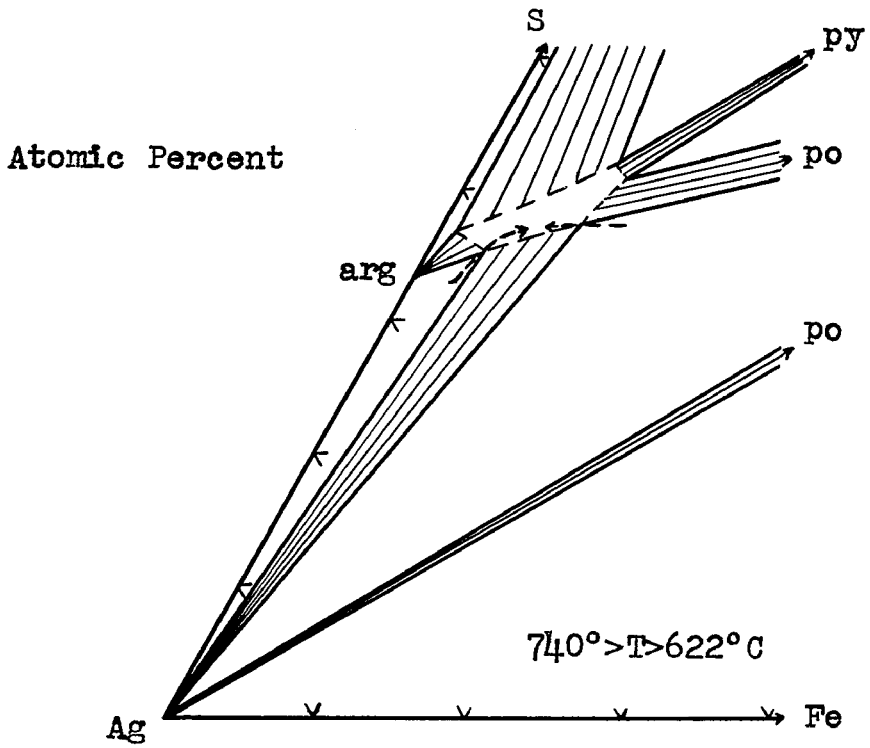

Figure 14. Schematic diagram depicting the composition change of the ternary liquids associated with the univariant fields flanking the Ag + L_t + V field.

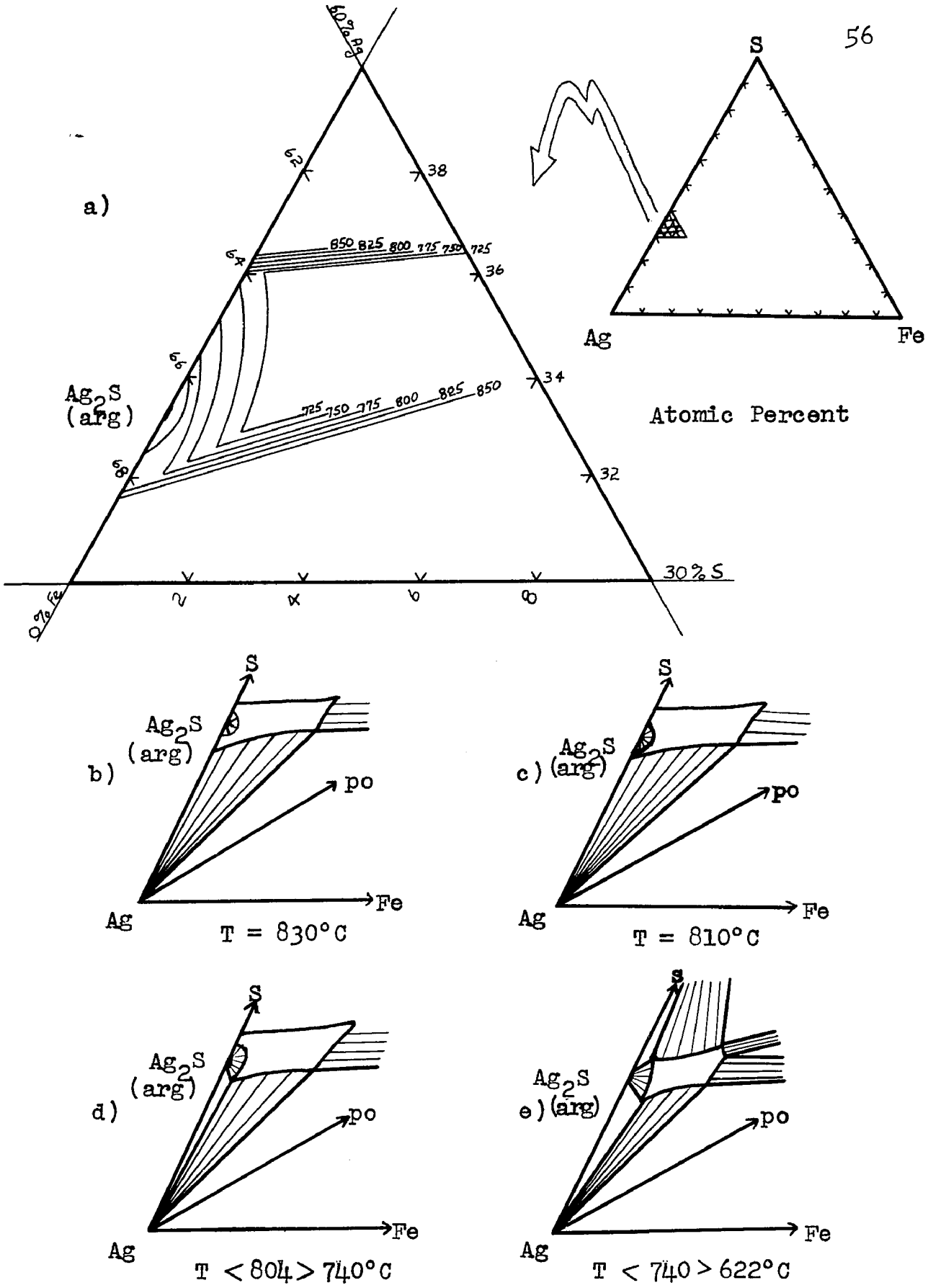

Figure 15. Schematic liquidus-surface diagram and selected isothermal sections of a portion of the Ag-Fe-S system.

Table 9 lists the experiments which were conducted to determine the temperature and nature of the reaction associated with the development of the Ag + arg + po + V assemblage. Preliminary to these experiments, the charges were melted in the flame of an oxygen-natural gas torch. After such melting, the tubes were opened and the charges were broken into small fragments which were used as reactants in quench-type experiments. The temperature of the experiments was raised in intervals and signs of insipient melting, as indicated by welding of the chips, were looked for. The temperature of appearance of liquid within the Ag + arg + po + V field was determined in this way as 622±2°C.

Table 9. Experiments on the invariant reaction at 622±2°C.

Composition, at.% Ag	Fe	S	Temp., °C	Time	Products at Temp.
53.0	10.3	36.7	600±2	1/2h	No liquid
			610±2	1/2h	No liquid
			615±2	1/2h	No liquid
			620±2	1/2h	No liquid
			625±2	1/2h	Liquid- Ag + po + L_t + V
53.0	10.3	36.7	630±2	2d22h	Ag + po + L_t + V
53.0	10.3	36.7	626±2	12h	Ag + po + L_t + V
54.1	9.4	36.5	625±2	1/2h	Liquid
54.1	9.4	36.5	620±2	1h	No liquid
70.0	5.0	25.0	620±2	5d	No liquid
70.0	5.0	25.0	625±2	1h	Liquid
61.0	4.0	35.0	626±2	16d	Ag + arg + L_t + V
po = 48.4 at.% Fe					
42.5	17.5	40.0	626±2	6d	Ag + po + L_t + V
po = 48.0 at.% Fe					
42.5	17.5	40.0	628±2	16d1h	Ag + po + L_t + V
po = 47.5 at.% Fe*					
42.5	17.5	40.0	628±2	5d1h	L_t + po + V
po = 47.0 at.% Fe*					

*Starting materials are Ag_2S and $Fe_{1-x}S$ with an approximate bulk composition as indicated.

Development of the Ag + arg + po + V field was found to involve a ternary invariant point: Ag + $L_t \rightleftharpoons$ arg + po, in the presence of vapor, as shown in Figure 16. The pyrrhotite composition in this univariant field slightly below 622±2°C is 48.6±0.1 at.% Fe (see pages 104-108). The ternary liquid involved in this reaction must lie on the sulfur-rich side of the arg-po join for this reaction to be valid. Experiments listed in Table 9 demonstrate this statement. In order to completely rule out the possibility of a ternary eutectic associated with the formation of the Ag + arg + po + V field, several DTA experiments (Table 10) were performed. These experiments show a decrease in stability of the arg-po join as the charges become more sulfur rich (Fe content of the pyrrhotite decreases from 48.6 at.%) and, thereby, demonstrate that argentite can coexist with pyrrhotite at 622±2°C only when the pyrrhotite contains 48.6 at.% Fe. Below this temperature liquid is absent on the metal-rich side of the arg-po join.

Table 10. DTA experiments on arg-po assemblages.

Composition, at.%			Thermal Effect, °C*		
Ag	Fe	S	heating	cooling	Interpretation
50	12	38**	518	517	Ag_2S - bcc $\rightleftharpoons$ fcc
po = 49.0 at.% Fe			623	620	$Ag_2S + L_t \rightleftharpoons$ arg + po
50	12	38**	517	516	Ag_2S - bcc $\rightleftharpoons$ fcc
po = 48.4 at.% Fe			618	624	liquid
50	12	38**	514	512	Ag_2S - bcc $\rightleftharpoons$ fcc
po = 48.0 at.% Fe			607	621	liquid
50	12	38**	506	504	Ag_2S - bcc $\rightleftharpoons$ fcc
po = 47.5 at.% Fe			595	614	liquid

* The thermal effect of quartz is omitted.

**Starting materials: $Ag_2S + Fe_{1-x}S$.

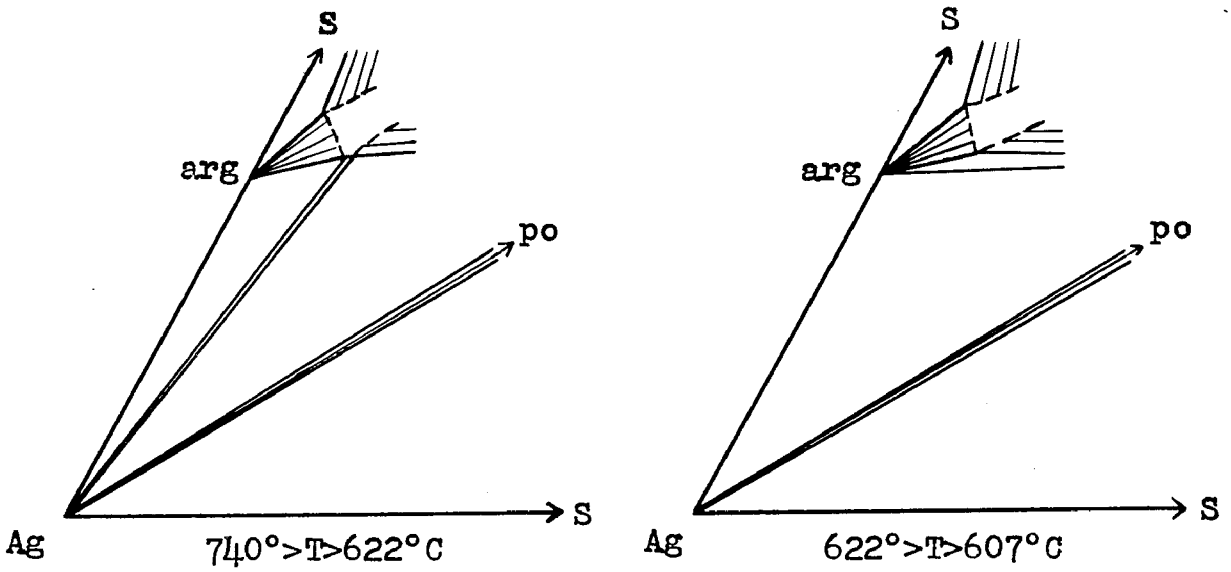

Figure 16. Schematic diagrams illustrating the invariant reaction at 622±2°C associated with the development of the Ag + arg + po + V field.

Ag_2S - FeS Join

The Ag_2S-FeS join was investigated because of the reported eutectic between these two compounds at 610°C and 74.2 mol.% Ag_2S (Friedrich, 1909 in Lüder, 1924). The existence of this eutectic was not confirmed in this study, nor does Ag_2S ever exist stably with stoichiometric FeS. Figure 17 shows the phase relations between Ag_2S and FeS and Appendix 2 lists the pertinent experiments along this "cut". The reported thermal effect at 610°C would appear to be due to the development of a Ag + L_t + V tieline across a line joining Ag_2S to FeS at 622±2°C and 87±2 mol.% Ag_2S (Point X in Figure 17). Possibly, the discrepancy between these two temperatures is due to the supercooling of the metallic liquids as commonly observed in DTA experimentation.

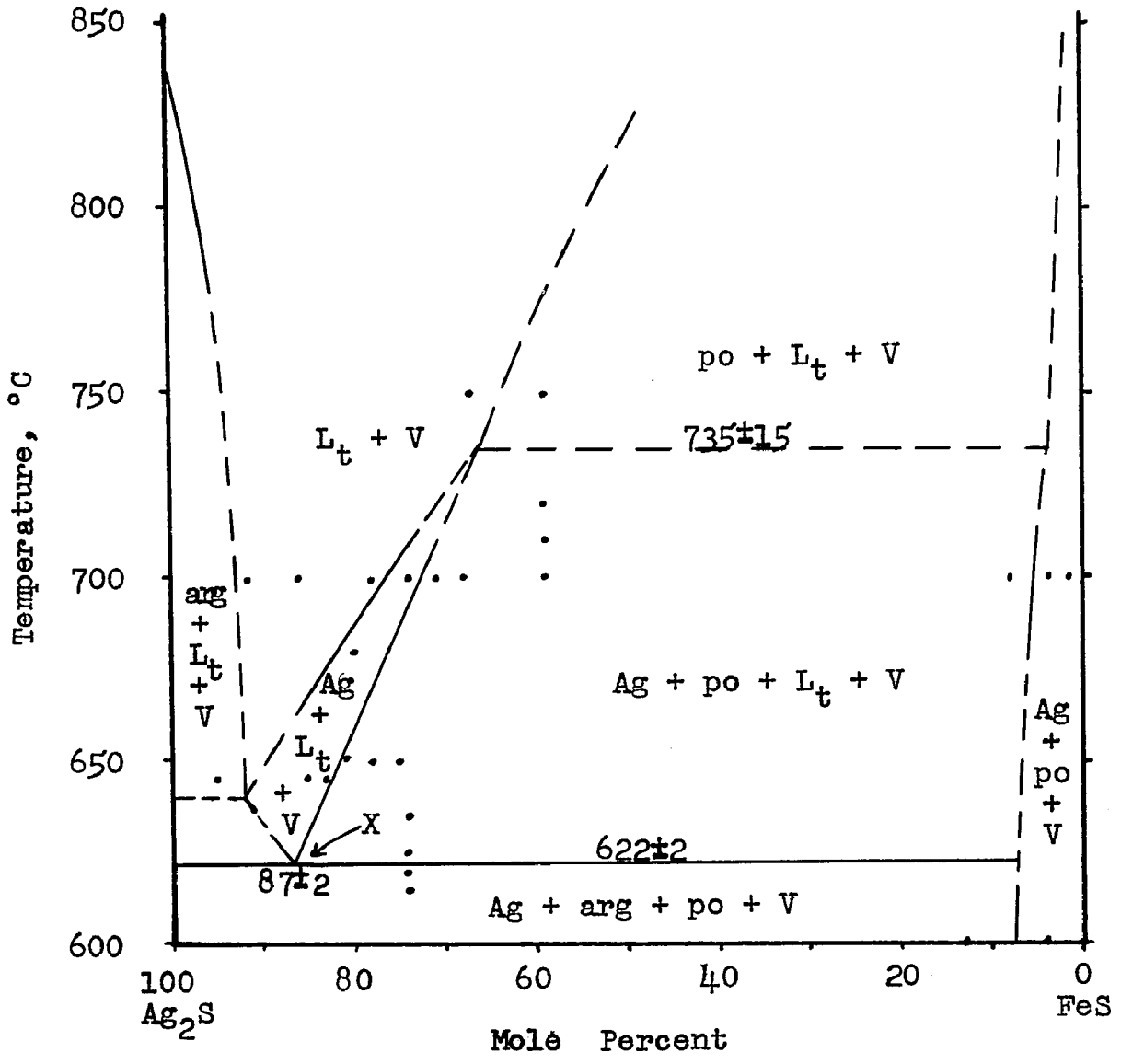

Figure 17. Condensed phase relations on the Ag_2S-FeS join. Points represent compositions of experiments listed in Appendix 2.

Development of the arg + py + L_S + V Field

As the po + L_S + L_t + V field expands into the ternary system with decreasing temperature, the composition of the metal-rich liquid (L_t; Point B of Figure 10c, page 46) follows an approximate straight-line path connecting the monotectic compositions on the FeS and Ag_2S joins (Points B and E of Figure 10b, respectively). This conclusion is based on experiments conducted at 800° and 700°C (Appendix 4 and 3).

Pyrite, FeS_2, is a stable phase in the Fe-S system below its incongruent melting temperature of 743±2°C (Kullerud and Yoder, 1959). Experiments listed in Table 11 demonstrate that tielines from pyrite to a ternary liquid phase become stable at about the same temperature (742±3°C). This development is shown schematically in Figure 18.

Table 11. Pyrite stability in the Fe-S and Ag-Fe-S systems.

Reactants	Comp., at.%	Temp., °C	Time, hrs.	Products at Temp.
FeS_2	100	740±3	121	py + V
FeS_2 + Ag_2S	89-21	740±3	121	py + L_S + L_t + V
FeS_2	100	745±2	51	po + L_S + V
FeS_2 + Ag_2S	89-21	745±2	51	po + L_S + L_t + V

The L_S + L_t + V field is unstable between argentite and sulfur below 740±2°C; below this temperature, an Ag_2S-rich liquid withdraws into ternary space and the arg + L_S + L_t + V field (Figure 15, a and e) is stable in the ternary system. With decreasing temperature, this field does not rapidly

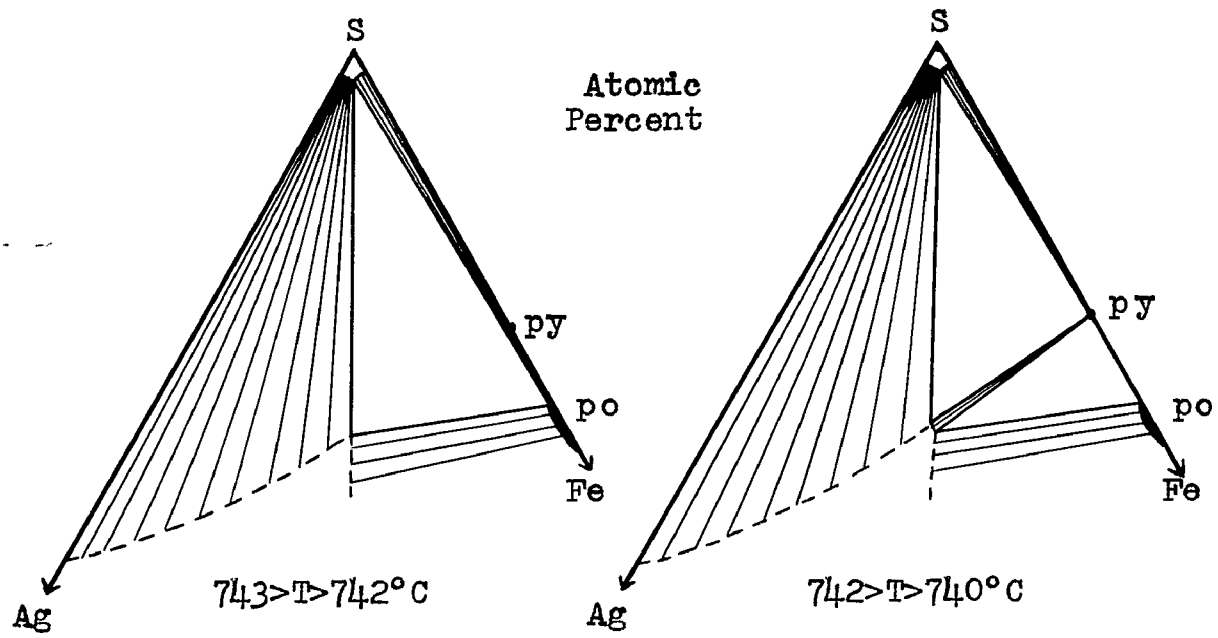

Figure 18. Schematic phase relations associated with the ternary reaction po + L_S ⇄ py + L_t, in the presence of vapor, at 742±3°C.

increase in size, extending less than 2 at.% Fe into the ternary system at 700°C (see page 66).

The composition of the ternary liquid of the py + 2L + V field lies on the metal-rich side of the arg-py (Ag_2S-FeS_2) join, whereas, the ternary liquid of the arg + 2L + V field lies on the sulfur-rich side (see Figure 20, page 66). With decreasing temperature, this latter ternary liquid composition crosses the arg-py join (Figure 19), the 2L + V field continually narrows and a ternary reaction: L_S + L_t ⇄ arg + py, in the presence of vapor, results in the formation of the arg-py join at 607±2°C.

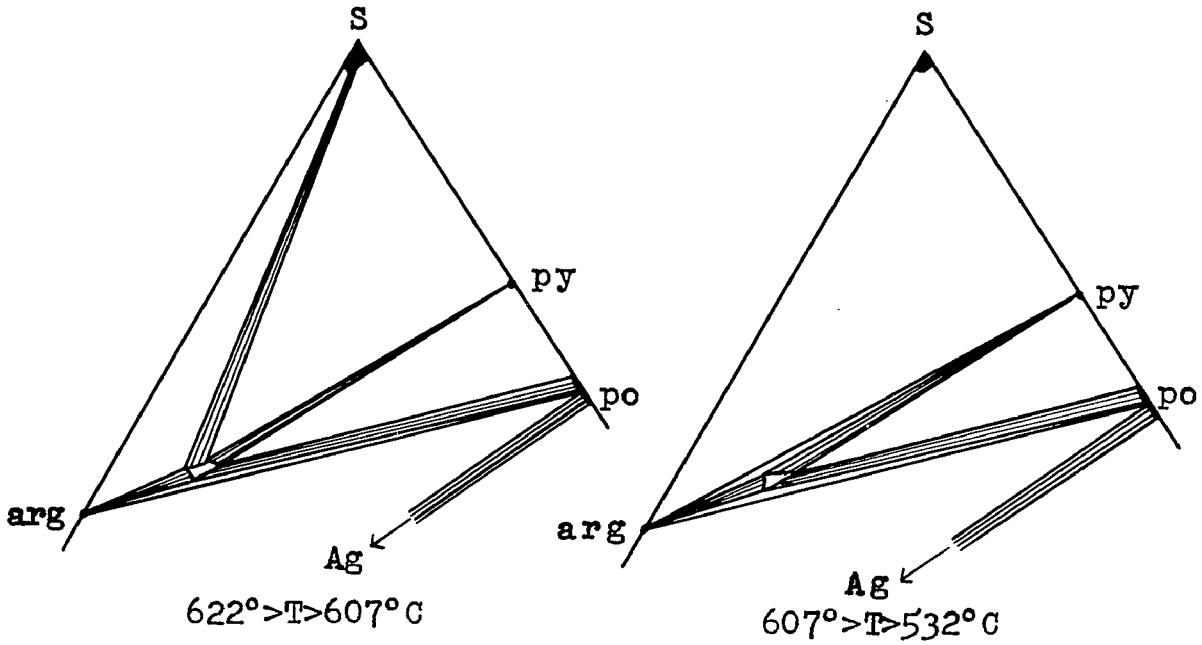

Figure 19. Schematic phase relations associated with the development of the arg + py + V assemblage at 607±2°C.

Experiments conducted in the investigation of the arg + py + L_S + V field (Table 12) above the invariant temperature, 607±2°C, contain a liquid phase (L_t) which, during rapid cooling, crystallizes to dendrites of arg + py + a maroon-colored interstitial "phase"*. If the experiment is allowed to cool in air, reaching 25°C in about 8-10 minutes, the maroon "phase" is completely absent, having recrystallized to arg + py + po. Also, the amount of sulfur-rich liquid present in the slowly-cooled experiment is approximately 1/3 that of the rapidly-cooled one. The observation suggests a

*"Phase" is used in this context to mean a homogeneous-appearing product which may not be a phase in the true sense.

reaction: $L_t + L_S \rightleftarrows$ arg + py which, upon cooling of the charge, uses up L_S. Such a reaction is valid if the ternary liquid has a composition in the arg-py-po field. Indexed X-ray powder-diffraction tracings of charges containing the maroon phase show no unidentified reflections, further supporting the conclusion that the maroon-colored product is not a distinct phase in the Ag-Fe-S system. It may be a metastable phase or a "quench" product consisting of a fine-grained intergrowth of the binary compounds.

Table 12. Experiments conducted on the reaction $L_S + L_t \rightleftarrows$ arg + py, in the presence of vapor, at 607±2°C.

Composition, mol.%			Temp., °C	Time	Products at Temp.
Ag_2S	FeS_2				
79	21		618±2	6d	py + L_S + L_t + V
82	18		612±2	2d	L_S + L_t + py(?) + V
82	18		610±2	9h	L_S + L_t + py(?) + V
82	18		606±2	2d	arg + py + V
86	14		602±2	11d	arg + py + V
60	40		596±2	3d	arg + py + V
Ag	Fe	S*			
57	3	40	618±2	4d	arg + L_S + L_t + V
40	10	50	615±2	3d	py + L_S + L_t + V
40	2	58	611±2	2d	arg + L_S + L_t + V
40	2	58	609±2	4d	arg + L_S + L_t + V
40	2	58	605±2	2d	arg + py + L_S + V
40	10	50	596±2	3d	arg + py + L_S + V

*Starting materials were Ag_2S, FeS_2, and S.

The 700°C Isotherm

The phase relations in the Ag-Fe-S system at 700°C are shown in Figure 20 as based on the results of experiments listed in Appendix 3. This isotherm is introduced at this point to illustrate the mutual relationships of the various univariant fields just discussed. It also emphasizes the position of the homogeneous L + V field in the region near Ag_2S composition at this temperature.

Development of the arg + py + po + V Field

With the establishment of arg-po and arg-py tielines at 622± and 607±2°C, respectively, the L_t + V field is restricted to the arg-py-po composition field as shown in Figure 21a. It persists to 532±2°C where it is involved in a ternary eutectic crystallization as schematically shown in Figure 21 a and b. This eutectic temperature was determined as 532±2°C by quench-type (Table 13) and DTA (Appendix 1) experiments. The eutectic composition is $Ag_{56}\ Fe_7\ S_{37}$ within ±2 at.%.

Table 13. Experiments to determine the temperature of the eutectic reaction, $L_t \rightleftharpoons$ arg + py + po, in the presence of vapor.

Composition, at.%			Temp., °C	Time	Products at Temp.
Ag	Fe	S			
40	16	44*	525±1	1h	No Melt
			530±1	1h	No Melt
			535±1	1h	Possible Melt
			540±1	1h	Melt
40	16	44	541±2	12d	py + po + L_t + V
52	9	39	535±2	17d	py + po + L_t + V
40	16	44	530±2	31d	arg + py + po + V

*Charge consisted of pieces of previously melted reactants.

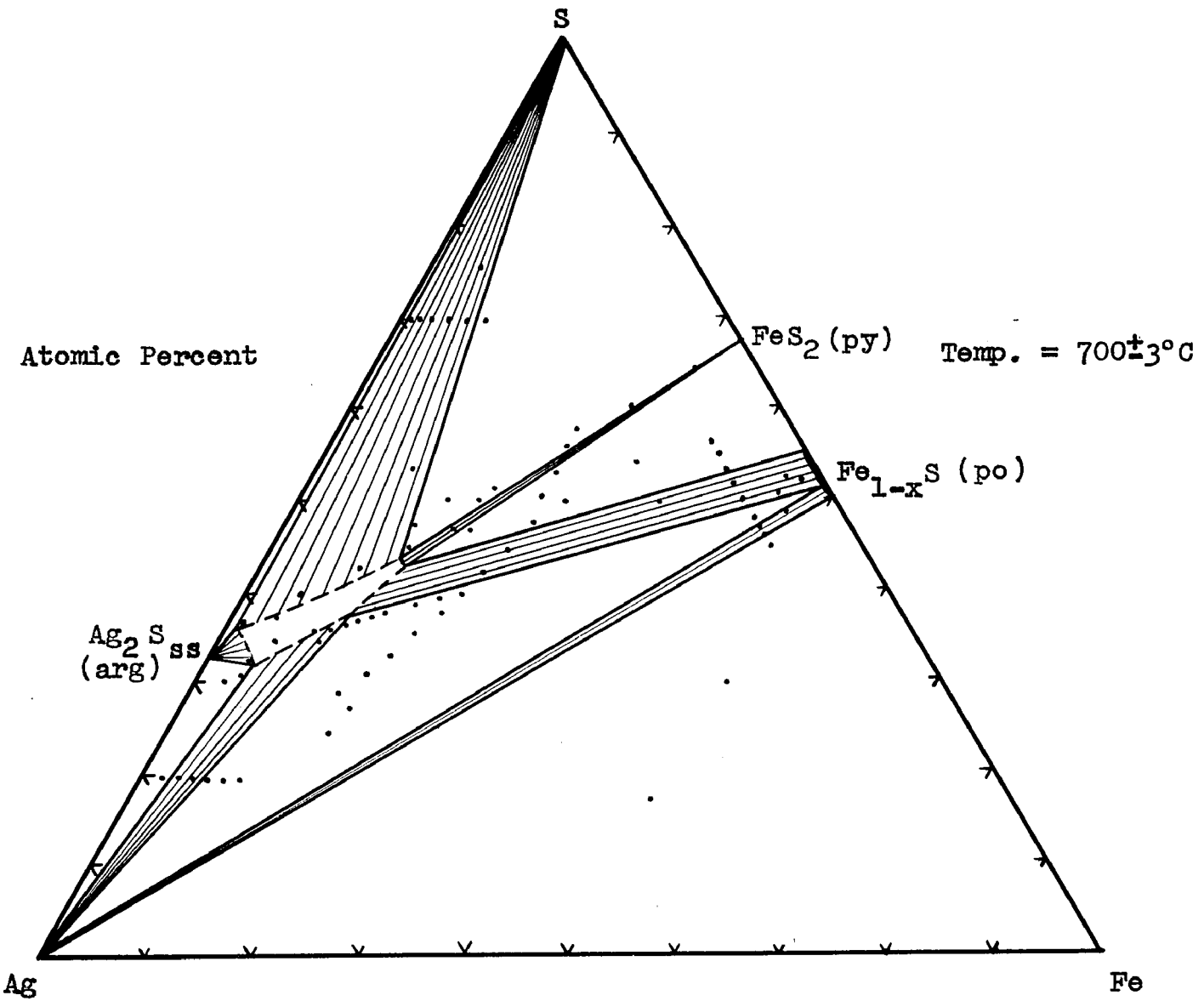

Figure 20. Condensed phase relations in the system Ag-Fe-S at 700°C. The points represent the compositions of experiments listed in Appendix 3.

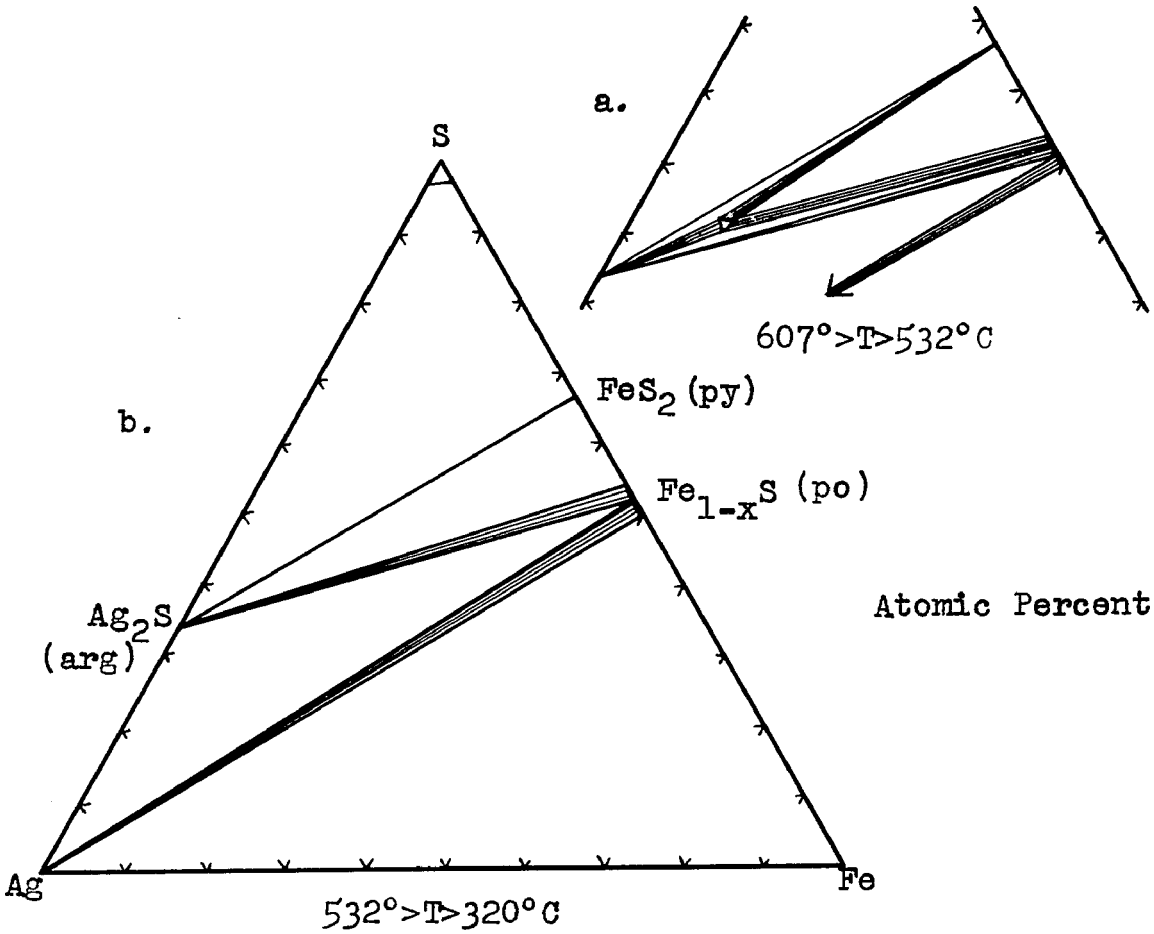

Figure 21. Schematic diagram of the eutectic reaction at 532±2°C and the subsolidus phase relations from 532° to 320°C in the Ag-Fe-S system.

The liquid present in experiments conducted at temperatures above 532°C, upon rapid chilling, crystallizes to an intimate intergrowth of pyrrhotite and pyrite in a groundmass of argentite (see Plate 4, page 151). This eutectic texture consists of alternating zones of argentite and pyrrhotite-pyrite and closely resembles a fingerprint. Slower cooling in air, reaching 25°C in about 8-10 minutes, almost completely erases this texture as a result of the coalescence of pyrrhotite and pyrite into rounded blebs. Similar textures have been described from the Fe-Pb-S system (Hewitt, 1938; Brett and Kullerud, 1967).

The phase relations in the Ag-Fe-S system remain essentially unchanged from 532° to approximately 320°C. The only changes, discussed on pages 72-78, are: 1) the compositional variations of pyrrhotite in the two ternary univariant fields, and 2) the fcc ⇌ bcc inversion in argentite.

Summary of Liquidus Relations

Below the ternary eutectic at 532±2°C, sulfur-rich liquid, L_S, is the only liquid remaining in the system. This liquid is present to a temperature slightly below 114°C, the melting point of pure sulfur. The low solubility of Ag and Fe in sulfur-rich liquid known from binary data suggests that the composition of this liquid is >99 at.% sulfur within this temperature range.

Figure 22 is a polythermal projection with cotectic crystallization paths depicting the course of events accompanying the cooling of the various liquids in the system. This diagram represents a convenient summation of the equilibrium events previously discussed.

Ternary Solid Solutions of Binary Phases

The binary phases in the Ag-Fe-S system do not extend appreciably into the ternary system, as shown by quench-type experiments listed in Table 14. The amounts of charges used in most of the experiments was 100-200 mg. The uncertainty in weighing of 0.1 wt.% of an element in 100 mg. of a compound is ≤±.1 wt.%. Therefore, although a solid solution would appear to be less than the at.% of the third element

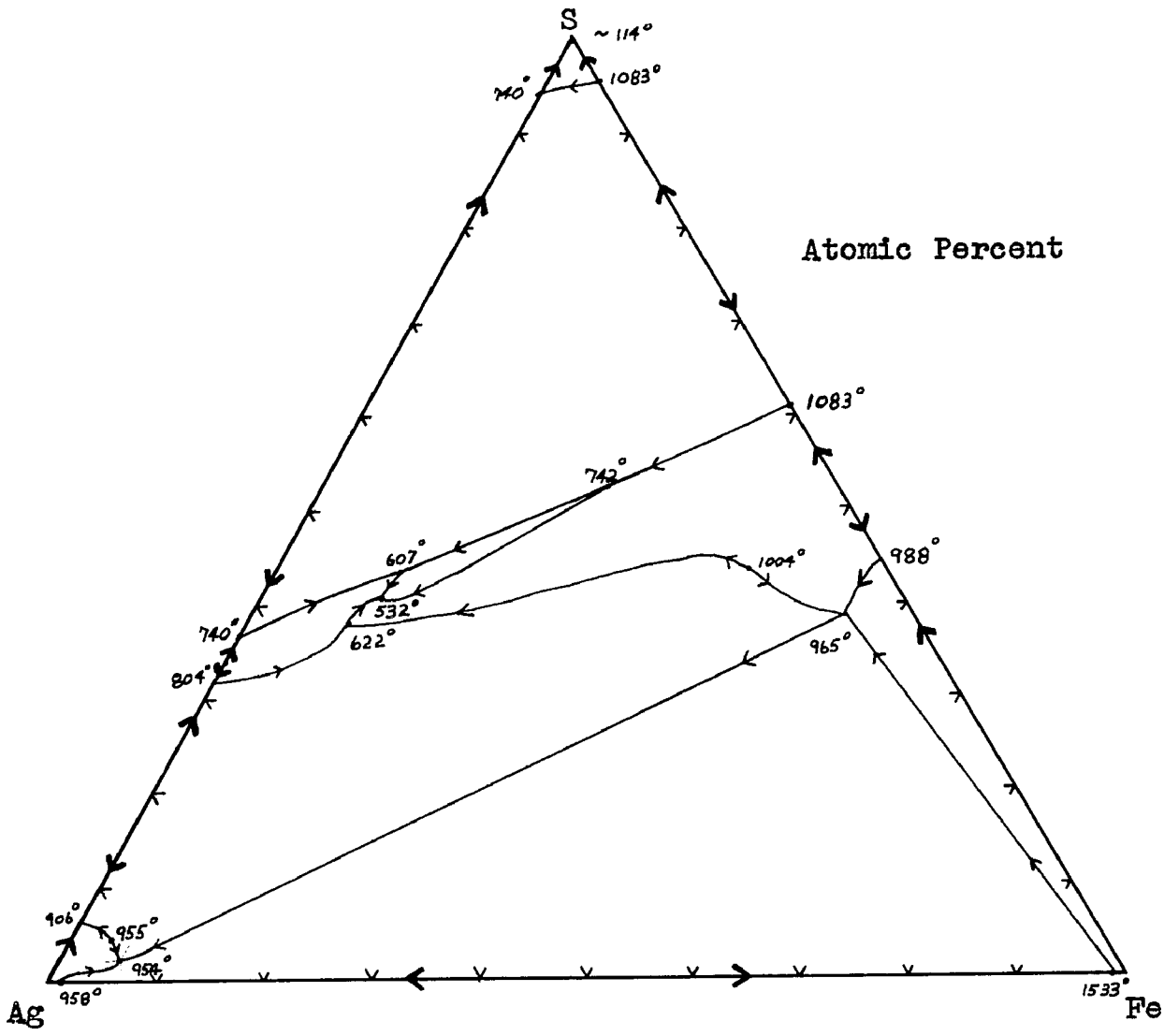

Figure 22. Polythermal liquidus diagram of the Ag-Fe-S system depicting cotectic crystallization paths.

Table 14. Experiments conducted on the ternary solid solution of binary phases.

a. Experiments conducted on the Ag solubility in pyrrhotite.

po Comp., at.% Fe	At.% Ag added	Temp., °C	Time	Product at Temp.
46.00	0.34	600±3*	58d	po + L_t + py(?) + V
46.00	0.26	600±3*	58d	po + L_t + V
46.1	0.10	600±3**	38d	po + L_t(?) + V
46.86	0.43	600±3*	58d	po + L_t + V
46.86	0.26	600±3*	58d	po + L_t + V
47.00	0.10	600±3**	38d	po + L_t + V
47.85	0.43	600±3*	58d	po + L_t + V
47.85	0.26	600±3*	58d	po + L_t + V
48.05	0.10	600±3**	38d	po + L_t(?) + V
49.75	0.25	600±3*	58d	po + Ag + V
49.75	0.10	600±3**	38d	po + Ag + V

* 18 hrs. at 970°C prior to anneal at 600°C + regrind at 30d.

**16 hrs. at 990°C prior to anneal at 600°C + regrind at 20d.

b. Experiments conducted on the Ag solubility in pyrite.

Comp., at.%		Temp., °C	Time	Products at Temp.
Ag_2S	FeS_2			
0.30	99.70	600±3	74d	py + arg + V
0.15	99.85	600±3	74d	py + arg + V
0.30	99.70	500±5	167d	py + arg + V

c. Experiments conducted on the Fe solubility in argentite.

Comp., at.%			Reactants	Temp., °C	Time	Products at Temp.
65.0	1.0	34.0	(1)	701±2	6d	arg + L + V
99.0	1.0		(2)	498±3	12d	arg + py + po(?) + V
98.3	1.7		(3)	500±5	89d	arg + po + V
96.0	4.0		(4)	500±3	114d	arg + po + V
96.0	4.0		(5)	600±5	173d	arg + po + V
97.5	2.5		(2)	600±5	173d	arg + py(?) + V
98.7	1.3		(2)	600±5	173d	arg + V

(1) Ag + Fe + S (melted in torch); (2) Ag_2S + FeS_2; (3) Ag_2S + $Fe_{1-x}S$ (47.0 at.% Fe); (4) Ag_2S + $Fe_{1-x}S$ (46.5 at.% Fe); (5) Ag_2S + $Fe_{1-x}S$ (48.5 at.% Fe).

as given (e.g., <.1 at.% Ag in pyrrhotite at 600±3°C), the amount is reported with the uncertainty of weighing taken into consideration (e.g.,<.2 at.% Ag in pyrrhotite at 600±3°C).

The solubility of Ag in pyrite at 600±3°C as determined by quench-type experiments is less than 0.2 at.%. Because the cell edge of pyrite, as reported in Table 15, is not measably affected by the presence of argentite, the solubility is probably much less than this amount, and in fact, no exsolution of any phase from pyrite was observed during this study. The solubility of Ag in pyrrhotite of various compositions at 600±3°C is also less than 0.2 at.%. The $\underline{d}_{(10\cdot2)}$ values of the pyrrhotites in experiments containing 0.1 at.% Ag were identical to the starting $\underline{d}_{(10\cdot2)}$ values and Ag was observed in polished sections, further suggesting that the amount of Ag solid solution may be considerably less than 0.2 at.%.

Table 15. Cell edge of pyrite in the Ag-Fe-S system.

Comp., at.% FeS_2	Comp., at.% Ag_2S	Temp., °C	Time, days	Product at Temp.
90.0	10.0	662±3	51	py + L_t + V ($\underline{a}_{25°}$ = 5.4174±0.0003Å)
99.7	0.3	500±5	167	py + arg + V ($\underline{a}_{25°}$ = 5.4175±0.0002Å)

Limited solubilities of pyrrhotite and pyrite in argentite are clearly evidenced in polished sections. Pyrrhotite and pyrite exsolved from argentite upon cooling are distinctly finer grained than these phases interpreted as being stable at the annealing temperature. Based on this assumption, the

solubility of Fe in argentite is derived to be less than 0.8 at.% at 500±5°C and less than 1.0 at.% at 600±3°C.

Pyrrhotite Compositions.

The composition of pyrrhotite in equilibrium with pyrite, vapor, and either ternary liquid or argentite was determined during the course of this study. The pertinent data are reported in Table 23 and shown on Figure 32 in the section on fugacity determinations (pages 104-108). These experiments, coupled with solubility data, demonstrate that the presence of Ag as a third component does not have a measurable effect on the $d_{(10.2)}$ values (i.e., the composition) of pyrrhotites and that the composition of pyrrhotite in the po + py + Ag-bearing phase + V field is predictable from Fe-S phase data.

Effect of Fe on the Ag_2S Inversions.

The Ag_2S compound exists in three polymorphic forms. The inversion from the low-temperature monoclinic form to the intermediate-temperature bcc form occurs at 177±1°C (Kracek, 1946). Ag_2S also has a high-temperature fcc modification. The temperature of this inversion is composition sensitive; 586±3°C for $Ag_{2+x}S$ in equilibrium with Ag and 622±3°C for $Ag_{2-x}S$ in equilibrium with L_S (Kracek, 1946).

The fcc ⇌ bcc inversion of Ag_2S in the univariant field arg + py + L_S + V occurs at 568±2°C -- lowered from 622±3°C on the Ag-S join. This temperature was determined by both DTA (Appendix 1) and quench-type (Table 16a) experiments. Experiments by the latter technique, annealed at temperatures

Table 16. Experiments conducted on the fcc ⇌ bcc Ag_2S inversion in the Ag-Fe-S system.

a. Experiments conducted in the arg + py + L_S + V field.

Composition, at.% Ag	Fe	S (1)	Temp., °C	Time	Nature of Ag_2S after Quench (see text)
40	10	50	555±2	3d	Not Cracked
40	10	50	575±2	3d	Cracked
40	10	50	596±2	3d	Cracked
21	8	60	543±2	49d	Not Cracked
21	8	60	579±2	8d	Cracked

b. Experiments conducted in the Ag + arg + po + V field.

Composition, at.% Ag	Fe	S (2)	Temp., °C	Time	Nature of Exsolution in Ag_2S
55	15	30	514±2	4d	po + Ag(?)
55	15	30	525±2	4d	po + Ag
60	10	30	506±2	4d	po
60	10	30	524±2	4d	po + Ag

c. Experiments conducted in the arg + py + po + V field.

Composition, at.% Ag	Fe	S (3)	Temp., °C	Time	Relative Amounts of Exsolved py + po in Ag_2S
50	11	39	472±2	4d	493°C exper. exsolves more
50	11	39	493±2	3d	
20	30	50	472±2	4d	493°C exper. exsolves more
20	30	50	493±2	3d	
25	25	50	470±2	10d	500°C exper. exsolves more
25	25	50	500±2	8d	

Starting Materials: (1) Ag_2S + FeS_2 + S (2) Ag + Ag_2S + $Fe_{1-x}S$ (48.4 at.% Fe) (3) Ag_2S + FeS_2 + $Fe_{1-x}S$ (46.5 at.% Fe).

above 568°C, contain argentite with a unique texture. A single grain of argentite contains many fine fissures. The material in the cracks is a maroon-colored material and is interpreted to be an exsolution product. Slow cooling of the charge, reaching 25°C in about 8-10 minutes, resulted in recrystallization of this maroon "phase" to a fine-grained

mixture of argentite, pyrite, and possibly pyrrhotite. This maroon product is identical in appearance to the maroon-colored "phase" described on pages 63-64 as resulting from crystallization of the liquid involved in development of the arg + py + L_S + V field. Experiments conducted at temperatures below 568°C do not contain argentite with a fissured texture and the amount of exsolved material is less (approximately 1/4). Therefore, this cracking observed in the argentite is interpreted as resulting from the fcc ⇌ bcc inversion which apparently involves a considerable volume change within the ternary system.

The fcc ⇌ bcc inversion in the univariant field Ag + arg + po + V occurs at 518±2°C as determined by DTA (Table 7, page 51) and quench-type (Table 16b) experiments. DTA experiments showed that the magnitude of the thermal effect at 518°C increases as the composition of the charge becomes more Ag_2S-rich suggesting a reaction with a composition near Ag_2S. Experiments conducted at temperatures just above and below this inversion temperature contained approximately the same amount of exsolved pyrrhotite. However, the high-temperature charge contained exsolved Ag as well; this larger solubility is compatible with the phase relations of an inversion such as depicted in Figure 23.

The fcc ⇌ bcc inversion in the argentite of the arg + py + po + V field occurs at 481±2°C as determined by DTA (Appendix 1), high-temperature X-ray camera (Table 17), and

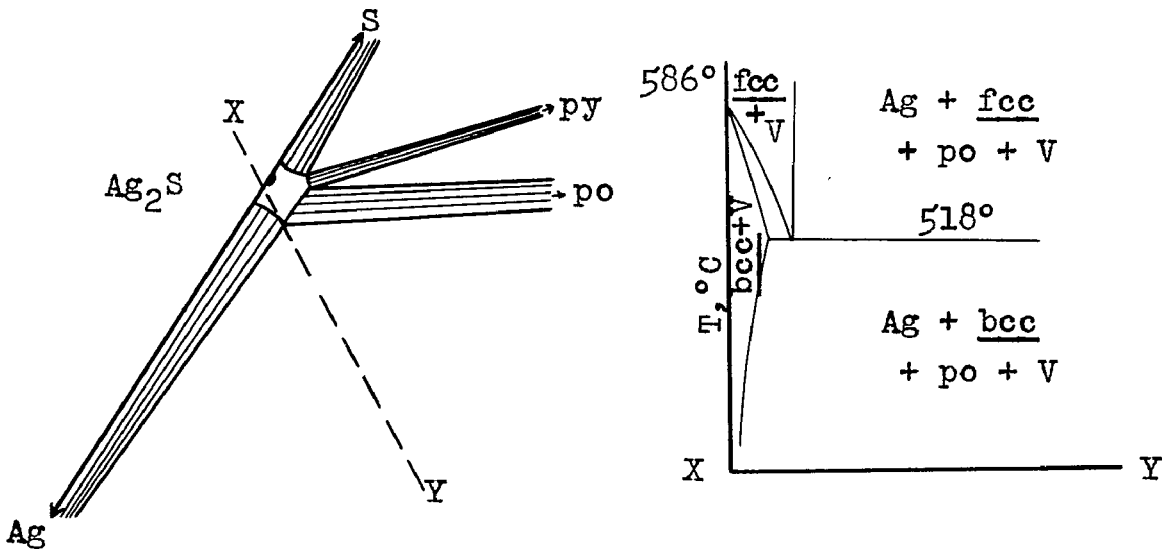

Figure 23. Schematic diagrams illustrating the fcc ⇌ bcc inversion in Ag_2S in the Ag-Fe-S system.

quench-type (Table 16a) experiments. DTA experiments showed that the size of the thermal effect at 481±2°C increases as the composition of the charge becomes more Ag_2S-rich. Unicam X-ray powder-camera experiments (Table 17) were made at 450±10° and 490±10°C and showed weak bcc (200 and 211) and fcc (220) Ag_2S reflections, respectively. Quench-type experiments showed that the amount of exsolution of pyrrhotite and pyrite from Ag_2S is less (approximately 1/2) in runs below 481±2°C than above. A cut through the ternary system from Ag_2S into the arg + py + po + V field would look similar to Figure 23b.

The bcc ⇌ mono. inversion of Ag_2S in Ag-Fe-S assemblages was not observed to be measurably different (i.e., 176±3°C) from the pure compound (DTA experiments, Appendix 1).

Table 17. High-temperature X-ray diffraction data of the assemblage arg + py + po + V using Cu unfiltered radiation.

Temp., °C	d_{obs}, Å	Cause of Reflection
490±10	2.69	py-po
	2.45	py
	2.29	py
	2.18	arg fcc 220
	2.08	po
	1.75	po
450±10	3.03	po
	2.68	po-py
	2.43	py-arg bcc 200
	2.076	po
	2.00	arg bcc 211
	1.749	po

It is apparent from the above discussion that iron has a large effect on the fcc ⇌ bcc inversion temperature, whereas the bcc ⇌ mono. inversion is not measurably changed. Barton and Skinner (1966, 1967) state that reactions involving large ΔH values will be less effected by small amounts of impurities than reactions with small ΔH, such as certain polymorphic transitions. The $\Delta H_{trans.}$ for the fcc ⇌ bcc and bcc ⇌ mono. inversions of pure Ag_2S are 100-200 (Rosenqvist, 1949) and 1410 cal/mole (Richardson and Jeffes, 1952) respectively. The differences in the magnitudes of the changes in inversion temperatures caused by the presence of iron can be explained thermodynamically by reference to Figure 24. This diagram shows schematically a free energy (ΔG) versus temperature (1/T) plot of the three polymorphic forms of Ag_2S, the inversions of which involve two greatly different $\Delta H_{trans.}$ values. The presence of iron as a third component changes

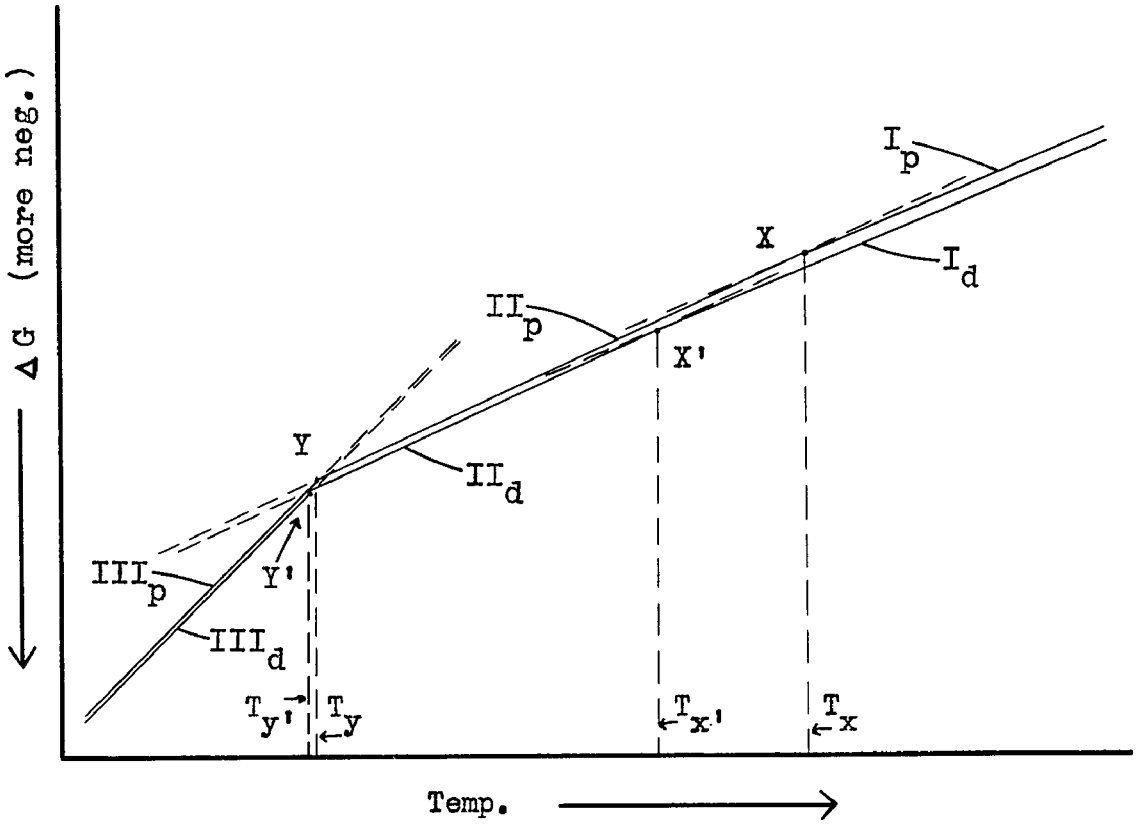

Figure 24. Schematic free energy versus temperature diagram showing the apparent effect of iron on inversion points of Ag_2S polymorphs. Subscripts p and d refer to pure Ag_2S and Ag_2S doped with iron. X and Y designate the inversions of pure Ag_2S and X' and Y', the inversions of iron-bearing Ag_2S. I, II, and III refer to fcc, bcc, and monoclinic structures of Ag_2S, respectively.

the position but not the relative slopes of the three curves. The amount of change is assumed to be directly related to the magnitude of iron soluble in the phase. Therefore, the change in ΔG for the fcc phase is greater than for the bcc phase which is greater than the mono. phase. Figure 24 explains the fact that although the fcc ⇌ bcc inversion temperature of Ag_2S is greatly affected (i.e., about 100°C lowering) by iron in solid solution, the bcc ⇌ mono. inversion remains relatively unchanged.

Phase Relations Between 320° and 200°C

A transition in pyrrhotite takes place at 320°C. Below this temperature, pyrrhotite has a hexagonal superstructure, 2A5C, based on the NiAs-type subcell. For purposes of discussion, monoclinic pyrrhotite, Fe_7S_8, is considered stable on the Fe-S join below 310°C. Based on theoretical considerations, two reactions must occur, with decreasing temperature, between 310° and 248°C: 1) tielines are established between m-po and arg (Figure 25a) and 2) tielines are established, by a reaction; arg + h-po ⇌ Ag + m-po, in the presence of vapor, from Ag to monoclinic pyrrhotite (Figure 25b). Neither of these temperatures were experimentally determined.

One of the most important developments in the Ag-Fe-S system concerns the reaction: arg + m-po ⇌ Ag + py, in the presence of vapor, and is diagrammatically presented in Figure 25 b and c. Experiments listed in Table 18 show this

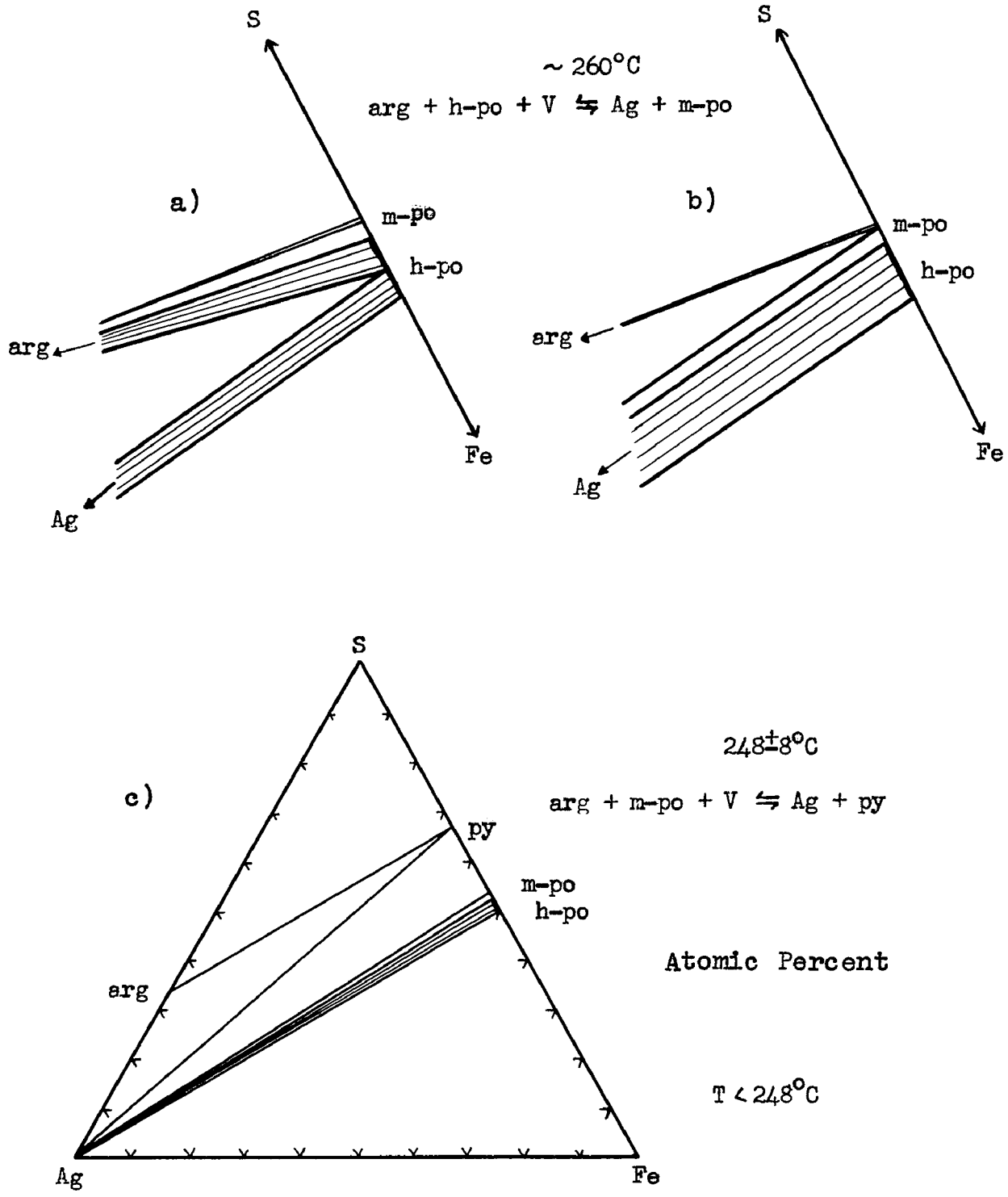

Figure 25. Schematic presentation of the phase relations associated with the development of the Ag + py + V join at 248±8°C in the Ag-Fe-S system. Vapor (V) is placed on the side of the equation with the condensed phases which are stable to higher temperatures.

Table 18. Experiments in the Ag-Fe-S system between 300° and 200°C.

Reactants		Temp., °C	Time, days	Products at Temp.*
Ag + py	(1)	300±5	32	Ag + py + arg + po
Ag + py	(1)	200±5	103	no reaction
arg + m-po	(1)	200±5	103	arg + m-po + Ag + py
Ag + py	(1)	265±3	32	Ag + py + arg + m-po
arg + m-po	(1)	265±3	103	no reaction
Ag + py	(1)	238±8	103	no reaction
arg + m-po	(1)	238±8	103	arg + m-po + Ag + py
Ag + py	(1)	256±3	152	Ag + py + arg + m-po
arg + m-po	(1)	240±3	88	arg + m-po + Ag + py
Ag + py	(1)	245±3	75	no reaction
arg + m-po	(1)	245±3	75	no reaction
arg+py+FeS	(2)	232±8	33	arg + py + m-po + Ag
Ag+py+m-po	(2)	225±8	63	no reaction
arg+py+FeS	(2)	200±5	103	arg + py + m-po + Ag
Ag+arg+py	(3)	200±5	103	no reaction
Ag + py	(4)	265±3	33	Ag + py + arg + m-po
see footnote	(5)	225±	28	decrease in arg + m-po

*These products are nonequilibrium assemblages, from incomplete reactions. Vapor is an additional phase in all assemblages.

(1) Composition = $Ag_{36.4}$ $Fe_{21.2}$ $S_{42.4}$; (2) Composition = $Ag_{16.7}$ $Fe_{33.3}$ $S_{50.0}$; (3) Composition = $Ag_{60.0}$ $Fe_{10.0}$ $S_{30.0}$; (4) natural Ag + py; (5) product from previous experiment.

invariant temperature to be 248±8°C. Because of the slow reaction rates at these temperatures, appearance of phase(s) was used as criterion for this reaction. Experiments with Ag_2S-Fe_7S_8 reactants at temperatures below 248±8°C, commonly contained Ag but no pyrite when examined by X-ray and in polished section. Either the pyrite was finely disseminated, making detection difficult or, more probably, monoclinic

pyrrhotite has a stable or metastable solid solution field which extends to the sulfur-rich side of Fe_7S_8 composition (see page 35).

The temperature 248±8°C is the upper-stability limit of Ag + py in the presence of vapor. Table 18 lists two experiments conducted with a natural assemblage of Ag + py from a specimen collected at Timmons, Ontario, Canada. The reaction times (28-33 days) involved demonstrate the feasibility of readjustment of a natural Ag + py assemblage to arg + po and vice versa.

The phase relations as shown in Figure 25c are shown present at approximately 200°C. No ternary solid phases were encountered in the Ag-Fe-S system at or above this temperature.

Phase Relations Below 200°C

Numerous experiments conducted by both dry and aqueous techniques were performed below 200°C. Because of the slow reaction rates, only signs of reaction were looked for which would indicate that the starting assemblage was metastable under annealing conditions.

Dry Experiments.

"Quench-type" experiments (Table 19a) were conducted in an attempt to determine the presence of any ternary phases in the system. Various starting materials were used, including the breakdown products of natural sternbergite annealed at 500°C. One experiment at 100±5°C consisting of

Table 19. Experiments conducted on the phase relations below 200°C.

a. Dry experiments

Reactants	Temp., °C	Time	Results
arg-py-po	177±3	111d	arg going to Ag
Ag-py-po	177±3	111d	no reaction
stern. breakdown	152±5	405d	arg going to Ag
arg-py-po	152±5	221d	arg going to Ag
Ag-py-po (pellet)	152±5	234d	no reaction
arg-po-S	100±5	167d	formation of Ag & py
Ag-po-py	100±5	156d	no reaction
Ag-po-py (pellet)	100±5	259d	arg-like rime on Ag & py
stern. breakdown	100±5	202d	arg going to Ag
Ag-po-py	100±5	358d	no reaction

b. Aqueous experiments

Ag-po-py + 2m NH_4Cl	100±10	201d	arg-like rim on Ag & py
stern. breakdown	100±10	202d	no reaction
Ag-arg-py + 2m NH_4Cl	100±10	202d	no reaction
arg-po-S + 2m NH_4Cl	100±10	377d	formation of Ag and py
arg-po + 2m NH_4Cl	100±10	201d	formation of Ag and py
cp + .4m $AgNO_3$	25±3	98d	ppt. Ag
cp + .025m Ag_2SO_4	25±3	97d	ppt. Ag
cb + .4m $AgNO_3$	25±3	96d	ppt. Ag
cb + .025m Ag_2SO_4	25±3	109d	ppt. Ag
po + .025m Ag_2SO_4	25±3	78d	ppt. Ag

a pressed pellet of Ag + m-po + py contained a thin reaction rim of an arg-like phase on some of the Ag and py grains. This experiment suggests that the assemblage Ag + m-po + py is not stable at 100°C; however, no concrete conclusions can be drawn from this experiment. All of the other dry experi-

ments listed in Table 19a were negative (i.e., no evidence for a ternary phase).

Aqueous Experiments.

Several types of aqueous experiments, including precipitation and recrystallization methods, were conducted and are summarized in Table 19b.

The precipitation experiments consisted of mixing solutions of various combinations of the salts: $AgNO_3$, Ag_2SO_4, $FeSO_4$, $FeSO_4 \cdot 7H_2O$, $FeCl_2 \cdot 4H_2O$, $Fe(NH_4)_2(SO_4)_2 \cdot 6H_2O$, $(NH_4)_2S$, and $(NH_4)_2S_x$ to give an Ag:Fe:S ratio of 1:2:3. Difficulty was encountered in keeping the Ag^+ in solution long enough to react with the other ions. Ag usually precipitated immediately and underwent gradual reaction with the solution to form Ag_2S. Several experiments resulted in black amorphous precipitates which crystallized to mixtures of Ag, Ag_2S, py, $AgFeS_2$(?), and Ag or Fe salts. No conclusive results were obtained concerning low-temperature phase relations of the Ag-Fe-S system.

The recrystallization experiments (Table 19b) consisted of placing various solid-phase reactants in a sealed silica tube containing approximately 2ml of 2m NH_4Cl solution. This salt solution did not appear to speed up the reaction rates appreciably over those of dry experiments. Perhaps the two ends of the reaction tube should have been at different temperatures, effecting a "driving" force for solution, transportation, and deposition of the phases. One experiment with

a charge consisting of Ag + m-po + py contained reaction rims on some of the Ag and py grains similar to the argentite-like phase of the dry experiment described above (Table 19a). This additional support for the metastable nature of the Ag + m-po + py assemblage at 100°C may be an expression of metastable m-po. This would lend support to the contention of Hall and Yund (1966) who believe that monoclinic pyrrhotite is never stable.

Several experiments (Table 19b) were also conducted in an attempt to replace the Cu atoms of chalcopyrite ($CuFeS_2$) and cubanite ($CuFe_2S_3$) with Ag. The chalcopyrite or cubanite was placed in an Erlenmeyer flask with 20-25 ml of an Ag-salt solution and mixed continuously on a shaker table. Here, as with the precipitation experiments, the Ag present in solution was easily removed as a pure Ag phase with no apparent replacement of the Cu of the sulfide.

Experiments with Natural Sternbergite and Argentopyrite

The breakdown temperatures of natural sternbergite and argentopyrite (both $AgFe_2S_3$) were investigated by quench-type experiments. The specimens used were not pure and contained small amounts (<5%) of pyrite, proustite, and possibly other minerals. The starting materials were finely ground under toluene and split into portions to insure similar charges for each experiment. Evidence of breakdown was looked for by 1) magnet, 2) X-ray diffractometer tracings, and 3) polished-section examination.

Experiments conducted in the 230° to 150°C temperature

range show that sternbergite and argentopyrite initially break down to arg + m-po + py + V developing a eutectoidal texture. However, $AgFe_2S_3$ composition lies in the Ag + m-po + py + V field, and sternbergite and argentopyrite should break down to this assemblage at temperatures below 248±8°C. If the initial breakdown product is replaced at the annealing temperature for additional time, the argentite phase decreases in amount with a corresponding formation and increase in Ag and pyrite. This phenomenon is explained by "Ostwald's step rule" (Ostwald, 1902) which can be stated as translated from German: -- "In general, one finds the rule that, with the breakdown of an unstable state [phase], a given chemical composition will form not the most stable state, but rather the adjacent, that is, transitory state, which can be reached directly from the existing one with the least loss of energy."-- It would appear that the formation of arg + m-po + py + V involves such an intermediate level of free energy. However, the fact that the breakdown products are metastable is not important to the following discussion.

Data from experiments listed in Table 20 were used to construct the reaction curve shown in Figure 26. The breakdown of sternbergite and argentopyrite are zero-order reactions, i.e., the rate is independent of the concentrations. This breakdown curve is linear on a log time versus T plot, which is to be expected when the rate-controlling mechanism (probably nucleatiion in this case) is the same over the

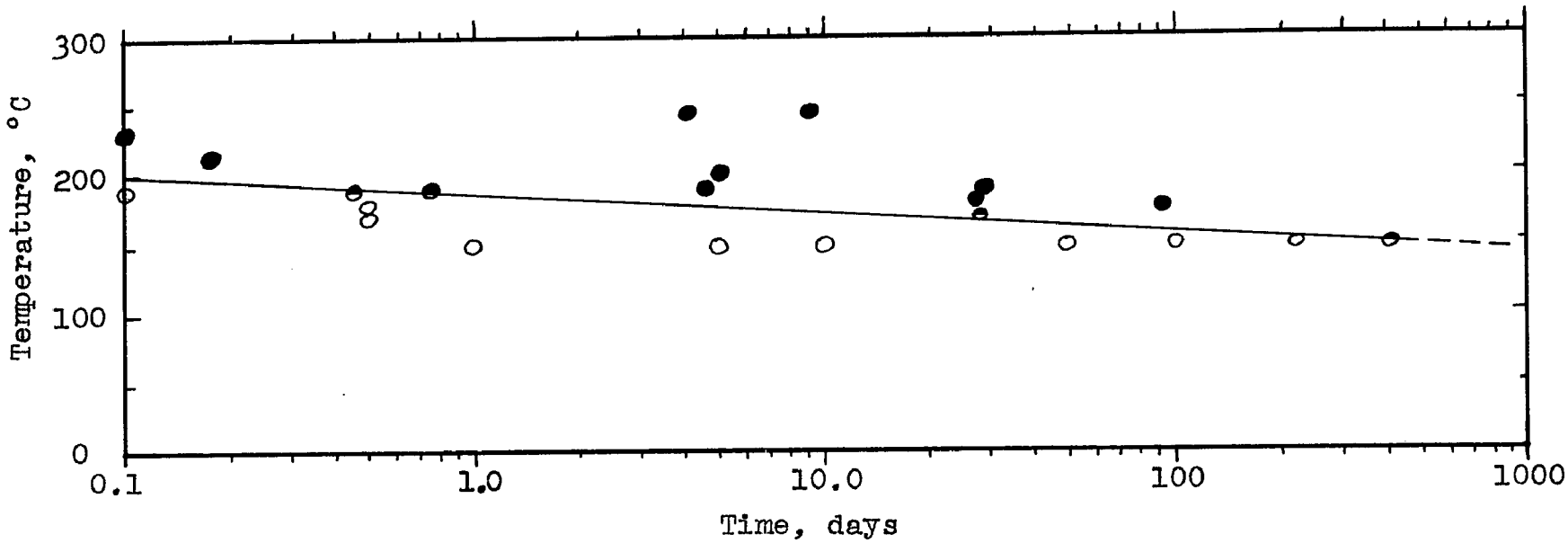

Figure 26. Reaction curve associated with the breakdown of natural sternbergite based on data from "quench-type" experiments listed in Table 20. The solid circles represent complete breakdown, whereas, the open circles represent stable sternbergite at the annealing conditions. Intermediate degrees of breakdown are shown as incompletely shaded circles.

temperature range of investigation.

$$k = A\, e^{\frac{-E_a}{RT}}$$

This is the Arrhenius equation for the rate constant, k = rate constant (sec^{-1}), A = frequency factor (sec/mole), R = universal gas constant (cal/mole-°K), T = temperature (°K), E_a = activation energy (Kcal/mole). From the log time versus T plot, where °C not °K has been used, (Figure 26), the value of k can be read directly at several different temperatures. If a plot of ln k versus 1/T (°K) is made, a straight line results which has a slope of $-E_a/R$. In this manner it was determined that the activation energy (E_a) for the breakdown of sternbergite is 66.6±1.0 Kcal/mole. Activation energies for the decompositions of pyrite and chalcocite are reported as 26.8 Kcal/mole (Samal, 1965) and 59.8 Kcal/mole (Pavlyuchenko and Samal, 1964), respectively.

A limited number of breakdown experiments were conducted on argentopyrite. The activation energy was not determined precisely; however, the breakdown data obtained suggest a value similar to that for sternbergite. The reaction rate at a given temperature is approximately 3 to 4 times faster than for sternbergite breakdown.

Sternbergite and argentopyrite, reported as possible polymorphs of $AgFe_2S_3$, were both observed to break down at 152±3°C. The breakdown products and activation energies are identical, suggesting the same rate-controlling mechanism.

Table 20. Experiments on the breakdown of natural sternbergite and argentopyrite.

Sternbergite - Roepper Collection, Lehigh University, Joachimsthal, Czechoslovakia.

Temp., °C	Time, Days	Estimated % Breakdown
245±3	9	100
245±2	4	100
233±1	0.1	100
215±2	0.17	100
200±2	5	100
190±2	0.1	0
190±2	0.45	50
190±2	0.75	80
190±2	4.5	100
188±2	28	100
180±2	0.5	0-?
178±2	27	80
177±3	93	>90
172±5	27	30-40
170±3	0.5	0
152±2	1	0
152±2	5	0
152±2	10	0
152±3	49	0
152±3	101	0
152±3	219	0-?
152±5	403	10-20
Argentopyrite-National Museum #R 9630, Andreasberg.		
177±3	14	>75
177±3	38	100
152±2	12	0
152±2	102	20-30
152±3	196	>75

Therefore, because argentopyrite breaks down faster than sternbergite at a given temperature, it is suggested that argentopyrite is the lower temperature phase.

It is an empirical fact that many reactions near room temperature, approximately double their velocities for a 10°C rise in temperature (Daniels and Alberty, 1955). However, in

the case of argentopyrite and sternbergite, a 10°C temperature increase results in approximately a five-fold increase in breakdown rate.

Fugacity Determinations

Richardson and Jeffes (1952) pointed out that, for most reactions of geologic and metallurgic importance, the Gibbs free energy (ΔG) can be expressed as a linear function of temperature. Because $\Delta G = RT\ln f_S$, therefore, $\ln f_S$ (which equals $\Delta G/RT$) is a linear function of 1/T. These facts make it convenient to use a log f_S versus 1/T plot to present pressure-temperature equilibria.

The vapor which is in equilibrium with liquid sulfur is composed of various molecular species -- S_2, S_4, S_6, and S_8. The equilibrium constants for these species, as well as data for undersaturated sulfur vapor, are given by Braune et al. (1951). At any given temperature, the mol. percent of S_2 species in the vapor increases greatly as the total fugacity (f_{S_t}) is decreased from the sulfur-condensation curve into the undersaturated vapor region (see Figure 27). Line 3 of Figure 27 demonstrates this; the region to the low-pressure side of this line consists almost entirely of S_2 species. The amount of sulfur occurring as species other than S_2 is negligible (<1 mol.%) and the vapor may be considered to behave ideally (Braune et al., 1951). Most univariant curves for various sulfide assemblages of importance to ore petrology lie in this region.

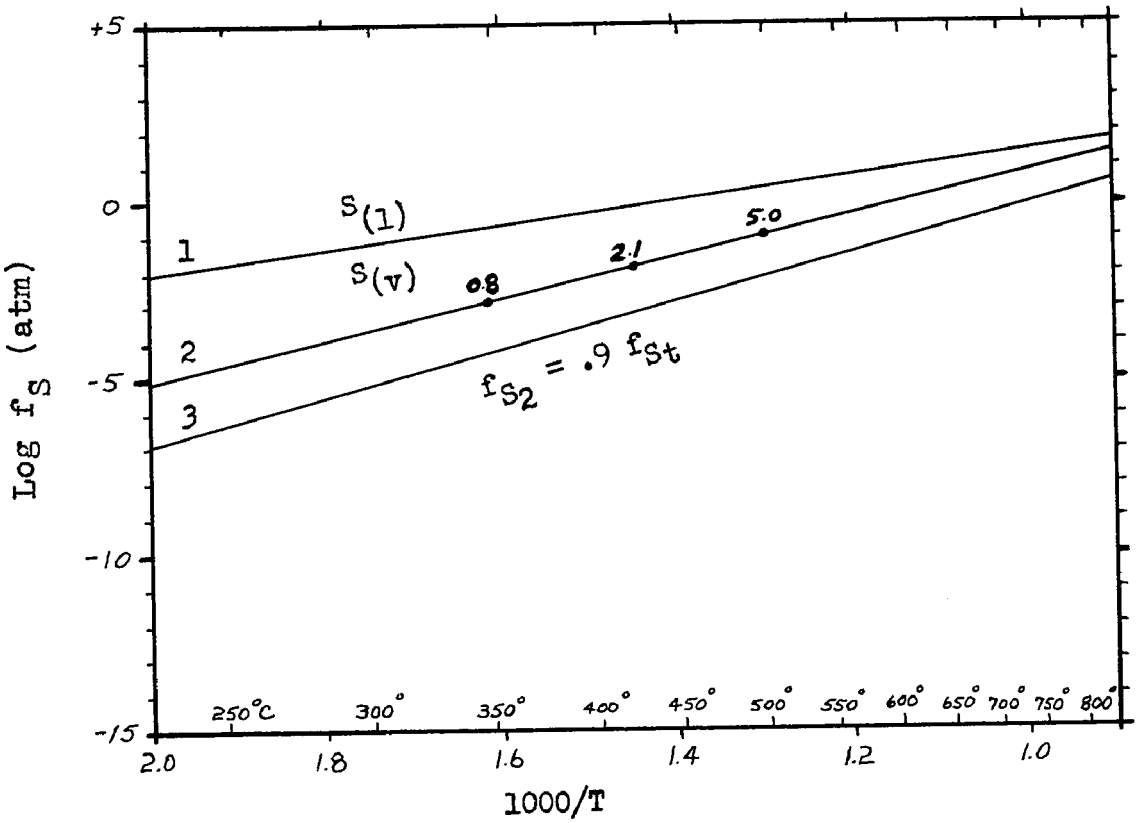

Figure 27. Considerations of sulfur species in sulfur vapor. 1) $S_L = S_V$ curve expressed as $f_{S_t} = f_{S_2} + f_{S_4} + f_{S_6} + f_{S_8}$ after West (1950); 2) f_{S_2} component of f_{S_t} associated with the $S_L + S_V$ curve; numbers show f_{S_2}/f_{S_t} in percent at selected temperatures; 3) undersaturated portion of the diagram where $f_{S_2} = 0.9\ f_{S_t}$, based on data of Braune et al. (1951). The region below this curve consists of > 90 mol.% S_2 species in the vapor.

Sulfur-fugacity data in the present investigation were obtained through use of the electrum-tarnish and pyrrhotite-indicator methods as presented by Barton and Toulmin (1964) and Toulmin and Barton (1964), respectively. Brief discussions of some of the principles and assumptions underlying these methods are given below along with the results from the present study.

Electrum-Tarnish Method.

Equilibrium between Ag and Ag_2S*, in the presence of vapor, in a closed system containing only Ag and S determines a univariant curve, Ag + Ag_2S + V, in P-T-X space (Figure 28) with an association reaction:

$$4Ag_{(s)} + S_{2(g)} \rightleftharpoons 2Ag_2S_{(s)};\ K = (aAg_2S)^2 \cdot (aAg)^{-4} \cdot (f_{S_2})^{-1}$$

where K = equilibrium constant, a = activity, and f = fugacity. At a given temperature, a certain f_{S_2} is necessary to tarnish Ag (i.e., form Ag_2S) and form the equilibrium univariant assemblage Ag + Ag_2S + V. The data concerning this curve, compiled by Richardson and Jeffes (1952), can be read directly off the log f_{S_2} versus 1/T plot of Figure 28.

If silver is diluted with gold (Au) in solid solution (electrum), the activity of silver diminishes, thereby increasing the f_{S_2} necessary to tarnish the alloy. A series of curves (several shown in Figure 28) for the tarnish of electrum, dependent on the mol. fraction of Ag in the electrum, were calibrated by Barton and Toulmin (1964) using the two-bulb, liquid-sulfur procedure of Allan and Lombard (1917). One bulb contained pure sulfur and was held at a given low temperature; the other bulb which was held at a higher temperature contained a piece of electrum of known composition. The temperature at which a sulfide tarnish appeared or dis-

*$Ag_{2+x}S$ is the correct formula for silver sulfide in equilibrium with Ag. However, for brevity this silver sulfide will be written Ag_2S.

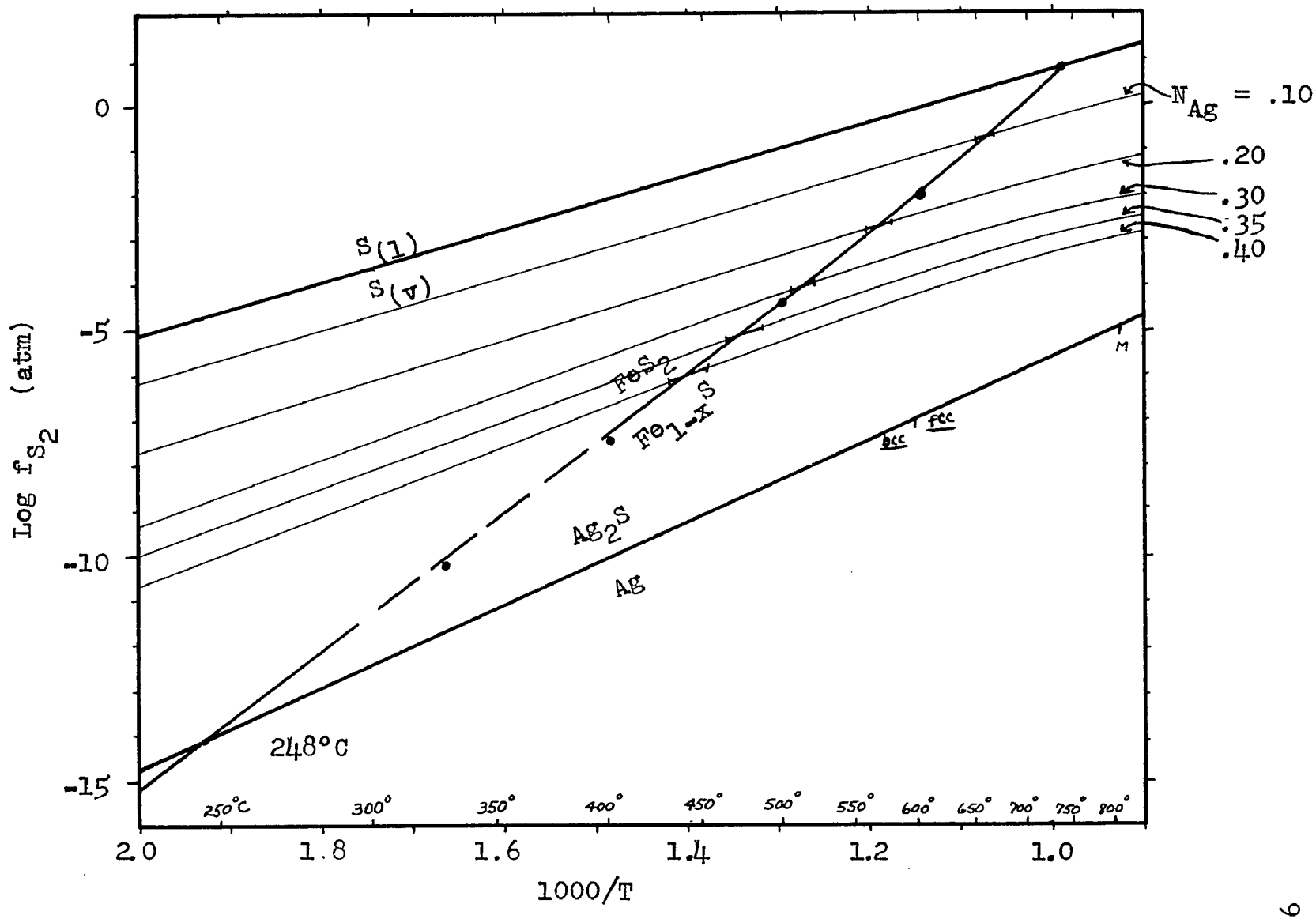

Figure 28. Log f_{S_2} versus 1/T diagram of the py + po + V curve determined during the present study. Several electrum-tarnish curves with tarnish intervals indicated (see text) are plotted. The points represent data determined by Toulmin and Barton (1964).

appeared on the electrum were determined to 5 to 10°C. Using the data of West (1950), assuming that the vapor was essentially pure sulfur, the total pressure of all sulfur species over the liquid sulfur was assumed to equal P_{S_2} over the electrum + tarnish + V assemblage. On the further assumption that the gas is ideal, the partial pressure of S_2 species equals its fugacity. In this manner, several calibration points on the curve associated with each composition of electrum were determined resulting in log f_{S_2} versus 1/T plots of the respective curves.

The electrum-tarnish method, as used during the present study, consisted of placing a small piece (1-2 mg.) of electrum of known composition in a sealed, evacuated silica tube along with, but mechanically separated from, a larger amount (100 mg.) of a univariant sulfide assemblage (e.g., po + py + V) whose f_{S_2} was to be determined (see Figure 29).* The temperature was then raised or lowered in increments and the resulting development or decomposition of a sulfide tarnish on the electrum was observed visually. In this manner, it is usually possible to bracket the equilibrium temperature, of the electrum-sulfide tarnish, produced by the vapor from the sulfide assemblage, within a 10-20°C interval. This

*The bulk composition of the condensed phase assemblage changes slightly due to the loss of S to form the equilibrium vapor; however, it is the number of phases, and not the amount, which governs the degrees of freedom. Thus, the fugacity is constant over the assemblage regardless of the relative amounts of the phases.

tarnish interval is noted on the appropriate electrum tarnish curve of Figure 28. The f_{S_2} associated with this tarnish, assumed to be also the equilibrium fugacity of the univariant assemblage, is found by reference to the electrum-tarnish curves of Barton and Toulmin (1964). If several experiments are performed using various known compositions of electrum, several "points" are determined through which a straight line or smooth curve can be drawn. Because of the shallow slopes of the log f_{S_2} versus 1/T curves of the various electrums with respect to the slope of the univariant curve being determined (see Figure 28), the ±5-10°C precision is sufficient for the precise fitting of a smooth curve to the data on a log scale. The total uncertainity of the calibrated electrum curves is reported as ±0.13 log f_{S_2} units (Barton and Toulmin, 1964); therefore, any univariant curve determined using this technique will be about ±0.13 log f_{S_2} units.

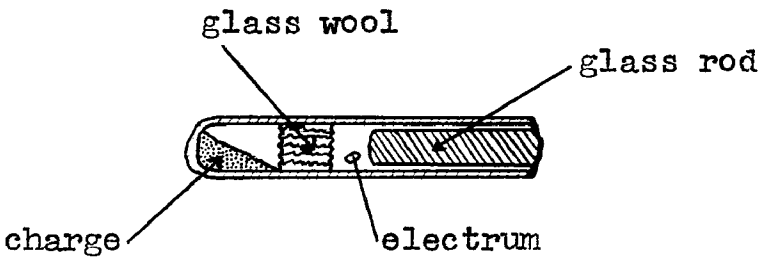

Figure 29. Electrum-tarnish silica-tube arrangement used in the present investigation.

Discussion of Assumptions. A complete evaluation of the various assumptions and principles underlying the electrum-tarnish method will not be attempted here; however, several

points are worthy of discussion.

The Allan and Lombard method (1917) for the determination of sulfur fugacities was used by Barton and Toulmin (1964) to establish their electrum-tarnish curves. The container for these determinations consisted of a sealed, evacuated tube with liquid sulfur at one end (at T_1) and the electrum at the other (T_2). The P_{S_t} over liquid sulfur was assumed (with a few exceptions at high temperatures) to be equal to P_{S_2} over the electrum. The electrum temperature was always higher (i.e., hundreds of degrees C) than that of the liquid sulfur with the result that mol. fractions of S_8, S_6, S_4, and S_2 species in the vapor (i.e., the mean molecular weight of sulfur vapor) must decrease drastically from the low to the high temperature portions of the tube. Thus, this procedure, based on gradients of temperature and partial pressures (mole fractions) of the respective sulfur species, is not an equilibrium method. Barton and Toulmin (1964) determined only one point on the Ag + Ag_2S + V curve which plots on the accepted curve (Richardson and Jeffes, 1952), suggesting that the disequilibrium factors just mentioned apparently do not have an appreciable net effect on the empirical curves obtained. This calibration scheme should be cross-checked by other methods and at several temperatures.

The tarnish in the electrum-tarnish experiments behaves in a variety of ways. Barton and Toulmin (1964) mentioned several of these, and certain problems concerning tarnish

development experienced during the present study are discussed below. Sometimes a tarnish will appear at anomalously low f_{S_2}. Barton and Toulmin (1964) suggest that this tarnish probably occurs because of the metastable composition of one phase in the univariant assemblage --- e.g., po of an initial FeS + py charge; the equilibrium pyrrhotite is not FeS but some $Fe_{1-x}S$ composition on the pyrite-pyrrhotite solvus. Preequilibration of the charge before the addition of the electrum reduces the occurrence of this metastable tarnish. The appearance of tarnish observed during the present study may be described by such terms as films, spots, clusters, pox, etc. Some types of spottedness may be due to slight compositional inhomogeneities of the electrum, the tarnish occurring at silver-rich regions. In the present study, certain tarnish pecularities were correlated with the condition of the surface of the electrum chip. Pieces of electrum cut up with a razor blade possessed smooth surfaces; those cut with dull wire cutters gave rough, striated, ridged surfaces. Tarnish commonly occurred at temperatures of 10-15°C less with electrum possessing rough surfaces than with smooth-surfaced electrum. The tarnish appeared unevenly along the crests of the ridges and other angular projections. This surface phenomenon can be explained by consideration of energy distribution on the surface of the electrum chip. The regions of the surface with the smallest internal radii of curvature will have the highest chemical potentials (sur-

face energy) and be the most chemically active. This may lead to preferred, and possibly metastable, tarnish formation on the sharpest portions of the surface.

The nonstoichiometry of the "Ag_2S" tarnish results in the activity of Ag_2S being less than one. Because the electrum-tarnish curves were empirically determined, the actual consideration of activity is not important to the accuracy of these curves.

Yund (personal communication as per G. Kullerud, 1967) found that the $(Ag, Au)_2S$ field actually contains intermediate compounds showing that this sulfide-tarnish field is not homogeneous as depicted by Barton and Toulmin (1964). The presence of these phases apparently did not affect the electrum-calibration curves measurably. The calibration of the electrum was based on "reaction - no reaction" criteria, and the nature of the reaction phase (tarnish) was probably assumed to be $(Ag, Au)_2S$ possibly resulting in non-detection of any intermediate phases.

Pyrrhotite-Indicator Method.

This method for the determination of sulfur fugacities was developed by Toulmin and Barton (1964). In the pure Fe-S system the composition of pyrrhotite is fixed at a given temperature and a given f_{S_2}. The log f_{S_2} versus 1/T plots for various pyrrhotite compositions were determined by Toulmin and Barton (1964) using the electrum-tarnish method described above. The pyrrhotite-indicator method consists of heating

a univariant assemblage whose f_{S_2} is to be determined, with synthetic pyrrhotites of suitably chosen compositions in a sealed, evacuated, silica tube. The pyrrhotites and the assemblage are mechanically separated as shown in Figure 30 so that sulfur, because of its high vapor pressure, but not silver or iron, can pass freely between all phases in the tube. The experiment is annealed at a given temperature with the result that the compositions of the pyrrhotites and the phases in the univariant assemblage (but not the number of phases) change until they are all in "equilibrium" with sulfur vapor. The pyrrhotite compositions are then determined and the fugacity of sulfur is obtained from Toulmin and Barton's data (1964). Initial pyrrhotite compositions were selected to bracket an estimated final composition; therefore, the pyrrhotite compositions converge toward the final composition, and at the end of the annealing period, the compositions were usually measurably equal. This was taken as evidence that equilibrium with respect to sulfur in the vapor phase was attained throughout the tube. The total uncertainty of the pyrrhotite-indicator method is reported as ± 0.35 log f_{S_2} units (Toulmin and Barton, 1964).

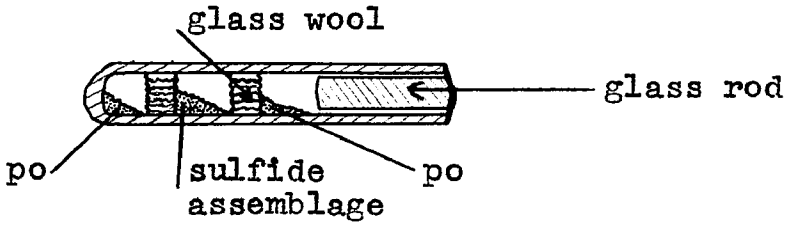

Figure 30. Pyrrhotite-indicator silica-tube arrangement used in the present investigation.

Discussion of Assumptions. The inherent assumption in this method is that the chemical potential of sulfur is equal in all phases, whereas, the chemical potentials of the metal components may or may not be equal. This is due to the fact that many metals (e.g., silver and iron in this study) are transported mainly by solid diffusion and to only a small extent in the vapor phase in silica-tube experiments. To check on the effect of this possible disequilibrium, the composition of the pyrrhotite in the univariant assemblage arg + py + po + V was compared to the composition of the pure pyrrhotite indicators on either side of the glass wool (Table 21). All three pyrrhotite compositions, as indicated by $\underline{d}_{(10.2)}$ values, were found to be measurably equal. This demonstrates that, although, the chemical potential of silver (and iron) may not be equal in all the pyrrhotites, the disequilibrium effect upon the pyrrhotite-indicator compositions is not measurable. As previously discussed, the effect of silver on pyrrhotite $\underline{d}_{(10.2)}$ values is not measurable by techniques used during this study. The pyrrhotite-indicator method was modified for further use during this study. No mechanically-separated pyrrhotite portions were needed in the experiments because the pyrrhotite composition of any assemblage in the Ag-Fe-S system is indicative of the fugacity of sulfur present at the annealing temperature.

Table 21. Experiments conducted to check disequilibrium effect of the po-indicator method in the Ag-Fe-S system.

Starting Materials		Temp., °C	Time	Products*	
po-indicator comps.	univariant assemblage			po-indicator comps.	po comp. in assem.
46.0 at.% Fe 47.0 at.% Fe	arg+py+po	500±3	49d	46.45 at.%Fe 46.50 at.%Fe	46.55

*The uncertainty of po compositions of the products is ±10 at.% Fe.

Results from the Present Study.

Experiments conducted during the present investigation utilized both the electrum-tarnish and pyrrhotite-indicator methods for the determination of the fugacity of sulfur. Because the pyrrhotite-indicator method was derived from the electrum-tarnish method and has considerable potential as a sulfur barometer, it was considered important to cross check some of the results of Toulmin and Barton (1964).

The f_{S_2} over the univariant assemblage py + po + V at various temperatures was determined using electrums of five compositions (Table 22) prepared according to the procedure of Barton and Toulmin (1964). With mechanical mixtures of po and py, problems concerning the metastable formation of electrum tarnish were encountered. Therefore, po + py mixtures were allowed to equilibrate for approximately 1 month at temperatures of 650, 550, 500, 475, and 450°C prior to use in the fugacity determinations. The results of the fugacity

Table 22. Fugacity experiments to determine the py + po + V curve.

N_{Ag} in electrum	Pre-equil. Temp., °C*	Temp., °C	Time, hrs.	Tarnish vs. No Tarnish		
0.10	650	650±2	42			X
0.10	650	660±2	60	X		
0.10	650	647±2	50			X
0.10	650	665±2	36	X		
0.10	650	647±2	194	X	went to	
0.20	550	560±3	74			X
0.20	550	580±2	88	X		
0.20	550	560±2	49			X
0.20	550	585±3	98	X		
0.20	550	550±5	720	X	went to	X
0.30	500	505±2	162			X
0.30	500	525±5	654	X		
0.30	500	504±3	180			X
0.30	500	520±5	713	X		
0.30	500	500±5	720	X	went to	X
0.30	500	503±2	144			X
0.30	500	516±2	192	X		
0.30	500	502±2	216	X	went to	X
0.35	475	460±3	611			X
0.35	475	490±3	574	X		
0.35	475	465±3	342			X
0.35	475	490±3	582	X		
0.35	475	460±3	720	X	went to	X
0.40	450	420±5	746			X
0.40	450	455±5	582	X		
0.40	450	430±3	510			X
0.40	450	455±3	588	X		
0.40	450	420±3	744	X	went to	X

*This is the temperature at which the py + po charge was pre-equilibrated for 30 days before incorporation into the fugacity experiment.

experiments on the univariant curve po + py + V are given in Table 22 and diagrammed in Figure 28, page 92. The experiments are reported as "tarnish or no tarnish", and the reac-

tions are shown to be reversible. The data bracket a temperature range on each tarnish curve. As previously mentioned, the shallow slopes of the log f_{S_2} versus 1/T plots of the various electrum compositions, as compared with the curve being determined, allow a fit for electrum-tarnish data with a precision of ±10-20°C.

The po + py + V curve shown in Figure 28 is not measurably different from the curve determined by Toulmin and Barton (1964) except below approximately 320°C. The beta inversion in pyrrhotite at 320±5°C terminates the stable portion of the measured po + py + V curve. For the purposes of discussion, the low temperature Fe-S phase relations are assumed to be those shown by Kullerud, 1967a (see page 31).

Figure 31 presents a schematic plot, based on theoretical considerations, of the univariant curves around the invariant points at 320° and 310°C in the Fe-S system. The py + h-po + V curve must lie above the metastable extension of the py + po + V curve discussed above, and likewise, the py + m-po + V curve must lie above py + h-po + V metastable curve. Toulmin and Barton (1964) state that the position of the py + h-po + V curve cannot be definitely fixed from their data; however, they give data of 300±5°C and approximately -11.5 log f_{S_2} for a point on this curve and state that the curve may cross the Ag + Ag_2S + V curve at about 200°C. If monoclinic pyrrhotite is stable to 310°C, the point they have determined is for the py + m-po + V curve, and it would be

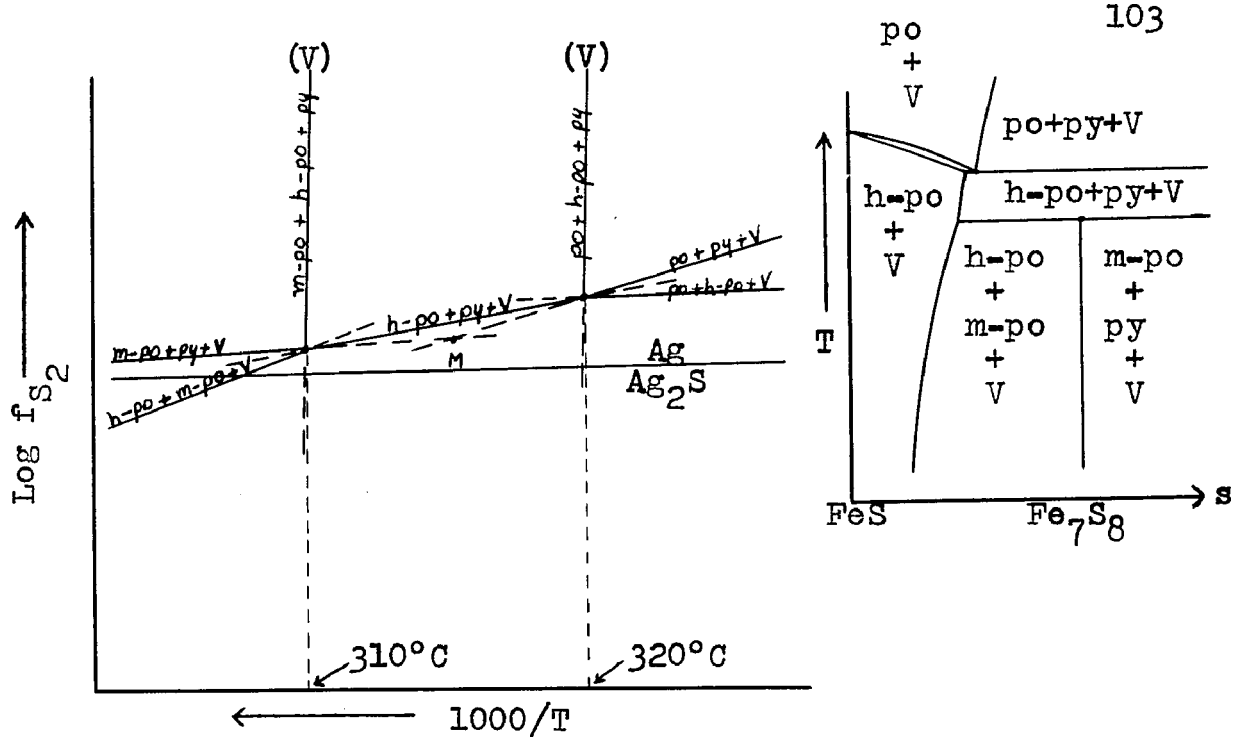

Figure 31. Schematic P-T diagram of univariant curves associated with the invariant points at 320° and 310°C in the $Fe_{1-x}S$ portion of the Fe-S system.

this curve which would cross the Ag + Ag_2S + V curve.

It is also noteworthy to consider Point M of Figure 31 which represents the intersection in P-T-X space of the metastable extensions from the invariant points associated with the stabilities of monoclinic and low-temperature hexagonal pyrrhotites. Point M represents the metastable transformation of m-po to hexagonal pyrrhotite of the same composition.

The invariant reaction arg + m-po ⇌ Ag + py, in the presence of vapor, at 248±8°C gives a control point for the py + m-po + V curve which must intersect the Ag + Ag_2S + V curve at this temperature. The assumption is made that the Ag + Ag_2S + V curve is correct and the py + m-po + V curve is

drawn to intersect it at 248°C.

For reactions in which all activities other than that of sulfur are constant --- no solid solution --- log f_{S_2} versus 1/T plots will be linear. The gradually changing solid solubility of pyrite in pyrrhotite with temperature causes the a_{FeS} to vary in pyrrhotite associated with the py + po + V univariant curve (e.g., a_{FeS} at 700°C = 0.40, 350°C = 0.56). The effect of this changing activity is to cause the curve to deviate from a linear relationship by being concave toward higher values of log f_{S_2}. Toulmin and Barton (1964) showed this curve to have a larger degree of concavity than was determined during the present study. According to the present experimental results, this curve is nearly linear (Figure 28, page 92).

The pyrrhotite-indicator method, as stated previously, was modified for use during the present study. Because the assemblages of interest in the Ag-Fe-S system contain pyrrhotite, the mechanically-separated pyrrhotite phase was omitted from the charges. In addition, a check on the attainment of equilibrium was conducted by preparing two experiments with initial pyrrhotite compositions bracketing the expected equilibrium composition under the same heating conditions. Thus, the pyrrhotite compositions could be observed to converge on a final equilibrium composition. Experiments conducted in the univariant fields arg + py + po + V, Ag + arg + po + V, and Ag + Fe + po + V (Table 23) demonstrate that the

Table 23. The compositions of pyrrhotite in univariant fields of the Ag-Fe-S system.

a. Compositions of po in the arg + py + po + V field.

Starting po Comp. At.% Fe*	Temp., °C	Time	Final po Comp. At.% Fe±0.1	po Comp. from Binary Data
50.0	700±2	8d	45.40	45.35
50.0	600±2	19d	46.05	46.00
50.0	500±3	24d	46.45	46.55
46.0	500±3	99d	46.50	46.55
47.0	500±3	99d	46.55	46.55
50.0	400±5	67d	46.81	47.00
50.0	400±5	50d	46.80	47.00
46.5	400±5	50d	47.18	47.00
47.5	400±5	50d	46.95	47.00
50.0	350±5	96d	47.28	47.15
46.5	350±5	96d	46.97	47.15

*All charges consisted of mechanical mixtures of arg, py, and po.

b. Compositions of po in the Ag + arg + po + V field.**

50.0	700±3	8d	48.60	48.70
48.0	620±3	31d	48.60	48.55
50.0	600±3	34d	48.60	48.50
48.0	600±3	49d	48.43	48.50
49.0	600±3	49d	48.55	48.50
50.0	500±5	35d	48.55	48.30
50.0	500±5	34d	48.45	48.30
48.0	500±5	49d	48.37	48.30
49.0	500±5	49d	48.45	48.30
47.5	400±3	59d	48.02	48.05
48.4	400±3	59d	48.11	48.05
50.0	350±5	96d	48.00	47.90
47.0	350±5	96d	47.82	47.90

**All charges consisted of mechanical mixtures of Ag, arg, and po.

c. Compositions of po in the Ag + Fe + po + V field.***

50.0	855±5	3d	50.00	50.0
49.75	802±3	2d	50.10	50.0
50.0	802±3	2d	50.05	50.0
50.0	700±3	2d	50.00	50.0
50.0	700±3	2d	50.08	50.0
48.0	596±3	7d	49.90	50.0
50.0	596±3	7d	49.95	50.0
49.5	498±5	38d	49.95	50.0
50.0	498±5	38d	50.10	50.0

***All charges consisted of mechanical mixtures of Ag, Fe, and po.

phase relations in the Fe-S system are not measurably affected by the presence of Ag as a third component. This is readily apparent (Table 23) by comparison of the pyrrhotite composition in a ternary field to that of the composition in the respective binary field.

A graphical presentation of pyrrhotite compositions in the various fields of the Ag-Fe-S and Fe-S systems is shown in Figure 32. The compositions of pyrrhotite in the arg + py + po + V assemblage (right-hand solvus of Figure 32) are measurably equal to the pyrrhotite of the binary assemblage, py + po + V as determined by Arnold (1962) and Toulmin and Barton (1964). The presence of liquid above 532±2°C in the ternary assemblage does not measurably affect the pyrrhotite composition; in fact, liquid significantly shortens the time required for attainment of equilibrium. The compositions of pyrrhotite in the Ag + arg + po + V field are shown by the left-hand solvus of Figure 32. Several reference compositions are shown through which a curve is drawn. The determination of these reference points is based on the principle that the composition of pyrrhotite is fixed at a given temperature and f_{S_2}. At a given temperature, the log f_{S_2} associated with the Ag-Ag_2S curve is read off Figure 28. On the assumption that iron-solubility in the Ag phases will have a negligible effect on this curve, the composition of pyrrhotite at this particular T and f_{S_2} is obtained from the data of Toulmin and Barton (1964). The close correspondence

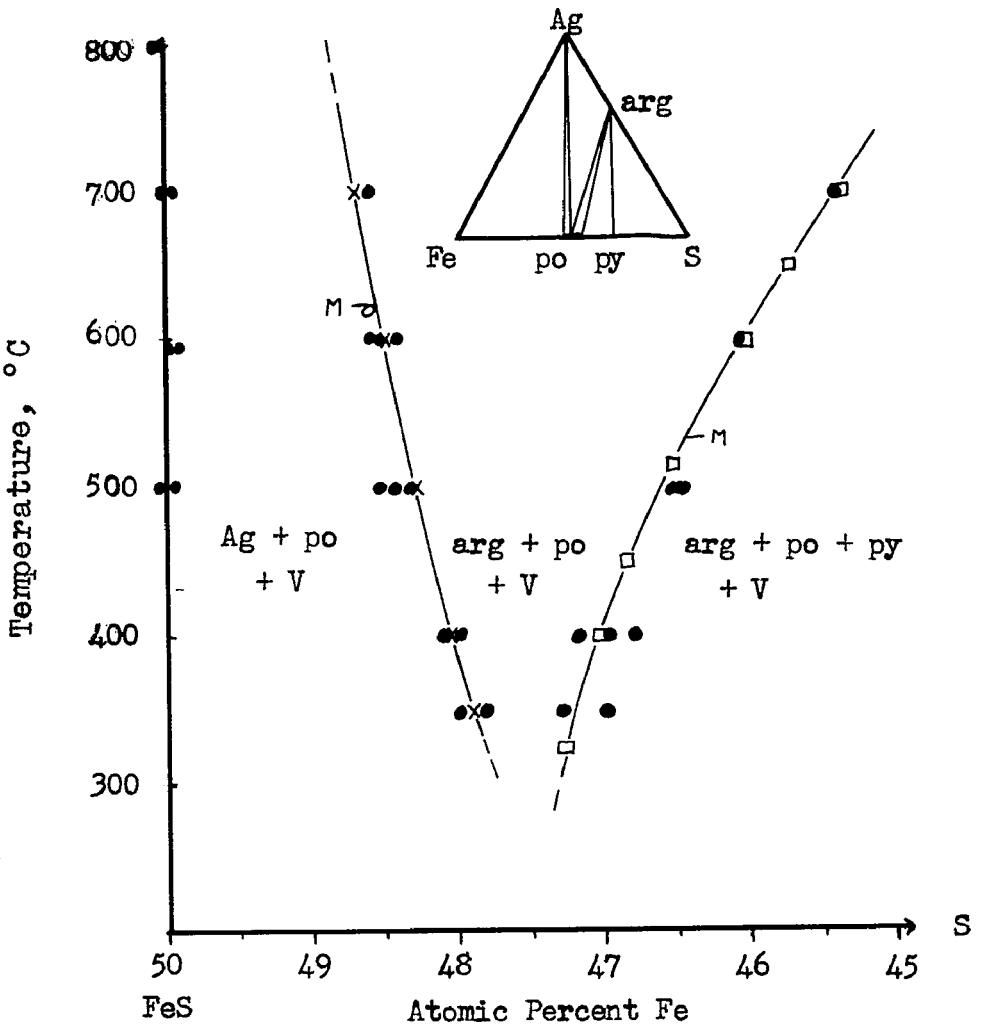

Figure 32. Compositions of pyrrhotites in ternary assemblages of the Ag-Fe-S system. The positions of the ternary fields are projected onto the Fe-S binary join for purposes of presentation. The solid circles represent pyrrhotite compositions as determined by experiments listed in Table 23. The squares represent pyrrhotite compositions on the pyrite-pyrrhotite solvus as determined by Arnold (1962) and Toulmin and Barton (1964). The crosses represent pyrrhotite compositions in the Ag + arg + po + V field as predicted from binary considerations (explanation in text). The pyrrhotite compositions were determined with a precision of ±0.10 at% Fe.

of the experimentally determined values to the theoretical values demonstrates that the amount of ternary solid solution of the binary phases is not sufficient to cause sulfur fugacities over the ternary phase assemblages to differ measurably from those predictable from binary consideration.

With the knowledge that in this particular system, the third component does not measurably affect the fugacity of sulfur over a binary univariant assemblage, the complete log f_{S_2} versus temperature data for the Ag-Fe-S system can be read directly off Figure 28. These data are compiled on Table 24.

Presentation of P-T-X Data

In the present study, f_{S_2}-T-X data for the Ag-Fe-S system were determined (Table 24). These dataare presented below in two different graphical forms illustrating certain principles of phase chemistry.

It is only possible to draw a complete P-T-X diagram of a system if each parameter (i.e., P,T,X) requires one dimension (one orthogonal axis). Therefore, it is not possible to construct a complete P-T-X diagram for systems containing more than two components.

If composition is allowed two dimensions and temperature one, the familiar T-X plot of a ternary system results. It is common to show T-X data as a series of isothermal sections; because the equilibrium vapor pressure over each assemblage is different, these sections are polybaric. Figure 33 shows a plot of several isotherms of the Ag-Fe-S system on which the log f_{S_2} data (compiled in Table 24) for the univariant assemblages have been superposed.

In order to restrict the compositional variable of a ternary system to one dimension, a cut can be chosen to pass

Ag + arg + po + V Field	Temp., °C	Log f_{S_2}
	600	- 6.9
	550	- 7.5
	500	- 8.3
	450	- 9.1
	400	-10.0
	350	-11.1
	300	-12.4
	250	-14.0
arg + py + po + V Field		
	530	- 3.6
	500	- 4.4
	450	- 5.7
	400	- 7.4
	350	- 9.2
	300	-11.4
	250	-14.0
Ag + arg + py + V Field		
	248	-14.0
	200	-15.9
	150	-18.4
Ag + py + po + V Field		
	248	-14.0
	200	-17.1
	150	-20.9
arg + py + L_S + V Field		
	600	- 0.1
	550	- 0.5
	500	- 1.0
	450	- 1.5
	400	- 2.1
	350	- 2.8
	300	- 3.7
	250	- 4.7
	200	- 5.8
	150	- 6.0
Ag + Fe + FeS + V Field		
	600	-12.5
	500	-14.8
	400	-18.0
	300	-22.0
	200	-27.8
	100	-36.8

Table 24. Log f_{S_2} data over univariant assemblages in the Ag-Fe-S system. These data were obtained from Figure 39 as explained in the text.

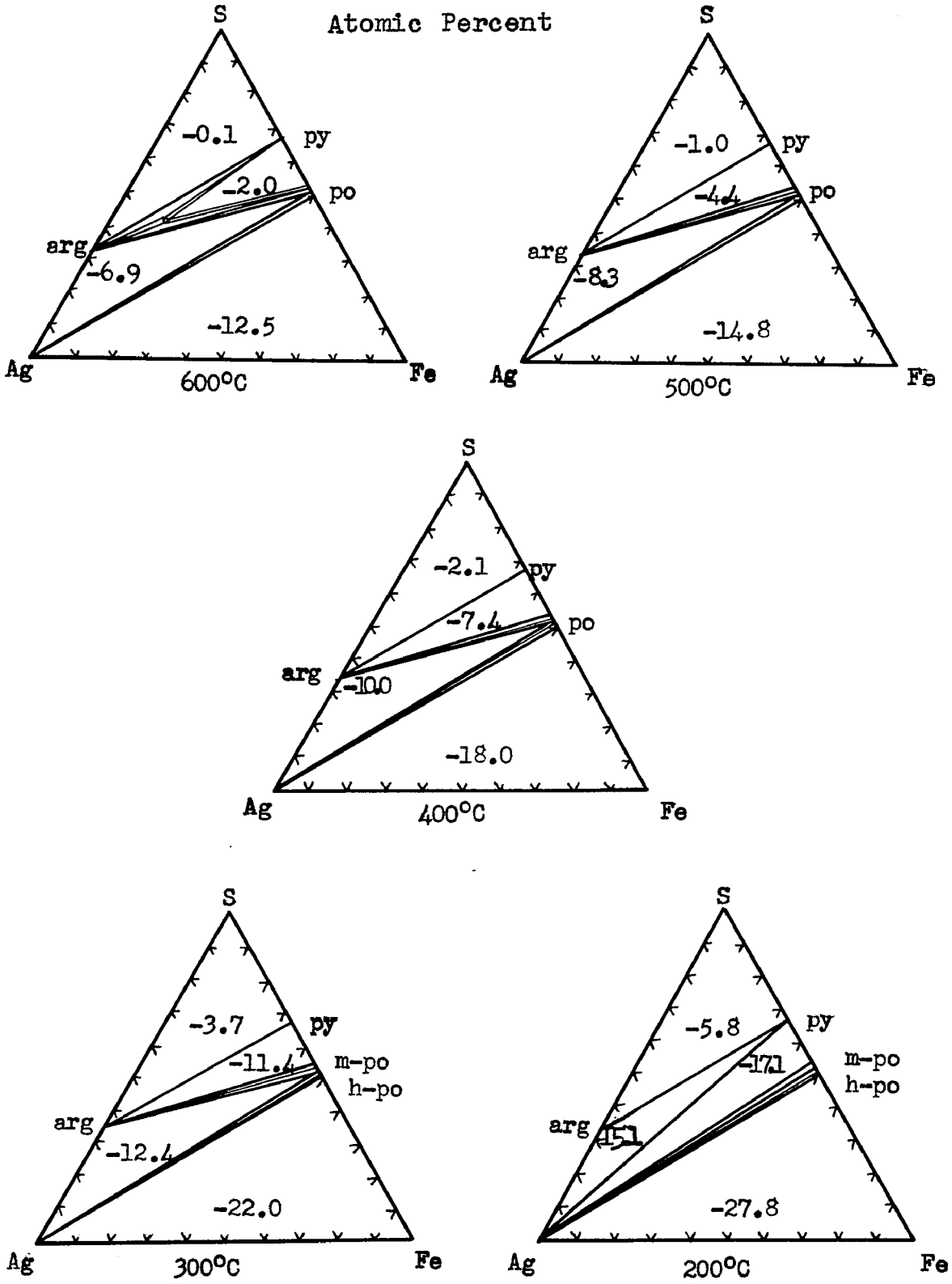

Figure 33. Polybaric, isothermal sections of the Ag-Fe-S system with log fS_2(atm.) data indicated for the various univariant fields.

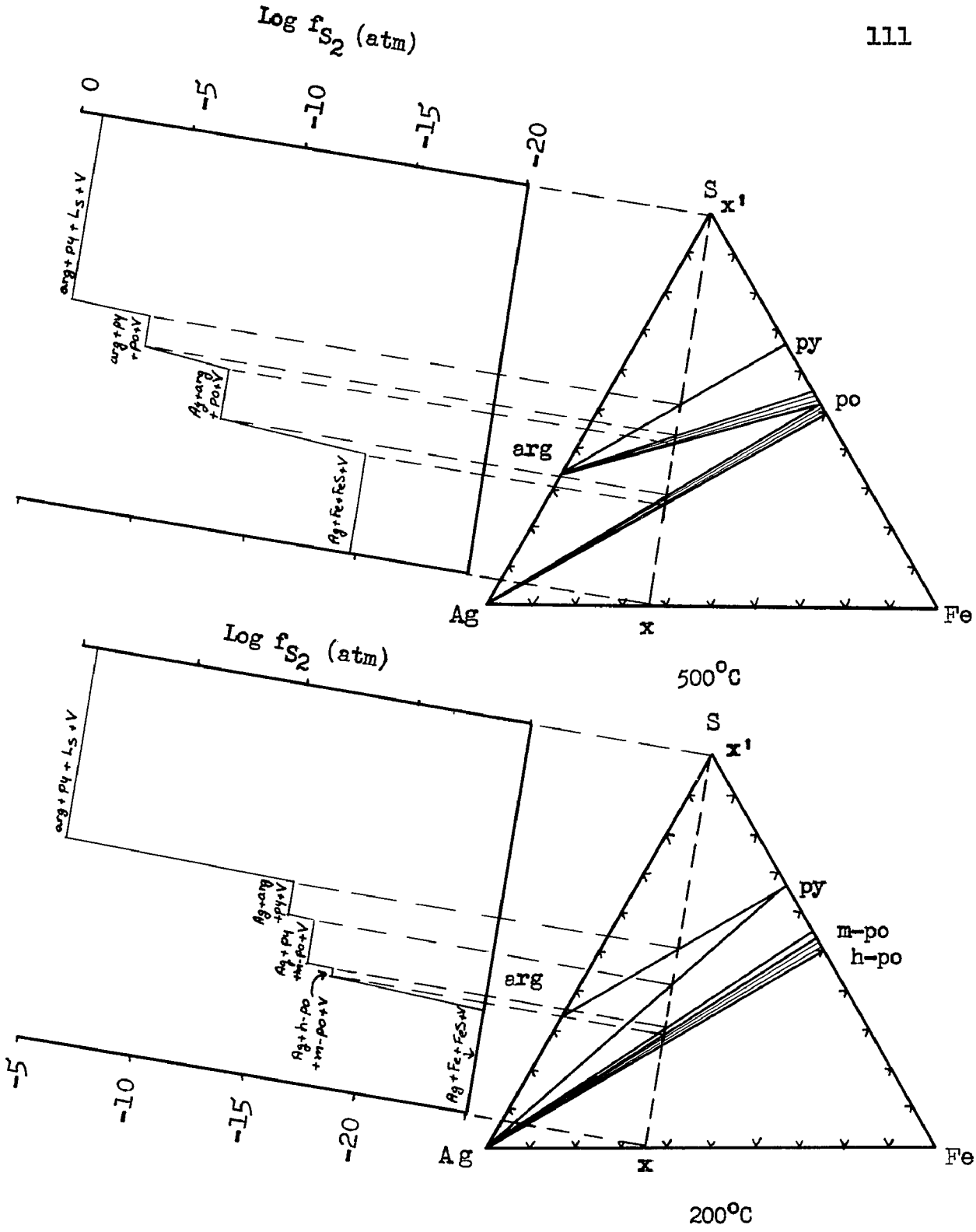

Figure 34. Schematic isotherms of the Ag-Fe-S system at 500° and 200°C with accompanying log f_{S_2} versus composition diagrams along the compositional cut x-x'.

through the system (e.g., Figure 34, X-X'). With this procedure, the compositional variable can be restricted to two components (one independent variable) and a P-X plot can be constructed at various selected temperatures.

A compositional cut in the Ag-Fe-S system was chosen to pass from sulfur through the reaction point of arg + m-po ⇌ Ag + py (248±8°C) at $Ag_{36.4}Fe_{21.2}S_{42.4}$. Figure 34 depicts such a cut and the accompanying log f_{S_2}-X plots.

The step-like change of f_{S_2} with composition illustrates the principle that at a given temperature, the vapor pressure over a univariant field is constant (independent of composition). A univariant assemblage, by definition, possesses one degree of freedom and if temperature is fixed, the variance is reduced to zero and the vapor pressure cannot vary over the assemblage, regardless of the relative proportions of the condensed phases.

Figure 34 also depicts another principle of phase chemistry. Two fields with the same degrees of freedom cannot be ajoining but must be separated by assemblages with a variance of one above or below that of the fields in consideration. For example, univariant fields are separated by divariant assemblages. Examination of these graphs will show that the size of the "steps" vary greatly but the sequence is for "flat-rise-flat-...".

At the temperatures used for the graphs of Figure 34, the fugacity of S_2 species is 99.9+% of the total sulfur

pressure in all fields except those involving sulfur-rich liquid as a phase. As the sulfur fugacity approaches the sulfur-condensation curve, the percentages of sulfur species other than S_2 increases (see Figure 27, page 90). It is assumed that the f_{S_2} of the arg + py + L_S + V assemblage is not significantly different from the f_{S_2} of the pure L_S + V assemblage.

GEOLOGIC APPLICATIONS

Introduction

In recent years several publications have been devoted to the application of experimentally determined sulfide systems to ores. Inherent in these attempts are certain basic scientific principles and certain necessary assumptions. Many geologists seem reluctant to accept the results of investigations based on synthetic minerals, especially if these minerals were produced in dry systems. This aversion is a result of incomplete understanding of the various parameters which control mineral stabilities. The experimentalist tries to create certain mineral assemblages in the laboratory under rigidly controlled conditions and to define these assemblages in terms of the most significant physical-chemical variables. He must evaluate the presence of certain fugitive components such as water, and thereby reduce natural assemblages to their least complicated form. With the necessary precautions, the laboratory derived data can be used to limit the physical-chemical environment of ore genesis.

The phase relations as determined in "pure" anhydrous systems are unchanged by the presence of water or other components provided these elements and compounds do not participate in the compositions of any of the minerals or phases. These inactive components may greatly affect the kinetics concerned with the attainment of equilibrium; however, they

cannot affect the state of this equilibrium. In sulfide systems, the presence of volatiles such as water can influence phase relations involving melts; the magnitude of this effect is largely dependent on the solubility of the volatile in the liquid. In contrast, these volatiles cannot influence subsolidus equilibria if they do not appear as components in the solid phases. Therefore, the presence of non-participating (i.e., inactive) volatiles is immaterial.

Vapor is an inherent phase in silica-tube experiments. The vapor pressure associated with most metals is low, with the result that the composition of the vapor in most sulfide systems is almost entirely sulfur. Therefore, the vapor pressure of sulfur is effectively equal to the total pressure. In nature this is never attained. Kullerud and Yoder (1959) discuss this fact and illustrate the principle that vapor pressures of sulfur less than total pressure simply lower the upper stability of a phase(s). Therefore, the temperatures of reactions points determined by silica-tube techniques provide maxima for the lower-temperature and minima for the higher-temperature assemblages, in the presence of vapor.

The total pressure over a natural assemblage may be sufficient to prevent the formation of a vapor phase. The effect of total or confining pressure upon a reaction involving only condensed phases can be expressed by the Clapeyron equation. The vaporless curves for sulfide and sul-

fide-type phase assemblages commonly reflect only small pressure effects on the reactions involved (i.e., slopes of 10-20°C/Kbar P_t).

Trace amounts of elements in sulfide systems usually do not affect phase equilibria significantly. The effects can be evaluated in a semi-quantitative manner by careful considerations but may require experimental verification before extensive application of the phase data.

One of the principle objectives of an investigation such as the present study is to determine the physical-chemical nature of the ore-forming fluids that resulted in the mineral assemblages of a deposit. A thermodynamic variable which is applicable to both hydrous and anhydrous systems is necessary for a correlation between mineral stabilities and the composition of aqueous solutions. Several recent papers have discussed this problem, notably those by Barnes and Kullerud (1961), Gustafson (1963), Barton and Toulmin (1964), and Holland (1965), and have emphasized the fact that partial pressures of various molecular species provide this parameter. In many sulfide systems the composition of the vapor phase makes the partial pressure of sulfur a convenient variable to determine. Applications of thermodynamic studies of sulfides are not restricted to reactions involving a vapor phase but are valid regardless of the chemical form in which sulfur is present——as HS^- in aqueous solution, S_2 or H_2S in a gas or vapor, etc. (Barton and

Toulmin, 1964). The activity of a gas by definition is numerically equal to its fugacity. Thus, the fugacity of sulfur over a sulfide assemblage is equal to the activity of sulfur necessary for the equilibrium formation of that assemblage and is a limiting parameter of the ore-forming fluid.

The application of data from any one ternary sulfide system cannot solely determine the possible conditions of ore formation. These data must be integrated with information on other systems, non-sulfide as well as sulfide. Therefore, in the following sections, several significant points of geologic interest from the present investigation will be discussed briefly with appropriate examples from nature. The silver deposits of Cobalt, Ontario, will be discussed at some length and used to demonstrate the combined usage of various types of thermodynamic data in an effort to delineate ore-forming conditions.

Binary Phases

The phase relations in the low-temperature (i.e., <320°C) portion of the Fe-S system are not known with certainty. However, several points of significance have evolved during the present study.

The upper stability of monoclinic pyrrhotite is uncertain; several experiments conducted at temperatures above 285°C would seem to indicate that the pyrite-hexagonal pyrrhotite mineral pair is present, thereby, negating the presence of monoclinic pyrrhotite above that temperature. It is therefore suggested

that the upper stability of monoclinic pyrrhotite is below 285°C. This supports the findings of Kullerud et al. (1963) on natural monoclinic pyrrhotites. It would also appear that monoclinic pyrrhotite, which usually is referred to as having Fe_7S_8 composition, forms measurable solid solution towards pyrite. This conclusion was also reached by Hall and Yund (1966).

Carpenter and Desborough (1964) stated that all pyrrhotites observed in nature possess low-temperature superstructures. This necessitates that pyrrhotites originally deposited at high temperature reequilibrate upon cooling, and thus, serious doubt is cast on the use of the pyrrhotite geothermometer of Arnold (1962). Obviously, an explanation of the occurrence of these low-temperature phases involves consideration of reaction kinetics. A charge of hexagonal pyrrhotite of Fe_7S_8 composition, formed at 600°C, placed at 300°C for 15 minutes, was observed to completely convert to the monoclinic phase. Likewise, monoclinic pyrrhotite placed at 330°C for 15 minutes converted to hexagonal pyrrhotite. These data suggest that the activation energy of this transformation is very small and emphasizes the doubt of ever finding a pyrrhotite phase in nature which has not reequilibrated to a low-temperature phase(s).

Monoclinic pyrrhotites made during this study were observed to have 408 and $\bar{4}08$ X-ray diffraction peaks with unequal intensities. Commonly, an assemblage of hexagonal

pyrrhotite and monoclinic pyrrhotite results in a larger 408 than $\bar{4}08$ peak. This increased intensity is a result of a superposed 10•2 reflection from the hexagonal pyrrhotite and 408 reflection of the monoclinic phase. However, charges of Fe_7S_8 composition annealed at temperatures of 225±25°C commonly possessed monoclinic pyrrhotite with a $\bar{4}08$ peak (the higher angle 2θ reflection) larger than the lower angle 408 peak. Experiments conducted at 150°C contain monoclinic pyrrhotite with approximately equal 408-$\bar{4}08$ reflections. The exact meaning of these intensity differences are not known; Kullerud (1967a) stated that this variation in relative intensities may be due to structural changes (e.g., ordering) in the pyrrhotite and that the relative intensities may be related to the temperature of formation. This observation is not confined to synthetic products. During the present investigation, numerous specimens collected at Cobalt, Ontario, were examined and monoclinic pyrrhotite was found which yielded an X-ray powder-diffraction pattern with 408-$\bar{4}08$ reflections with intensity differences similar to those observed with the synthetic Fe_7S_8 formed at 225°C.

Careful examination of the pyrrhotites at Cobalt, Ontario, also revealed the mineral smythite, of reported Fe_3S_4 composition (Erd et al., 1957). Smythite was observed in assemblages containing monoclinic pyrrhotite, as well as other sulfides and non-sulfides. The X-ray data for this new occurrence of smythite are reported in Table 25 and com-

Table 25. X-ray powder-diffraction data for smythite from Cobalt, Ontario.

hk·l	d(obs.)Å (Erd et al., 1957)	I	d(obs.)Å (this study)	I
00·3	11.5	6	-	-
00·6	5.75	1/2	-	-
00·9	3.82	2	-	-
10·1	3.00	6	2.98	6
01·2	2.96	1/2	2.96	1
00·12	2.86	1/2	-	-
10·4	2.83	2	2.82	4
01·5	2.75	4	2.74	2
10·7	2.56	6	2.56	6
01·8	2.45	2	2.46	1
00·15	2.29	1/2	-	-
10·10	2.26	6	2.24	4
01·11	2.16	4	2.15	2
10·13	1.979	7	1.983	5
00·18	-	-	-	-
01·14	1.897	8	1.903	4B
10·16	-	-	-	-
11·0	1.732	10	1.732	10
11·3	1.715	1/2	-	-
01·17	1.687	1/2	-	-
11·6	1.672	4	1.664	2
00·21	-	-	-	-
11·9	1.577	1/2	-	-
10·19	1.546	1/2	1.549	1
02·1	-	-	-	-
20·2	1.496	1/2	1.499	1
01·20	1.496	-	-	-
11·12	-	-	-	-
02·4	-	-	-	-
20·5	1.465	1/2	-	-
00·24	1.435	2	-	-
02·7	-	-	-	-
20·8	1.427	6	1.427	3
02·10	1.375	1/2	1.373	1
20·11	1.351	1/2	1.349	1/2

pared to the X-ray data for smythite from the first described occurrence collected from a geode at Bloomington, (Erd, et al., 1957). An important feature of the Cobalt smythite is the complete absence of basal reflections. Dr. H. T. Evans, Jr. (personal communication, 1967) believes that this is due to some disorder in the atomic sites. Research concerning this new occurrence of smythite, a revision of the smythite structure, the mineral associations, stability, etc. is underway.

Aqueous experiments (page 35) conducted during the present study suggest that smythite is not stable in the Fe-S system at 100±10°C or above. Samples of metal-deficient pyrrhotite synthesized at high temperature, exsolved pyrite and monoclinic pyrrhotite, at 100±10°C. This does not completely negate the possibility of smythite stability at this temperature, however. The py + m-po may be exsolving metastably and the kinetic factor of nucleation may be hindering the formation of smythite.

Smythite should be much more common in nature than observed to date. It is optically and physically indistinquishable from monoclinic pyrrhotite and would be identified as pyrrhotite if not submitted to X-ray diffraction analysis. Also, smythite should form from monoclinic pyrrhotite + pyrite deposited above 100°C, by reequilibration with decreasing temperature; however, pyrite at these low temperatures is reluctant to participate in any reaction. If smythite cannot

form by reequilibration but must be deposited from a solution at some temperature <100±10°C, the presence of this mineral in an ore assemblage is noteworthy. Another explanation for the paucity of smythite in nature may be found in the kinetics of its nucleation. Perhaps, smythite nucleates so slowly that metastable monoclinic pyrrhotite + pyrite are deposited instead.

The presence of silver in solid solution was not observed to have any measurable effect on the phase relations in the Fe-S system. Ternary reactions involving pyrite and pyrrhotite were not observed to differ markedly in reaction rates from binary reactions, the $\underline{d}_{(10\cdot2)}$ values of pyrrhotite in po + py + Ag-bearing phase + V assemblages are the same as on the Fe-S join, and the melting point of pyrite in the presence of an Ag-bearing phase is not measurably different from 743±2°C.

The term "argentiferous pyrite" is well established in the literature and refers to pyrite which is thought to contain an appreciable amount of silver in solid solution. Petruk (1964) described a pyrite concentrate from a Bolivian mine which contained 163 oz. Ag/ton; this would correspond to about 0.8 at.% Ag in solid solution. Data from the present study demonstrate that the Ag solubility in pyrite at 600°C is considerable less than 0.2 at.%; in fact, the amount of Ag in solid solution is too small to influence the cell dimension of pyrite. The term "argentiferous" is

incorrectly applied to pyrite, and close examination with oil-immersion objectives of well-prepared polished sections of "argentiferous" pyrite reveals the presence of an admixed silver-bearing phase. A sample of the Bolivian pyrite concentrate was obtained from W. Petruk and examination of polished sections revealed the presence of small inclusions of sphalerite and questionable native Ag. Specimens of pyrite from Texas Gulf Sulfur's Timmons, Ontario, deposit show many small specks of native Ag which could go completely unnoticed by a cursory optical examination.

The inversion of Ag_2S from a bcc to monoclinic structure at 177±1°C produces inversion twinning. The presence of twinning in natural Ag_2S has been used as criterion for initial deposition above this temperature (i.e., as argentite). The present study has shown that twinning is also developed in Ag_2S well below this inversion temperature and is retained upon cooling to room temperature. These data negate the use of twinning in Ag_2S as evidence for formation of argentite until such time as criteria are established to distinguish inversion twinning from this lower-temperature twinning.

The inversion of $Ag_{2\pm x}S$ from a fcc ⇌ bcc structure occurs at 586-622±3°C on the Ag-S join. During the present, the presence of iron was observed to lower this inversion greatly——e.g., $Ag_{2+x}S$ from 586±3°C on the binary join to 518±2°C in the ternary system. However, the effect of iron on the monoclinic ⇌ bcc inversion was not measurable and

this inversion remains at 176±3°C in the presence of an iron-bearing phase.

Ternary Phases

The ternary minerals sternbergite and argentopyrite (both $AgFe_2S_3$) are stable somewhere below 152°C (see page 86). Samples of these minerals were broken down in silica tubes at 200°C and the products annealed at 100±10°C for 358 days, at which time there was no evidence of reaction of the products to reform the $AgFe_2S_3$ compounds.

The invariant reaction Ag + py + po ⇌ $AgFe_2S_3$, associated with the formation of the $AgFe_2S_3$ phase, is also of geologic significance. The temperature of this invariant point, here stated as less than 152°C, is a minimum for the Ag + py + po assemblage in nature. During the present study, examination of ore specimens and the literature concerning Ag-bearing ores, showed no well-documented occurrence of this assemblage in nature. Instead, various assemblages of sternbergite and/or argentopyrite and one or two of these minerals coexist. This observation suggests that the Ag + py + po deposited in nature has reequilibrated to a low-temperature assemblage containing $AgFe_2S_3$ compound.

The "silberkies" minerals are commonly reported (Ramdohr, 1955, 1960) as among the last to form in the paragenetic sequence of silver-bearing deposits. These minerals are stated to be much more common than previously reported or believed (Ramdohr, 1960; personal communication, 1967); they

may have been frequently overlooked or misidentified because of their small grain size and/or optical properties, which are similar to pyrrhotite and marcasite. The "silberkies" minerals are common in many typical epithermal deposits. However, they have also been reported from deposits classed as hypo- and meso-thermal. The deposits of Broken Hill, Australia, (mentioned previously) believed to have been formed at high temperatures and pressures, contain scattered grains of sternbergite (Stillwell, 1953). The presence of this mineral shows that the ore-forming processes were still active far below the temperatures of the initial formation of the early mineral phases.

Ternary Assemblages

Several invariant reactions in the Ag-Fe-S system are of geologic significance. The temperatures of 622±2°C, 607±2°C and 532±2°C, the upper stabilities, in the presence of vapor, of arg + po, arg + py, and arg + py + po, respectively, are generally higher than those attained during deposition of typical silver ores. Because these reactions involve ternary liquids, water, if soluble in this liquid, may lower the temperatures at which the reactions occur and they may have limited applicability.

The deposits at Broken Hill, New South Wales, Australia, ores of Pb, Zn, and Ag, are often cited as examples of hypothermal ore deposits. Ramdohr (1950, 1954) believed that these ores, subsequent to initial deposition, have been meta-

morphosed at high temperatures and pressures. He observed antimony which he interprets as having been partially melted, as well as pyrargyrite which had been completely melted, indicating a temperature of approximately 630°C. Edwards (1956), based on iron and manganese content of sphalerite, concluded a temperature of 600°C or higher, in agreement with Kullerud (1953), who estimated 620°C (without correction for pressure). Under conditions such as these, an arg + py + po assemblage could be expected to melt. Such an assemblage would probably consist mainly of pyrite and pyrrhotite with little argentite and the amount of liquid generated would be small; however, this liquid would be very rich in silver. This melt could conceivably undergo movement, thereby, effecting a remobilization of some sulfide minerals as well as bringing about an enrichment of silver. Thus, sulfide fluids may, indeed, play an important part in ore genesis as postulated by Brett and Kullerud (1967).

The reaction arg + po ⇌ Ag + py, in the presence of vapor, which occurs at 248°C is important for several reasons. As a general rule, it is exceptional in sulfide systems that a metal is stable with a disulfide, particularly pyrite. Most metals are very "sensitive" to even low fugacities of sulfur as would be depicted by an log f_{S_2} versus 1/T plot of the appropriate M + M_xS + V curves (e.g., Fe + FeS + V, Figure 39, page 142). Therefore, their sulfida-

tion curves do not approach the po + py + V curve. Other metals, such as copper, which do not have strong affinities for sulfur, have ternary compounds which block tielines to pyrite. Silver is not as chalcophile as most other metals with the result that the Ag + Ag_2S + V curve crosses the po + py + V curve. The silver deposits at Pachuca and Real del Monte, Chihuahua, Mexico contain appreciable amounts of native silver (Geyne, 1963), particularly in the "oxidized" zone. This silver is considered secondary, having been derived from argentite and other silver-bearing minerals. Some of the native silver is undoubtedly secondary; however, a lack of appreciation of the silver sulfidation curve has possibly led some geologists to conclude that almost all the silver, some present in Ag + arg + py assemblages, is a product of meteoritic ground-water reduction of silver-bearing minerals.

A minimum-temperature indicator is provided by the assemblage arg + po. Examination of numerous polished sections of specimens from worldwide localities, as well as a search of pertinent literature, failed to reveal the well-documented existence of this assemblage in nature. Either reequilibration of previously formed arg + po, or original deposition of Ag + py can account for this observation. The feasibility of reequilibration was demonstrated for natural specimens (page 80).

The assemblage Ag + py is not particularly common in

nature; but, it is important in some massive sulfide deposits (e.g., Texas Gulf Sulfur's Kidd Creek Deposit, Northern Ontario, Canada). It is not necessary that silver and pyrite be deposited simultaneously for application of this invariant temperature (248°C) to ores. The phase relations define the stability of the Ag + py assemblage and are not concerned with the paragenetic sequence of the phases involved. Much of the native silver found at the Kidd Creek deposit occurs as stringers, veinlets, and blebs in pyrite. It is evident from the present study that, regardless of the formation of the other minerals of this massive sulfide deposit, the Ag + py assemblage formed below 248°C at an f_{S_2} of less than 10^{-14} atm.

Ore-Forming Solutions

The conditions of ore formation must be intimately related to the nature of the ore-forming fluids; the fugacities (activities) of the components involved in formation of a mineral assemblage can be used as limiting parameters of this solution and can describe the chemistry of formation of any given assemblage directly and quantitatively.

It should be realized that the fugacity of any component does not tell us the concentration of that component in the ore-forming solution. Figure 35 (after Barnes and Kullerud, 1961) illustrates this statement. The f_{S_2} can be seen to vary greatly in this diagram, whereas the sum of the sulfur

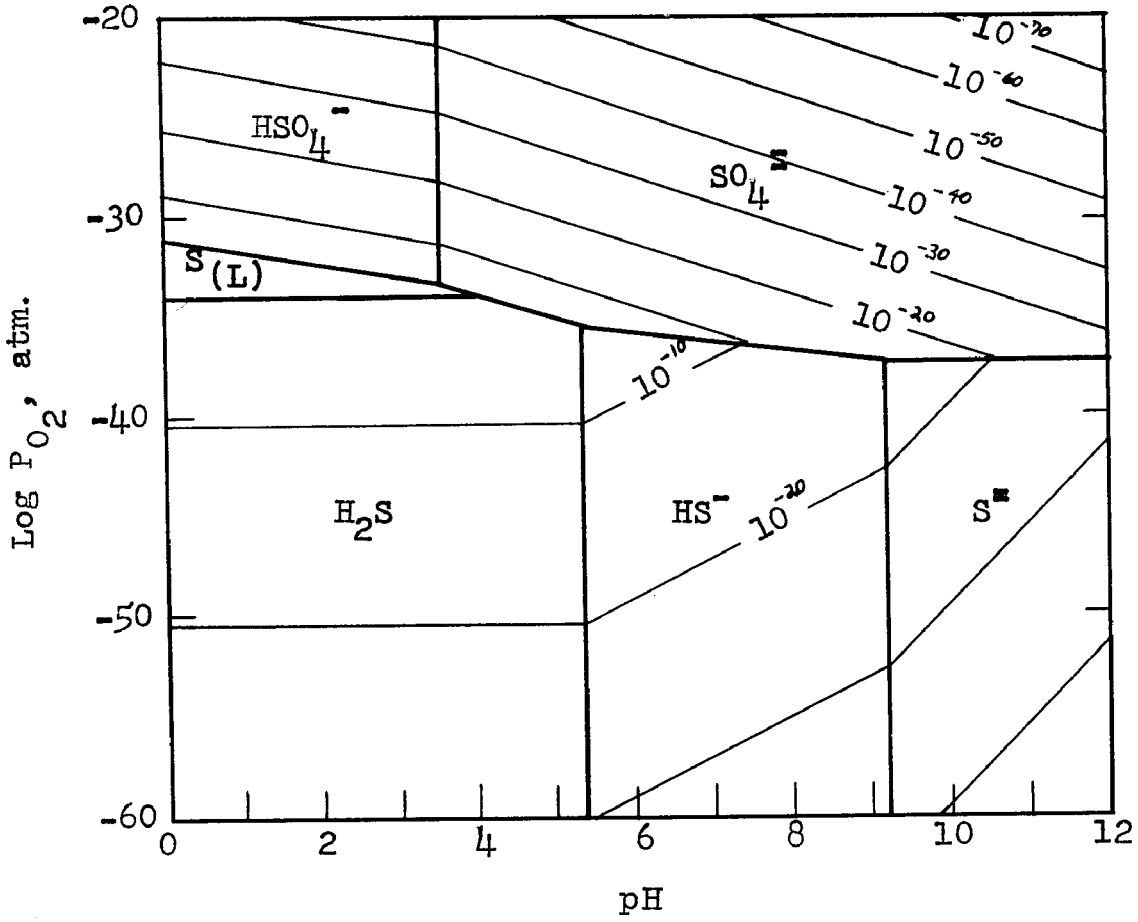

Figure 35. Distribution of predominant aqueous species and P_{S_2} (contoured in atm.) at (ΣS) = 0.1 m and 250°C (after Barnes and Kullerud, 1961).

species (i.e., HS^-, $S^=$, H_2S, etc.) at all points is constant (ΣS = 0.1 m).

Several methods are possible for presenting thermodynamic data on the formation and stabilities of minerals. Diagrams of log f_{S_2} versus 1/T provide a useful frame of reference upon which various curves representing univariant equilibria may be superposed to form a grid. This type of plot is similar to the petrogenetic diagrams as originally

developed by N. L. Bowen (1928) and presently in common use by oxide and silicate petrologists. An example of such a plot is shown in the next section on Cobalt, Ontario.

Activity versus activity plots are phase diagrams whose axes are the activities of two components of a three component system. The details of construction of such graphs are covered by Garrels (1960) and Garrels and Christ (1965) and numerous examples are given by Gustafson (1963) and Holland (1959, 1965). Such diagrams are based on the principle that the fugacity of an element is numerically equal to its activity. Figure 36 was constructed as an a_{S_2}/a_{Ag} plot of the Ag-Fe-S system at several temperatures as derived from the data compiled in Table 24, page 109. The activities of components in an ore-forming solution responsible for deposition of a particular assemblage can be read directly off the figure.

By plotting the activities of the three components of a ternary system on orthogonal axes, it is possible to construct a "saturation-surface" diagram such as depicted in Figure 37. Gustafson (1963) has discussed the possibility of the interpretation of such models as an aid to an understanding of the paragenesis of mineral assemblages.

Consider a hypothetical ore-forming solution containing, among other things, silver, iron, and sulfur. The various other possible components of the fluid phase, such as H_2O, CO_2, Cl^-, etc., are here considered as inactive for they do

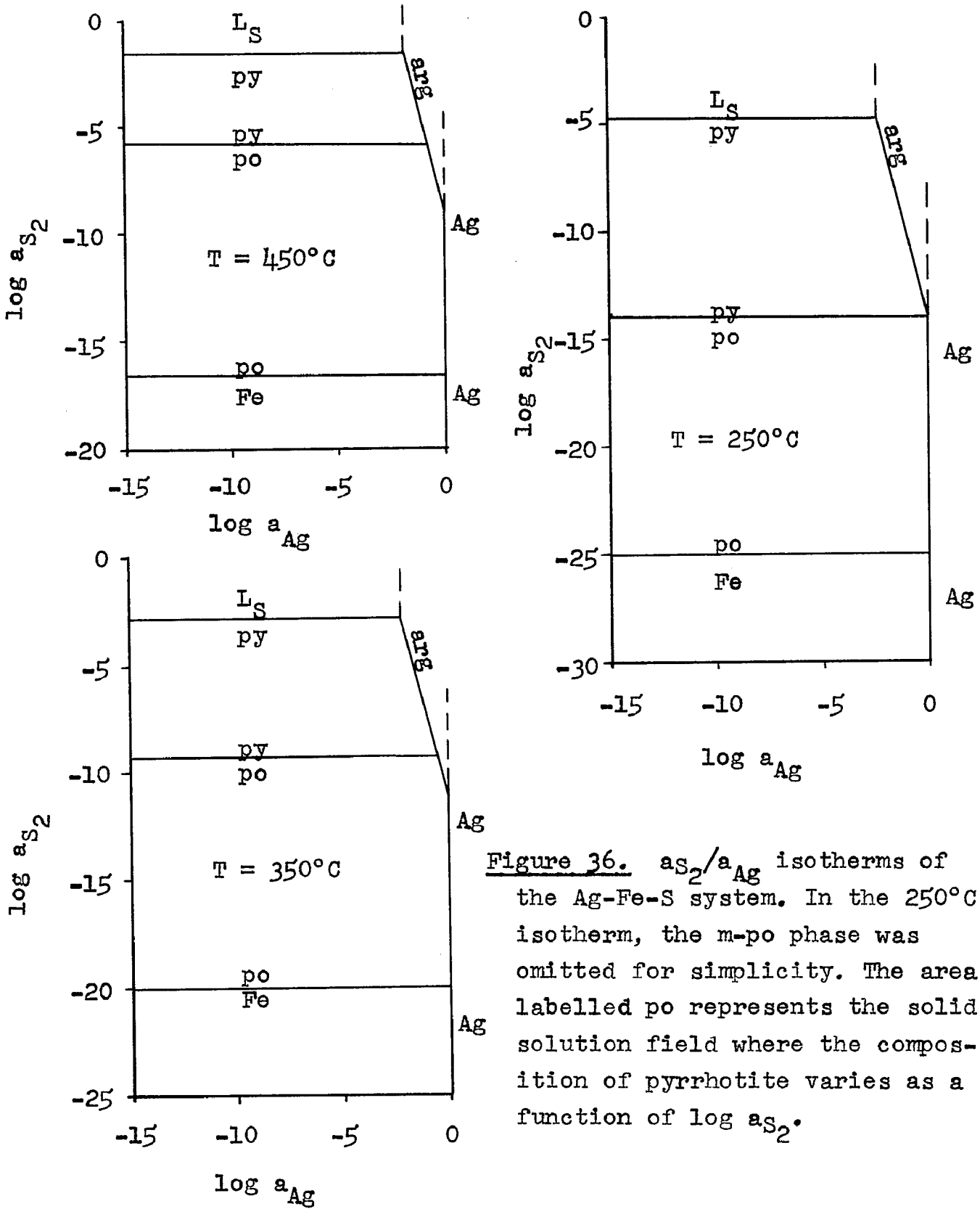

Figure 36. a_{S_2}/a_{Ag} isotherms of the Ag-Fe-S system. In the 250°C isotherm, the m-po phase was omitted for simplicity. The area labelled po represents the solid solution field where the composition of pyrrhotite varies as a function of log a_{S_2}.

not enter into the solid phases. The saturation surface shown in Figure 37 encloses a volume of space. Inside this volume the solution is undersaturated and no solid phases containing silver, iron, or sulfur are present. The volume above this surface is supersaturated, a disequilibrium situation, and will not be considered here. It is assumed that an ore phase is precipitated whenever the saturation surface for that phase is intersected --- that is, the solubility product is reached. For example, Point B of Figure 37 represents the point where pyrrhotite begins to precipitate from a solution originally at Point A. It can be assumed that the activities (fugacities) of the ore components are controlled by the external environment (e.g., composition of the fluid, temperature and pressure gradients, diffusion and reaction with the wall rocks). These are the factors which control the movement of A to B to C....Point A is inside the volume and is consequently undersaturated. The path A-B-C-D explains the sequential formation of pyrrhotite, then py + po, and finally arg + py + po. It should be remembered that the pyrrhotite forming along path B-C is constantly changing composition. As the activities of the components in solution move toward Point C, the pyrrhotite at B becomes unstable and redissolves and pyrrhotite at B' pre-precipitates, etc.*

---

* In general, if the activities of the components are lowered so that the activity product (solubility product) of some previously precipitated phase is no longer satisfied, that phase should go back into the fluid phase and be replaced by the currently stable phase(s).

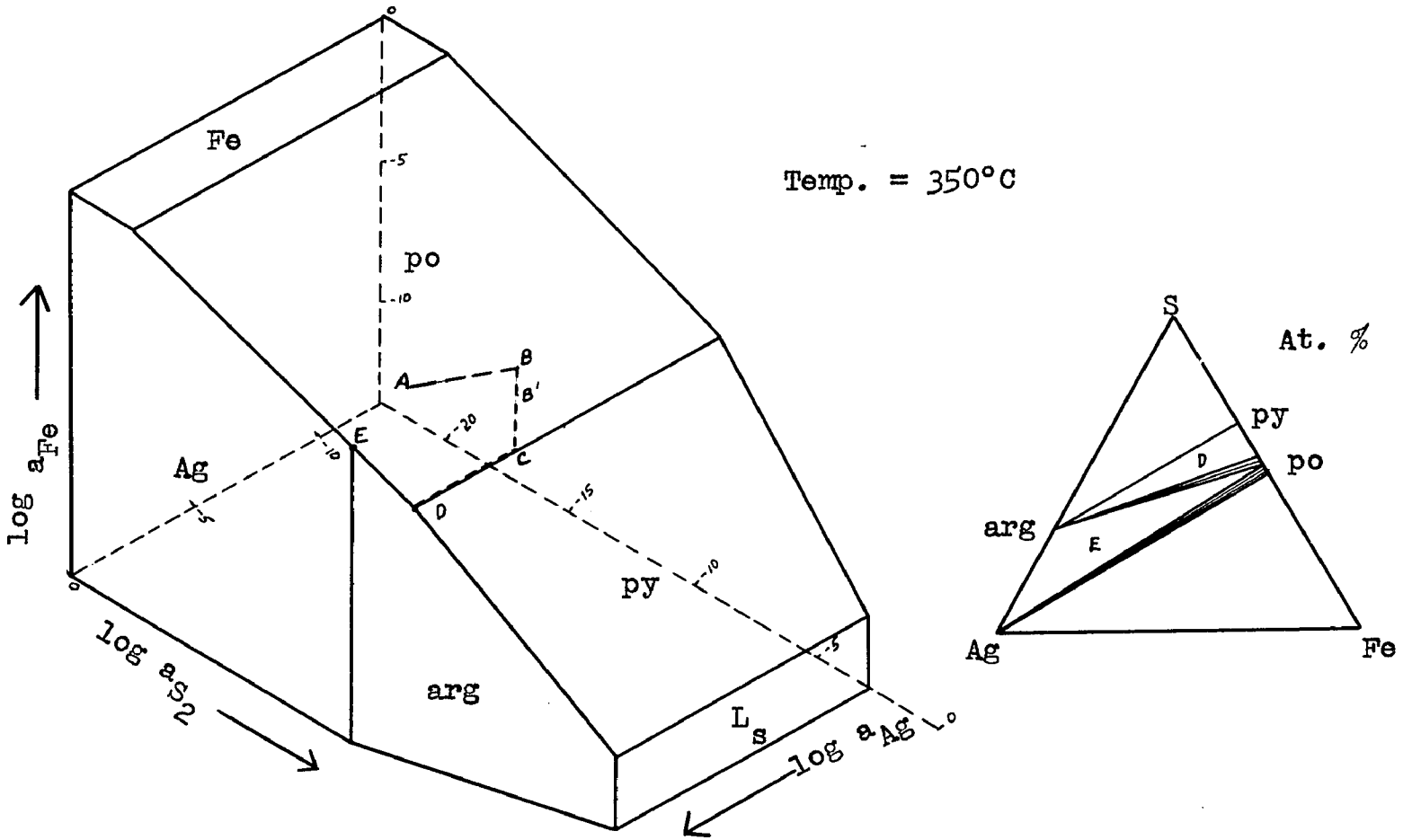

Figure 37. Saturation-surface diagram of the Ag-Fe-S system described in terms of the activities of Ag, Fe, and S_2 at 350°C. The portion of this surface which represents the stability field of each phase is a plane only if the phase is stoichiometric. Therefore, the surfaces labelled po and arg should be slightly curved, convex toward higher activities.

At temperatures below 248°C, Point D of Figure 37 will be situated so that the precipitated assemblage will be Ag + py + m-po as diagrammed on Figure 38. This portion of the diagram is most applicable to nature.

The complemented use of "saturation-surface" diagrams of several different systems can add to our knowledge of ore assemblages and their paragenesis. The principles of construction of such plots are simple and should be used to construct diagrams for other systems. However, a necessary prerequisite for their construction is a thorough knowledge of the activities (fugacities) within the systems involved. Many of these data, unfortunately, are either entirely lacking or need to be revised. The "saturation-surface" diagrams of the Ag-Fe-S system serve to illustrate the construction of this type of phase diagram and demonstrate the application of fugacity and temperature data as an aid to the understanding of ore-forming processes.

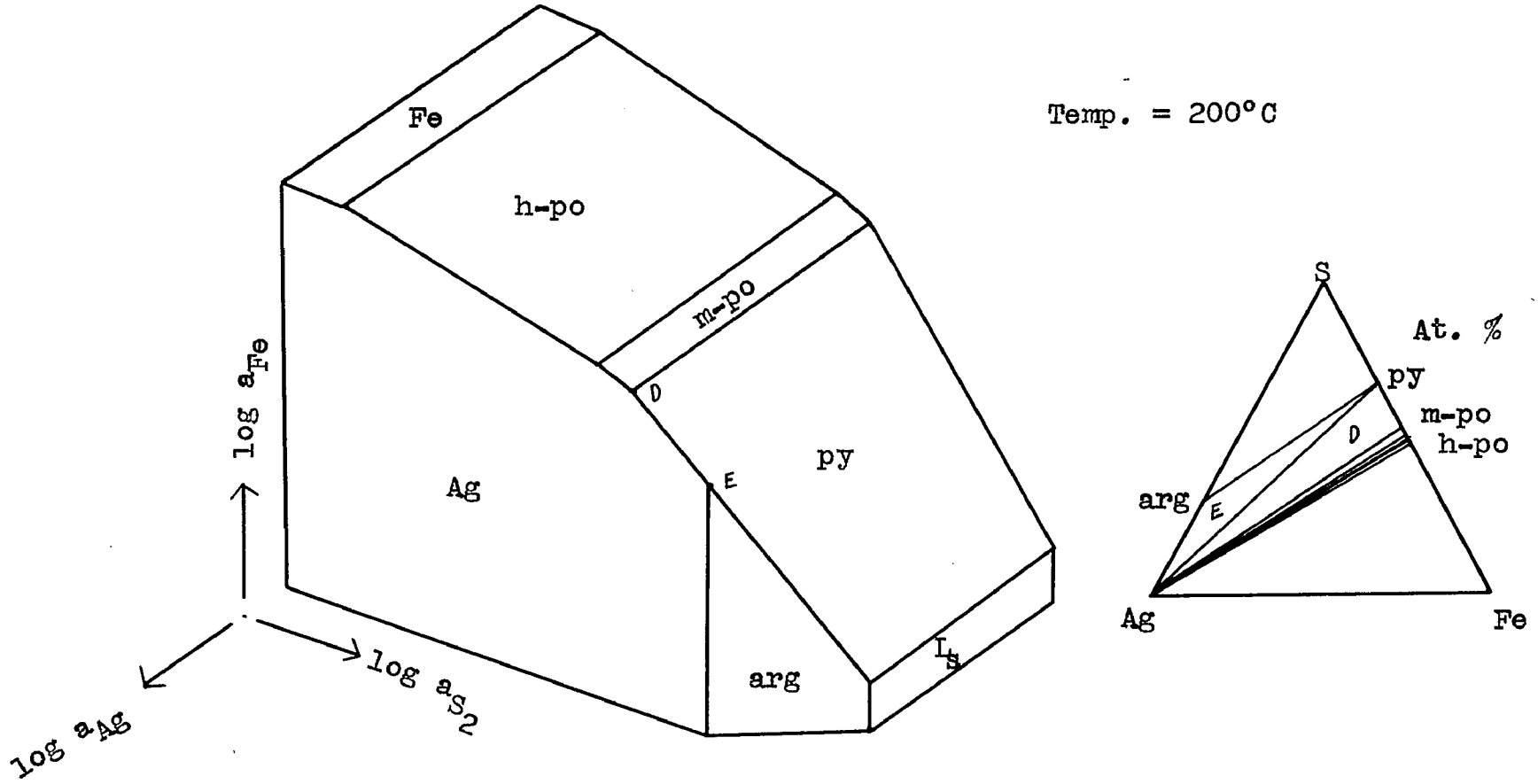

Figure 38. Saturation-surface diagram of the Ag-Fe-S system described in terms of the activities of Ag, Fe, and S_2 at 200°C. The portion of this surface which represents the stability field of each phase is a plane only if the phase is stoichiometric. Therefore, the surfaces labelled po and arg should be slightly curved, convex toward higher activities.

Cobalt, Ontario

The Cobalt district, Ontario, Canada, one of the most productive silver camps in the world, has been selected to demonstrate the applications of various types of experimental data to ores. Several mines in this district were visited and the specimens collected were subsequently investigated in the laboratory.

Geology.

The Cobalt district is underlain by three rock types. Oldest to youngest, these are: 1) Keewatin metavolcanics with interbedded iron formation; 2) Cobalt series sediments, consisting of boulder conglomerate, greywacke, slate, and quarzite; and 3) the Nipissing diabase which is present as a sill about 1000 feet thick. The detailed geologic setting of Cobalt is described by Thompson (1957).

The silver veins at Cobalt are fault and joint fillings varying from a fraction of an inch to over 12 inches in width. Attitudes are nearly vertical with strikes, in general, N to NW, and the veins are up to several hundred feet, in both vertical and horizontal extent. A set of post-ore fault veins cross and displace (on the order of inches) the major ore veins, and vary in attitude from vertical to horizontal. It is generally believed that both types of veins are genetically related to the diabase, although the exact nature of this association is not definite. Thompson (1957) believes that the ore-forming solutions were derived from the

magma which solidified to form the diabase sill.

Mineralogy of the Veins

The deposits consist of mineralized carbonate veins in which the mineral associations gradationally change from the central portions to the terminal portions and edges (Petruk, 1966). The central portions consist mainly of native silver and cobalt-nickel-iron arsenides and sulfarsenides in a carbonate matrix (commonly calcite, but often dolomite or siderite with rare quartz). In contrast, the terminal portions and edges are generally much higher in sulfide content but lower in native silver and the cobalt-nickel arsenides. The exact paragenesis is not agreed upon; however, a general trend may be stated as, early calcite, Co-Ni-Fe arsenides and sulfarsenides with native silver, and more sulfides in carbonate matrix.

Metallic Minerals and Assemblages

The metallic minerals in the veins at Cobalt occur in a wide variety of textures which have been described by Petruk (1966). The principle metallic minerals are native silver, safflorite, cobaltite, loellingite, arsenopyrite, and skutterudite. Important accessory minerals are dyscrasite, bismuth, "argentite", ruby silvers, stephanite, chalcopyrite, pyrrhotite, pyrite, sphalerite, niccolite, rammelsbergite, galena, and breithauptite. Various ore-mineral assemblages and their implied temperatures of formation are listed in Table 26. Some of the more important associations

Mineral Assemblage	Temperature Implication °C	Reference
asp + py	< 491±12°	Clark, 1961
proustite	< 495±1°	Roland, 1966
proustite + arg	< 469±3°	Roland, 1966
Ag + asp	< 440±25°	Taylor, unpublished
gn-matildite + Ag	< 380°	Craig, 1965
Ag + Bi	< 262°	Petrenko, 1906
Ag + py	< 248±8°	this study
xanthoconite	< 192±10°	Hall, 1966
proustite + Ag	< 192±8°	Roland, 1966
"silberkies"	< 152±5°	this study
mckinstryite	< 94.4±1.5°	Skinner et al., 1966
smythite	< 100°	this study, Kullerud, 1967a
Ag + Ag_6Sb	> 400°	Somanchi & Clark, 1966
Ag + Ag-Sb phases	> 275-350°	Carpenter & Fisher, 1932
gn-matildite (exsoln.)	> 215±15°	Craig, 1965
arg (cubes)	> 177±1°	Kracek, 1946

Table 26. Minerals and assemblages found at Cobalt, Ontario and the temperature implications regarding their formation (uncorrected for pressure).

are discussed below

The common assemblage native silver + arsenopyrite was deposited both early and late in the depositional sequence. It is stable below 440±25°C (Taylor, data to be published elsewhere), in the presence of vapor. The invariant reaction: po + lo + arg ⇌ asp + Ag which occurs at this temperature is illustrated in Figure 39. Knowledge of this invariant temperature provides an additional point (±25°C) on the po + lo + asp univariant curve and allows extrapolation of this curve from 702°C (the upper-stability temperature of

arsenopyrite) to lower temperatures and pressures of sulfur (see Figure 39, page 142).

Various minerals and assemblages of the Ag-Sb system are common in the Cobalt deposits. Carpenter and Fisher (1932) described exsolution intergrowths of Ag_3Sb (dyscrasite) and antimonial silver and, based on homogenization experiments, concluded that the temperature of formation was above 275-350°C. Somanchi and Clark (1966) recently reported the occurrence of an Ag_6Sb mineral with antimonial silver. They interpreted this assemblage as having originally precipitated at a temperature "well above" 400°C.

The native silver + pyrite assemblage was observed in polished sections examined during this study and has also been reported by Bell and Thompson (1924) from a similar silver deposit 20 miles SE of Cobalt. This assemblage was intermediate to late in the depositional sequence at Cobalt; its temperature of formation must have been below 248±8°C, in the presence of vapor (this study).

Ramdohr (1955) reported the presence of "silberkies" in the Cobalt district. Examination of numerous polished sections, during the present study, has revealed the rare occurrence of one of the Ag-Fe-S ternary minerals but the very fine grain size did not permit X-ray identification of the exact species. Breakdown experiments in this study showed that both sternbergite and argentopyrite, the only two well-documented "silberkies" minerals, are stable at some tempera-

ture below 152±5°C.

Skinner (1966) described a phase $Cu_{0.8}Ag_{1.2}S$, from the Cobalt district, which he named mckinstryite (Skinner et al., 1966). This mineral is present as pure masses and single crystals with native silver and stromeyerite. It breaks down at 94.4±1.5°C to jalpaite and a cation-disordered hexagonal compound, $Cu_{0.96}Ag_{1.04}S$. It is unlikely that these two phases were originally present in exactly the correct amounts and in such close contact that they could reequilibrate on cooling to produce pure masses of mckinstryite. This suggests that the mckinstryite at Cobalt only formed directly from solution below 94°C.

During this study an apparent two-phase pyrrhotite was observed in some of the ore specimens collected in Cobalt. X-ray powder-diffraction patterns showed the two phases to be monoclinic pyrrhotite and smythite, Fe_3S_4. Smythite was originally described by Erd et al. (1957) from a geode at Bloomington, Indiana and this occurrence at Cobalt is only the second reported occurrence in North America. Low-temperature experiments conducted during this study suggest that any Fe_3S_4 phase on the Fe-S join is stable only below about 100°C. Because much of the smythite is present as single pure masses and also small crystals, it is probably that this mineral was deposited directly from solution below 100°C.

The author has also examined crystals of Ag_2S which

display cubic morphology and are thus correctly called argentite. According to the data of Kracek (1946), cubic Ag_2S must be deposited at temperatures above 177°C, and thus, its presence indicates a minimum temperature of formation for this mineral and other contemporaneous minerals at Cobalt. Argentite is usually considered to have formed in the late-intermediate to late stages of mineral deposition at Cobalt.

Galena and matildite ($AgBiS_2$) intergrowths, interpreted as an exsolution texture, have been described by Ramdohr (1938). Craig (1965) reported that this exsolution is indicative of formation of a solid-solution phase stable above 215±15°C. This exsolution product also coexists with native silver. Craig (1965) showed experimentally that a solid solution with the composition of galena-matildite in a 1:1 proportion has a maximum temperature of coexistence with silver of approximately 380°C.

In summary, formation of the silver ores at Cobalt probably occurred at temperatures from above 400°C to below 100°C. The various mineral assemblages lead to ambiguous results with regard to temperatures of formation if they are not interpreted in time-space relationships. This would require a thorough study of the mineral paragenesis and was not undertaken in this study.

Ore-forming Conditions

Various methods of presentation of data can be used to discuss the important parameters concerned with the forma-

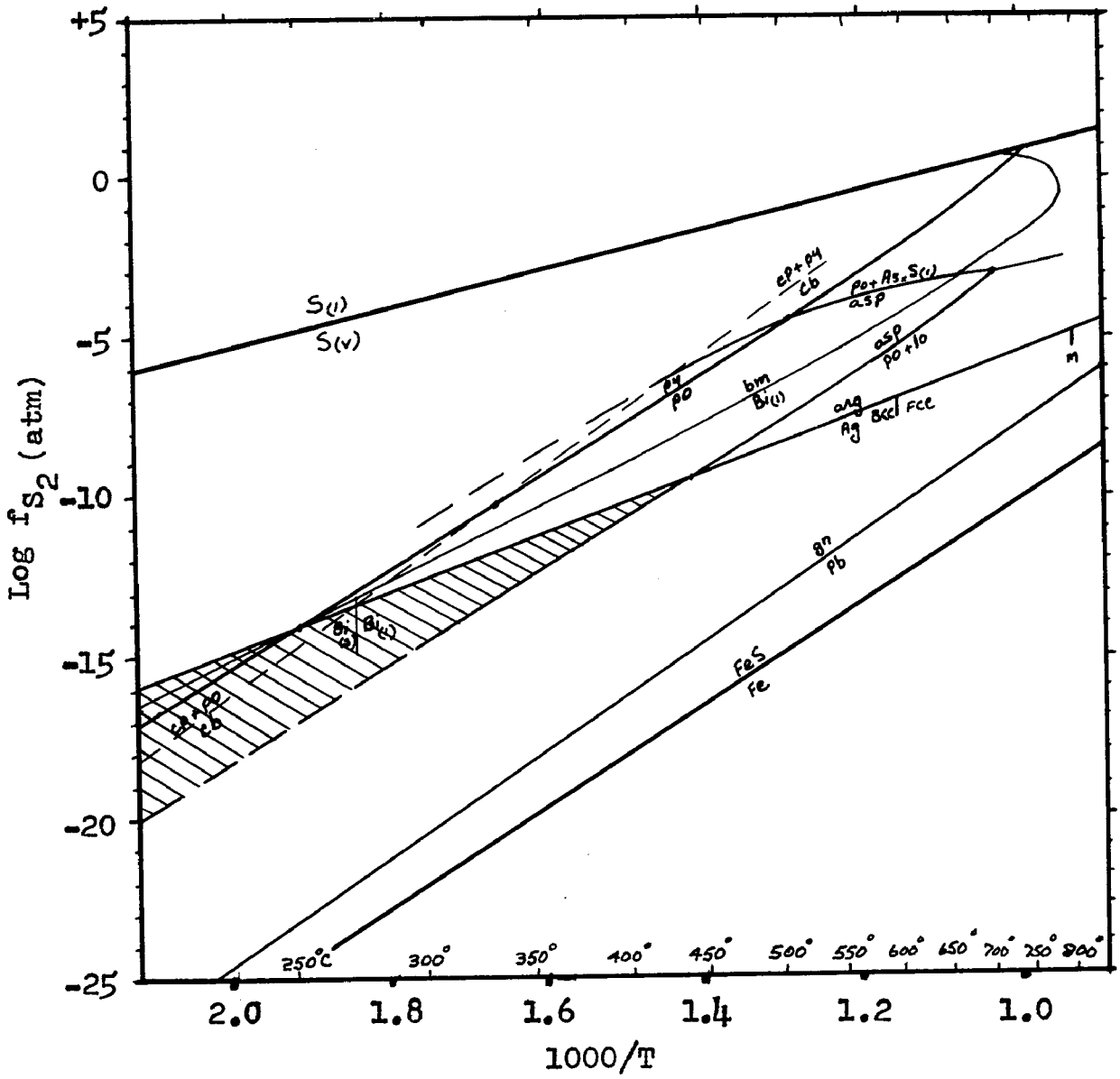

Figure 39. Log f_{S_2} versus 1/T diagram of the sulfidation curves (univariant curves) of several minerals and assemblages.

tion of an ore deposit. Two of these methods will be utilized in this discussion and will be shown that one compliments the other.

Phase relations can be depicted on a log f_{S_2} versus 1/T plot such as shown in Figure 39. One of the most important

curves on the diagram is the sulfur condensation curve. This curve marks the upper limit of sulfur fugacity pertaining during most geologic processes. Another important curve is that for the assemblage Fe + FeS + V. Most sulfide deposits formed at fugacities of sulfur above this curve, for native iron is not a common terrestrial mineral. Therefore, the region of geologic interest lies between these limiting curves.

Most of the silver in the Cobalt deposits is present in the form of native silver with only a minor amount as argentite. The region of Figure 39 which is compatible with deposition of native silver is located below (i.e., on the sulfur-deficient side) the Ag + arg + V curve. Arsenopyrite and loellingite commonly coexist with native silver throughout the paragenetic sequence. The curve asp + lo + po + V which originates at 702±2° C (Clark, 1961) and 10^{-3} atm. f_{S_2} (Barton, personal communication, 1967) intersects the Ag + arg + V curve at 440±25°C (Taylor, see above) and has been extrapolated to lower temperatures as a linear function. The ruled area of Figure 39 represents the region of f_{S_2} and temperature within which Ag + asp can stably coexist; this region involves rather narrow limits of f_{S_2} (activity). This plot illustrates the importance of fugacity data in phase equilibria studies as an aid to deciphering depositional environments.

Sulfide minerals, pyrite, chalcopyrite, galena, sphale-

rite, etc., are not common, but are locally abundant at Cobalt. They occur in a carbonate matrix which is calcite and/or siderite in association with argentite and native silver. These facts are considered in Figure 40. For purposes of the following discussion, a temperature of 250°C will be chosen to represent a temperature of deposition not imcompatible with the mineral assemblages at Cobalt.

Holland (1965) presents a compilation of thermodynamic data from which log f_{S_2}/log f_{O_2} plots can be drawn for various reactions of geologic interest. The C-CO_2 curve provides an important restriction on f_{O_2} because the absence of carbon minerals (i.e., graphite) at Cobalt and the abundance of carbonates requires that all considerations be confined to the CO_2 side of this curve. Similarly, the lack of native sulfur also restricts this discussion to the region below the S_L-S_V curve. Figure 40 shows these two bounding curves, as well as several other curves of interest.

It was determined during the present investigation that Ag + py are stable below 248°C. Therefore, the curve which defines the FeS_2-$FeCO_3$ assemblage must approach the Ag-Ag_2S curve at 250°C. This requires an f_{CO_2} = 10^0 atm. at 250°C. At lower fugacities, $FeCO_3$ does not plot within the area outlined by the C-CO_2 and S_L-S_V curves. At values above 10^0 atm., the FeS_2-$FeCO_3$ curve is displaced more than three orders of magnitude toward higher f_{S_2} values and is not near the Ag-Ag_2S curve.

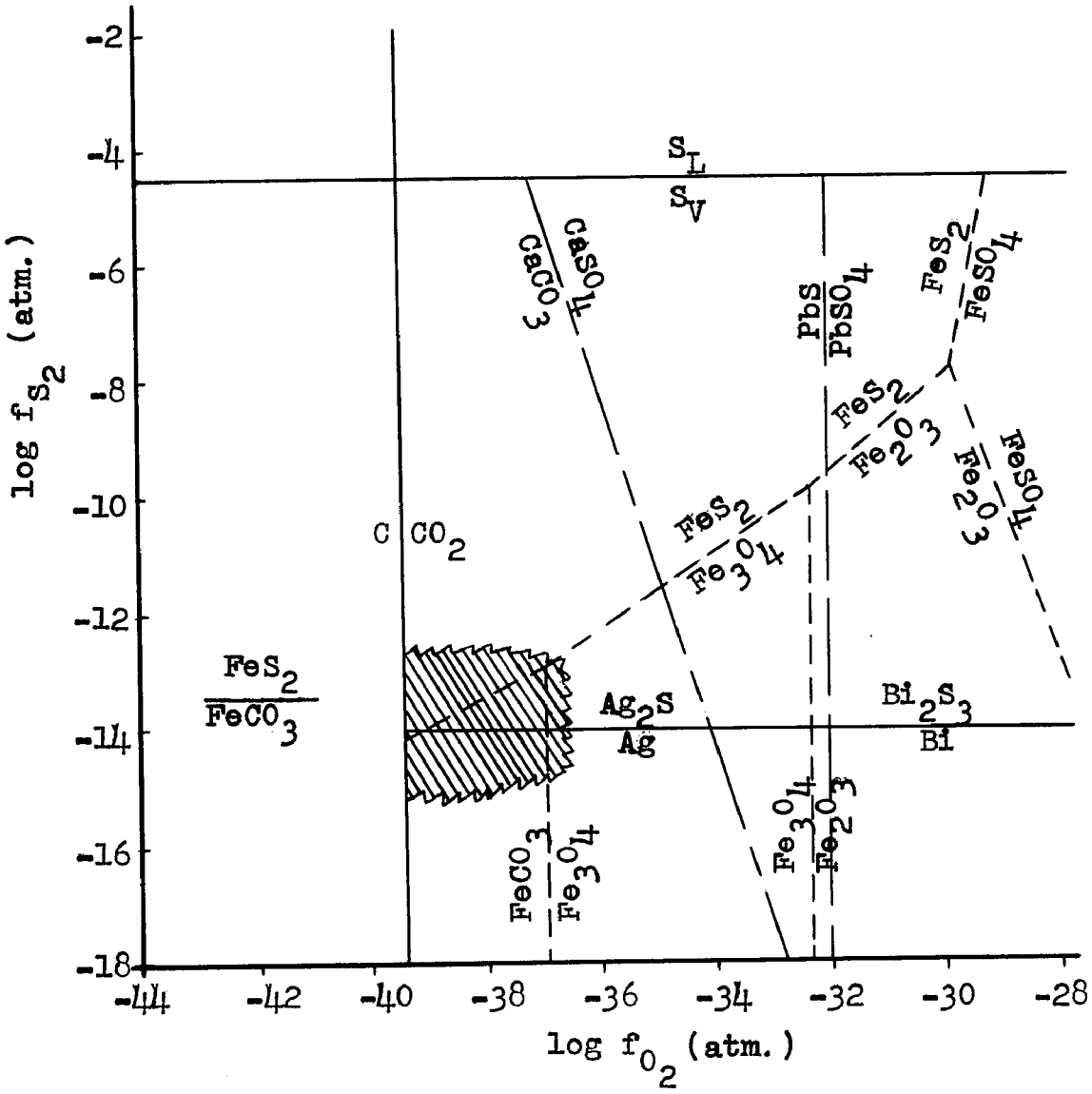

Figure 40. Mineral Equilibria at 250°C and f_{CO_2} = 10° atm. No silica present. The ruled area represents the region of mineral deposition at Cobalt, Ontario. Diagram is based on thermodynamic data from Holland (1965).

Considerations of the minerals and mineral assemblages deposited at Cobalt at a temperature of 250°C and $f_{CO_2} = 10^{0}$ atm. result in the placing of certain restrictions upon deposition as shown in Figure 40. Based on the further assumption that the fugacity of water in a vapor phase in equilibrium with an ore-forming solution at 250°C is about 40 atm. (i.e., the same as the vapor pressure of pure water at 250°C) and not correcting for P_{total}, a number of important parameters of the solution may be determined:

Temp. = 250°C (assumed)

$f_{S_2} = 10^{-14}$ atm.
$f_{O_2} = 10^{-38}$ atm.
$f_{SO_2} = 10^{-13}$ atm.
$f_{CO_2} = 10^{0}$ atm.
$f_{H_2} = 10^{-1}$ atm.
$f_{H_2S} = 10^{-2}$ atm.
$fH_2O = 10^{1.6}$ atm.

All of the species calculated are not necessarily present; however, those that are, will have the fugacities (= activities) given above. Further, if the $\Sigma S = 0.1$ m in the solution, reference to Figure 35, page 129, would suggest that the major sulfur species in the solution is HS^- at a pH of about 8.

Note that the $f_{S_2} = 10^{-14}$ atm. obtained by inspection of the log f_{S_2}/log f_{O_2} plot of Figure 40 is in agreement with the value which would be obtained by consideration of the Ag + asp assemblage at 250°C on the log f_{S_2} versus 1/T

plot of Figure 39.

Because ore-forming solutions may vary in composition from place to place at any given time, it is difficult to make generalizations concerning a_{S_2}, a_{O_2}, a_{Ag}, etc. For consideration of temperatures different from 250°C, it is only necessary to recalculate the various parameters of interest. Also, little thermodynamic data are available concerning the arsenide minerals (safflorite, loellingite, etc.), which are very important at Cobalt, making it difficult to estimate arsenic fugacities (f_{As}). The preceeding analysis of the Cobalt deposits has involved an approach to a better understanding of an ore-forming environment, and the results are open to all the inaccuracies that are inherent in the thermodynamic data. However, the general agreement in the data is noteworthy.

METALLURGICAL IMPLICATIONS

Introduction

In recent years, metallurgists have become increasingly interested in the study of eutectic textures. The microscopic examination of a cooled eutectic charge reveals the presence of two or more phases usually intimately grown together. By controlling the solidification process, it is possible to enhance certain properties of eutectic intergrowths. For instance, Albright and Kraft (1966) and Albright et al. (1967) applied controlled solidification techniques to mixtures of iron and troilite (FeS) to create a eutectic texture which consisted of a parallel array of needles and rods of magnetic iron in a sulfide matrix. This microtexture has certain characteristics which may be of importance in the production of permanent magnets.

Kraft (1967) discussed many of the fundamentals of controlling eutectic solidification and emphasized that the field of controlled eutectic textures is still in its infancy. The controlled microtextures may possess certain magnetic, electrical, optical, thermal, and mechanical properties giving directional features to almost all of the crystalline properties of solids.

Ag-Fe-S Microtextures

During the course of the present investigation, it was observed that many of the experiments involving melts resulted in distinctive intergrowths of phases in the Ag-Fe-S

system. Several of these microtextures appear to be similar to those produced by Albright and Kraft (1966) and Albright et al. (1967) during studies of solidification characteristics of the Fe-FeS eutectic.

Intergrowths of phases such as ferromagnetic Fe and antiferromagnetic pyrrhotite with soft, malleable phases such as silver and argentite possess magnetic, electrical, metallographic, and crystallographic characteristics which may have possibilities for industrial applications especially in the fields of electronics and solid-state physics.

Solidification of the melts in experiments conducted during the present investigation was not directionally controlled by intentional temperature gradients or slow cooling rates. The experimental charges were rapidly chilled from the annealing temperature to 25°C by immersion of the silica tubes in cold water. During the 3-5 second cooling time, the liquid nearest the wall of the tube cooled faster than the interior of the charge. In most experiments this slight difference in cooling rate, was sufficient to set up a temperature gradient which produced effects similar to those observed with controlled solidification (Kraft, 1967). That is, certain phases were oriented with respect to the gradient direction.

Photos of some of the interesting quench microtextures observed as a result of crystallization from melts in the Ag-Fe-S system are shown below.

Plate 1. Eutectic intergrowth of argentite (gray) and silver (white). The charge ($Ag_{73}S_{27}$) was annealed at 839±3°C for 2 1/2 days prior to quenching. (x 1600 oil)

Plate 2. Eutectic-like intergrowth of pyrrhotite (gray) and silver (white) resulting from crystallization of a pyrrhotite-rich liquid. The charge (50Ag + 50FeS) was annealed at 1010±5°C for 20 minutes prior to quenching. (x 510 oil)

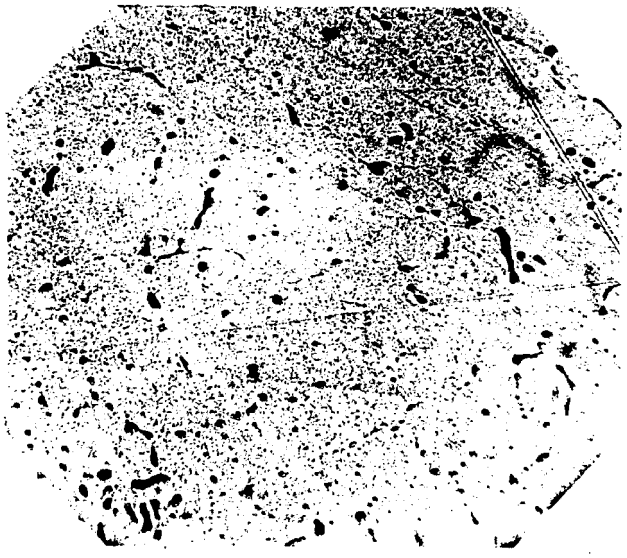

Plate 3. Intergrowth of silver (white) and pyrrhotite+ argentite (dark gray) resulting from crystallization of a silver-rich liquid. The charge ($Ag_{50}Fe_{23}S_{27}$) was annealed at 952±2°C for 1 hour prior to quenching. (x 240 oil)

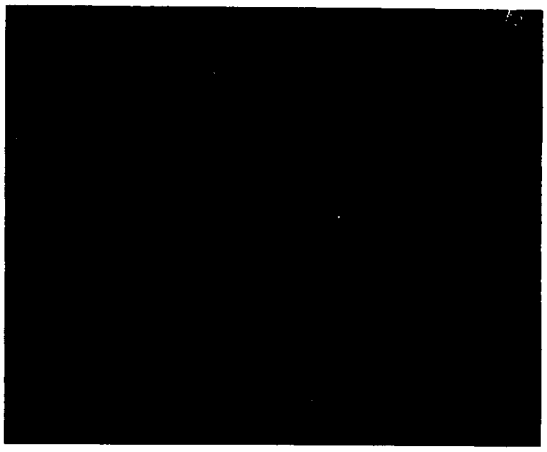

Plate 4. Eutectic intergrowth of argentite (gray groundmass) and pyrrhotite (lighter-colored stringers) and pyrite (white to light gray). The charge ($Ag_{50}Fe_{10}S_{40}$) was annealed at 630±5°C for 12 days prior to quenching. (x 1600 oil)

APPENDIXES

Appendix 1

DTA EXPERIMENTS WITHIN THE Ag-Fe-S SYSTEM

Composition, at.%			Thermal Effect, °C*		Interpretation
Ag	Fe	S	heating	cooling	
40.0	10.0	50.0(1)	568	-	Ag_2S fcc ⇄ bcc
			607	565**	arg + py ⇄ L_t + L_S
54.0	3.0	43.0(1)	608	560**	arg + py ⇄ L_t + L_S
			-	651	liquidus surface
45.6	10.2	44.2(1)	565	562	Ag_2S fcc ⇄ bcc
			608	585**	L_t + L_S ⇄ arg + py
54.7	6.0	39.3(2)	-	560	Ag_2S fcc ⇄ bcc
			605	566**	L_t + L_S ⇄ arg + py
47.5	10.0	42.5(3)	176	-	Ag_2S bcc ⇄ mono.
			482	481	Ag_2S fcc ⇄ bcc
			532	530	arg-py-po eutectic
20.0	29.0	51.0(3)	482	481	Ag_2S fcc ⇄ bcc
			533	534	arg-py-po eutectic
52.0	9.0	39.0(3)	178	-	Ag_2S bcc ⇄ mono.
			481	481	Ag_2S fcc ⇄ bcc
			532	531	arg-py-po eutectic
65.0	5.0	30.0(4)	519	518	Ag_2S fcc ⇄ bcc
			623	619	Ag + L_t ⇄ arg + po
60.0	20.0	20.0(5)	954	935	Ag + po upper stability
			1004	-	L_t ⇄ $L_{Ag\text{-}rich}$ + po
70.0	20.0	10.0(6)	954	950	L_t ⇄ Ag + Fe + po
			965	968	L_t ⇄ Fe + po + $L_{Ag\text{-}rich}$
20.0	50.0	30.0(6)	955	-	L_t ⇄ Ag + Fe + po
			964	-	L_t ⇄ Fe + po + $L_{Ag\text{-}rich}$
			955	-	L_t ⇄ Ag + Fe + po
			965	-	L_t ⇄ Fe + po + $L_{Ag\text{-}rich}$

* The thermal effect of the quartz internal standard is omitted.
**Supercooling of the liquid phase.

Starting materials: 1) Ag_2S, FeS_2, and S; 2) Ag_2S and FeS_2; 3) Ag_2S, FeS_2, and FeS; 4) Ag_2S, Ag, and FeS; 5) Ag and FeS; 6) Ag, Fe, and FeS.

Appendix 2

Experiments conducted on the Ag_2S-FeS join.

a. Experiments within the po + L_t + V field.

Composition, mol.% Ag_2S	FeS	Temp., °C	Time, days
58.7	41.3	750±2	6
66.7	33.3	750±2	5

b. Experiments within the Ag + po + L_t + V field.

58.7	41.3	710±2	3
58.7	41.3	719±2	4
8.3	91.7	700±2	8
58.7	41.3	700±2	12
68.0	32.0	700±2	3
71.0	29.0	700±2	4
75.0	25.0	650±2	5
78.0	22.0	650±2	5
81.0	19.0	650±2	5
74.2	25.8	630±2	7
74.2	25.8	625±2	1

c. Experiments within the arg + Ag + po + V field.

74.2	25.8	620±2	4
74.2	25.8	615±2	3
13.2	86.8	600±2	18

d. Experiments within the Ag + po + V field.

4.0	96.0	700±2	5
1.5	98.5	700±2	10
3.8	96.2	600±2	18

e. Experiments within the Ag + L_t + V field.

74.0	26.0	700±2	3
80.3	19.7	680±2	4
83.0	17.0	645±2	9
85.0	15.0	645±2	9

f. Experiments within the arg + L_t + V field.

95.0	5.0	645±2	9

g. Experiments within the L_t + V field.

91.5	8.5	700±2	3
85.7	14.3	700±2	3
78.2	21.8	700±2	18

Appendix 3

Experiments conducted to determine 700±3°C isotherm.

a. Experiments within $L_t + L_S + V$ field.

Composition at.%			
Ag	Fe	S	Time, days
29.5	0.5	70.0	3
28.5	1.5	70.0	10
27.0	3.0	70.0	10
25.5	4.5	70.0	10
24.0	6.0	70.0	10
20.0	4.4	75.4	8
38.0	9.0	53.0	7
62.0	1.0	37.0	6
55.0	5.0	40.0	7
47.6*	9.5	42.8	3
44.9	10.9	44.2	7

*Using $Ag_2S + FeS_2$ as starting materials; the remaining experiments were prepared from elemental Ag, Fe, and S.

b. Experiments within $py + L_t + L_S + V$ field.

Composition at.%			
Ag	Fe	S	Time, days
41.0	12.0	47.0	7
42.5	12.5	45.0	6
40.7*	13.0	46.3	3
36.0	14.0	50.0	7
33.0	17.0	50.0	6
31.5*	17.6	50.9	7
21.8*	22.4	55.8	7
13.8*	25.4	59.8	7
5.3*	30.6	64.1	7
20.0	22.5	57.5	6
22.0	8.0	70.0	6

*Using $Ag_2S + FeS_2$ as starting materials; the remaining experiments were prepared from elemental Ag, Fe, and S.

c. Experiments within py + L_t + V field.

Composition at.%			
Ag	Fe	S	Time, days
37.5*	16.0	46.5	6

*Using FeS_2 + Ag_2S as starting materials.

d. Experiments within py + po + L_t + V field.

Composition at.%			
Ag	Fe	S	Time, days
35.5*	17.5	47.0	7
29.0*	23.5	47.5	7
26.5*	22.5	51.0	6
24.5*	22.5	53.0	6
25.0*	25.0	50.0	7
16.3*	29.5	54.2	14
8.0*	38.0	54.0	8
8.0*	37.0	55.0	8
8.0*	36.0	56.0	8

*Elemental Ag, Fe, and S were used as starting materials.

e. Experiments within po + L_t + V field.

Composition at.%			
Ag	Fe	S	Time, days
33.5*	22.5	44.0	7
37.0*	21.0	42.0	3
16.3*	33.7	50.0	14
8.0*	43.0	49.0	6
8.0*	42.0	50.0	8
8.0*	39.5	52.5	7
3.0*	45.0	52.0	8
2.0*	46.0	52.0	7
4.5*	45.0	50.5	7

*Elemental Ag, Fe, and S were used as starting materials.

f. Experiments within Ag + po + L_t + V field

Composition at.%

Ag	Fe	S	Time, days
74.0	6.0	20.0	10
72.5	7.5	20.0	10
71.0	9.0	20.0	6
60.0	15.0	25.0	10
57.3	14.1	28.6	20
53.5	15.5	31.0	7
50.0	17.0	33.0	7
47.0	17.5	35.5	6
43.0	19.0	38.0	3
52.4*	10.7	36.9	4
50.7*	11.9	37.3	3
51.1	11.7	37.2	3
48.1	13.9	38.0	17
45.3	16.0	38.7	17
42.0	18.5	39.5	3
40.0	20.0	40.0	14
8.0	44.0	48.0	8

*Using Ag_2S+ FeS_2 as starting materials; the remaining experiments were prepared from elemental Ag, Fe, and S.

g. Experiments within Ag + L_t + V field.

Composition at.%

Ag	Fe	S	Time, days
77,0	3.0	20.0	10
75.5	4.5	20.0	10
56.5	8.5	35.0	3
54.0*	9.5	36.5	3

*Using Ag_2S + FeS as starting materials; the remaing experiments were prepared from elemental Ag, Fe, and S.

h. Experiments within Ag + arg + L_t + V field.

Composition at.%

Ag	Fe	S	Time, days
78.5*	1.5	20.0	10
67.0*	2.5	30.5	6
64.5*	4.0	31.5	6

*Elemental Ag, Fe and S were used as starting materials.

i. Experiments within arg + L_t + V field.

Composition at.%			
Ag	Fe	S	Time, days
63.0*	4.0	33.0	3

*Elemental Ag, Fe, and S were used as starting materials.

j. Experiments within homogeneous liquid (L_t) + V field.

Composition at.%			
Ag	Fe	S	Time, days
58.6*	4.0	37.3	4
56.2	7.8	36.0	18
60.0	5.0	35.0	3

*Using Ag_2S + FeS_2 as starting materials; the remaining experiments were prepared from elemental Ag, Fe, and S.

k. Experiments within the Ag + po + V field.

Composition at.%			
Ag	Fe	S	Time, days
3.9*	47.1	49.0	5
8.0	46.0	46.0	8
8.0	45.0	47.0	7
50.0	25.0	25.0	6
50.0	25.0	25.0	7

*Using Ag_2S + FeS as starting materials; the remaining experiments were prepared from elemental Ag, Fe, and S.

l. Experiments within the Ag + FeS + Fe + V field.

Composition at.%			
Ag	Fe	S	Time, days
33.6*	49.6	16.8	11
20.0	50.0	30.0	8
8.0	47.0	45.0	6

*Using Ag_2S + Fe as starting materials; the remaining experiments were prepared from elemental Ag, Fe, and S.

Appendix 4

Experiments conducted on L_t positions of po + L_S + L_t + V field.

Composition, at.%			Temp., °C	Time, Days	Products at Temp.
Ag	Fe	S			
20	10	70	798±2	4	$L_S + L_t + V$
15	15	70	798±2	4	$L_S + L_t$ + po + V
16	30	54	803±3	4	$L_S + L_t$ + po + V
20	30	50	803±3	4	L_t + po + V

Appendix 5

Experiments in the Fe-S system below 320°C.

a. Experiments conducted on the troilite--h-po solvus.

Starting Material po comp., at.% Fe	Type of Experiment	Temp., °C	Time	Comp. h-po at.% Fe(±0.10 at.%)
49.5	Dry	121±5	14d	49.35
49.0	Dry	100±5	31d	48.65
49.0	Dry	70±10	63d	48.30
49.5	Aqueous*	120±5	5d	49.35
49.0	Aqueous	100±5	17d	48.60
49.0	Aqueous	70±10	47d	48.35

*Reaction medium was 2cc of 2m NH_4Cl.

b. Experiments conducted on the m-po--py solvus.

Type of Experiment*	Temp., °C	Time, days	Products at Temp. (po in at.% Fe)
Dry	300±3	6	m-po(46.70) + py
Dry	200±5	15	m-po(46.50) + py
Dry	200±5	93	m-po(46.40) + py
Dry	100±10	93	m-po(46.35) + py
Dry	100±10	202	m-po(46.30) + py
Aqueous**	205±10	46	m-po(46.45) + py
Aqueous	100±10	93	m-po(46.30) + py

* All starting materials consisted of high-temperature h-po of 46 at.% Fe.

**Reaction medium was 2cc of 2m NH_4Cl.

c. Miscellaneous experiments

Starting Materials***	Type of Experiment	Temp., °C	Time, Days	Products at Temp. (po in at.% Fe)
po(47.0)+py	Dry	296±3	40	h-po(47.30)+py
po(47.0)	Dry	296±3	40	h-po(47.35)+py
po(47.0)	Dry	295±4	47	h-po(47.30)+m-po(?)
po(48.0)+py	Dry	295±4	87	h-po(47.40)+py
po(48.0)	Dry	295±4	87	h-po(47.95)
po(46.5)+arg	Dry	295±4	47	m-po(46.7)+arg+py
po(46.5(	Dry	295±4	47	m-po(46.75)+py

Appendix 5-c, continued

Starting Materials***	Type of Experiment	Temp., °C	Time, Days	Products at Temp. (po in at.% Fe)
po(47.5)	Dry	270±10	36	h-po(47.4)
po(47.0)	Dry	270±10	36	h-po + m-po*
po(47)+py	Dry	270±10	36	m-po(46.60)+py
po(46.5)	Dry	270±10	36	m-po*
po(47.5)	Dry	225±10	79	h-po(47.50)
po(47.0)	Dry	225±10	79	m-po*
po(46.5)	Dry	225±10	79	m-po*
po(47.0)	Dry	152±5	167	h-po + m-po
po(46.7)	Dry	152±5	167	m-po
po(48.0)+py	Aqueous**	205±10	46	h-po(47.8)+py
po(47.0)	Aqueous	205±10	46	m-po*
po(48.5)	Aqueous	100±10	63	h-po(48.45)
m-po(46.7)	Dry	305±3	67	No reaction
m-po(46.7)	Dry	315±2	13	h-po(47.30)+py

* $\bar{4}08$ reflection larger than 408.
** Reaction media was 2cc of 2m NH_4Cl.
*** The pyrrhotite (po) of the starting material is the high-temperature form; h-po of the products is the low-temperature form.

BIBLIOGRAPHY

Abrahams, S. G., 1955, The crystal and molecular structure of orthorhombic sulfur: Acta Cryst., vol. 8, 661-671.

Albright, D. L., and Kraft, R. W., 1966, Structural characteristics of the Fe-FeS eutectic: Trans. Met. Soc. AIME, vol. 236, 998-1003.

Albright, D. L., Conard, G. P., and Kraft, R. W., 1967, Magnetic behavior of a eutectic alloy featuring an aligned array of iron rods: Jour. Applied Phys., vol. 38, 2919-2923.

Allen, E. T., and Lombard, R. H., 1917, A method for the determination of dissociation pressures of sulphides, and its application to covellite (CuS) and pyrite (FeS_2): Am. Jour. Sci., vol. 43, no. 255, 175-195.

Alsén, N., 1925, Röntgengraphische Untersuchung der Kristallstrukturen von Magnetkies, Breithauptite, Pentlandite, Millerite, und Verbindungen: Geol. Foren. Forhandl. Stockholm, vol. 47, 19-72.

Arnold, R. G., 1962, Equilibrium relations between pyrrhotite and pyrite from 325° to 743°C: Econ. Geol., vol. 57, 72-90.

_____, 1967, Range in composition and structure of 82 natural terrestrial pyrrhotites: Can. Min., vol. 9, 31-49.

Barnard, W. M., and Christopher, P. A., 1966a, Hydrothermal synthesis of chalcopyrite: Econ. Geol., vol. 61, 897-902.

_____, 1966b, Further study on the effectiveness of aqueous solutions in the hydrothermal synthesis of chalcopyrite: Econ. Geol., vol. 61, 1287-1290.

Barnes, H. L., and Kullerud, G., 1961, Equilibria in sulfur-containing aqueous solutions in the system Fe-S-O, and their correlation during deposition: Econ. Geol., vol. 56, 648-688.

Barnes, H. L., and Czamanske, G. K., 1967, Solubilities and transport of ore minerals in Geochemistry of Hydrothermal Ore Deposits: Holt, Rinehart, and Winston, Inc., New York, 334-381.

Barton, P. B., Jr., 1957, Some limitations on the possible composition of the ore-forming fluid: Econ. Geol., vol. 52, 333-353.

Barton, P. B., Jr., Bethke, P. M., and Toulmin, P., 1963, Equilibrium in ore deposits: Min. Soc. Amer. Sp. Pap. 1, 171-185.

Barton, P. B., Jr., and Skinner, B. J., 1966, Reaction points of possible interest in geothermometry studies of ore deposits (Abstract): Geol. Soc. Am. Ann. Mtg, 12.

_____, 1967, Sulfide mineral stabilities in Geochemistry of Hydrothermal Ore Deposits: Holt, Rinehart, and Winston, Inc., New York, 236-333.

Barton, P. B., Jr., and Toulmin, P., 1964, The electrum tarnish method for the determination of the fugacity of sulfur in laboratory sulfide systems: Geochim. Cosmochim. Acta, vol. 28, 619-640.

Bell, J. M. and Thompson, E., 1924, The effect of deep-seated alteration upon the mineralogical and geological features of the Keeley silver mine: Univ. Toronto Studies, Geol. Ser., no. 17, 18-37.

Bell, P. M, England, J. L., and Kullerud, G., 1967, High-pressure differential thermal analysis: Carnegie Inst. Wash. Year Book 65, 354-356.

Berner, R. A., 1962a, Experimental studies of the formation of sedimentary iron sulfides: Biogeochemistry of Sulfur Isotopes, N.S.F. Conf., Yale Univ.

_____, 1962b, Tetragonal iron sulfide: Science, vol. 137, 669.

_____, 1964, Iron sulfides formed from aqueous solution at low temperatures and atmospheric pressure: Jour. Geol., vol. 72, 293-306.

Berry, L. G., and Thompson, R. M., 1962, X-ray powder data for ore minerals: The Peacock Atlas: Geol. Soc. Amer. Mem. 85.

Bertaut, E. F., 1953, Contribution a l'etude des structures lacunaires, la pyrrhotine: Acta. Cryst., vol. 6, 557-561.

_____, 1956, Structure de FeS stoichiometric: Bull. Soc. Franc. Mineral, vol. 79, 276-292.

Bowen, N. L., 1928, The Evolution of Igneous Rocks: Dover Publ., Inc., New York.

Braune, H., Peter, S., and Neveling, V., 1951, Die Dissoziation des Schwefeldampfes: Zeit. Naturf., vol. 6a, 32-37.

Brett, R., and Kullerud, G., 1967, The Fe-Pb-S system: Econ. Geol., vol. 62, 354-367.

Buerger, M. J., 1931, The crystal structure of marcasite: Amer. Min., vol. 16, 361-395.

_____, 1934, The pyrite-marcasite relation: Amer. Min., vol. 19, 37-61.

Burnham, C. W., 1962, Lattice constant refinement: Carnegie Inst. Wash. Year Book 61, 132-135.

Buseck, P. R., 1962, Pyrrhotite from Tem Piute, Nevada: Carnegie Inst. Wash. Year Book 61, 161.

Byström, A., 1945, Monoclinic magnetic pyrites: Arkiv. Kemi Mineral Geol: vol. 19B, no. 8., 1-8.

Carpenter, H. C. H. and Fisher, M. S., 1932, A metallographic investigation of native silver: Trans. Inst. Min. Met. London, vol. 41, 382-403.

Carpenter, R. H., and Desborough, G. A., 1964, Range in solid solution and structure of naturally occurring troilite and pyrrhotite: Amer. Min., vol. 49, 1350-1365.

Clark, A. H., 1966a, Stability field of monoclinic pyrrhotite: Trans. Inst. Min. Metal., vol. 75, 232-235.

_____, 1966b, The mineralogy and geochemistry of the Ylojarvi Cu-W deposit, Southwest Finland: mackinawite-pyrrhotite-troilite assemblages: Rend. Soc. Geol. Finlande, vol. 38, 331-342.

Clark, L. A., 1961, The Fe-As-S system: phase relations and applications: Econ. Geol., vol. 55, 1345-1381, 1631-1652.

Clark, L. A., and Kullerud, G., 1963, The sulfur-rich portion of the Fe-Ni-S system: Econ. Geol., vol. 58, 853-885.

Corlett, M., 1968, Low-iron polymorphs in the pyrrhotite group: In press.

Craig, J. R., 1965, A systematic study of phase equilibria in the Ag-Bi-S system and exploration of the geologically significant portion of the Ag-Bi-Pb-S system: Unpubl. Ph.D. thesis, Lehigh Univ.

Daniels, F., and Alberty, R. A., 1955, Physical Chemistry: John Wiley and Sons, Inc., New York.

Desborough, G. A., and Carpenter, R. H., 1965, Phase relations of pyrrhotite: Econ. Geol., vol. 60, 1431-1450.

Djurle, S., 1958, An X-ray study on the system Ag-Cu-S: Acta Chem. Scand., vol. 12, 1427-1436.

D'Or, L., 1931, Dissociation thermique de la pyrite: Jour. Chim. Phy. et Phys. Chem., vol. 28, 377-408.

Edwards, A. B., 1956, Manganese and iron in Broken Hill sphalerites: Proc. Australasian Inst. Mining Metal., no. 180, 97-117.

Elliott, R. P., 1965, Constitution of binary alloys, first supplement: McGraw-Hill Book Co., New York.

Emmons, S. F., Stockwell, C. H., and Jones, R. H. B., 1926, Argentite and acanthite: Amer. Min., vol. 11, 326-328.

Erd, R. C., Evans, H. T., and Richter, 1957, Smythite, a new iron sulfide and associated pyrrhotite from Indiana: Amer. Min., vol. 42, 309-333.

Evans, H. T., Berner, R. A., and Milton, C., 1962, Valleriite and mackinawite (abstract): Geol. Soc. Amer. Sp. Pap. 73, 147.

Evans, H. T., Milton, C., Chao, E. C. T., Adler, I., Mead, C., Ingram, B., and Berner, R. A., 1964, Valleriite and the new iron sulfide mackinawite: U.S. Geol. Surv. Prof. Pap. 475-D, 64-69.

Fink, C. G., and deMarchi, V. S., 1938, Alloys of silver and iron: Trans. Electrochem. Soc., vol. 74, 271-280.

Frueh, A. J., 1958, The crystallography of silver sulfide, Ag_2S: Zeit. Krist., Bd. 110, 136-144.

Garrels, R. M., 1960, Mineral Equilibria: Harper and Bros., New York.

Garrels, R. M., and Christ, C. L., 1965, Solutions, Minerals, and Equilibria: Harper and Row, New York.

Geyne, A. R., Fries, C., Segerstrom, K., Black, R. F., and Wilson, I. F., 1963, Geology and mineral deposits of the Pachuca-Real del Monte District, State of Hidalgo, Mexico: Consejo de Recursos Naturales no Renovables, Publ. 5E, 203 p.

Gibbons, G. S., 1967, Optical anisotropy in pyrite: Amer. Min., vol. 52, 359-370.

Grønvold, F., and Haraldsen, H., 1952, On the phase relations of synthetic and natural pyrrhotites ($Fe_{1-x}S$): Acta Chem. Scand., vol. 6, 1452-1469.

Gustafson, L. B., 1963, Phase equilibria in the system Cu-Fe-As-S: Econ. Geol., vol. 58, 667-701.

Haidinger, W,, 1828, Description of sternbergite, a new mineral species: Trans. Roy. Soc. Edinburgh, vol. 11, 1-7.

Hägg, G., and Sucksdorff, I., 1933, Die Kristallstructure von Troilit und Magnetkies: Zeit. Physik. Chem., vol. 22, 444-452.

Hall, H. T., 1966, The systems Ag-Sb-S, Ag-As-S, and Ag-Bi-S: Phase relations and mineralogical significance: Unpubl. Ph.D. thesis, Brown Univ.

Hall, H. T., and Yund, R. A., 1966, Pyrrhotite phase relations below 325°C (Abstract): Geol. Soc. Amer. Ann. Mtg.

Hansen, M., and Anderko, K., 1958, Constitution of Binary Alloys: McGraw-Hill Book Co., New York.

Haraldsen, H., 1941, Uber die Eisen-Sulfidmisch-Kristalle: Zeit. Anorg. u. Allgem. Chem. vol. 246, 169-194.

Hewitt, R. L., 1938, Experiments bearing on the relation of pyrrhotite to other sulfides: Econ. Geol., vol. 33, 305-338.

Holland, H. D., 1959, Some applications of thermochemical data to problems of ore deposits. I. Stability relations among the oxides, sulfides, sulfates, and carbonates of ore and gangue minerals: Econ. Geol., vol. 54, 184-233.

_____, 1965, Some applications of thermochemical data to problems of ore deposits. II; Mineral assemblages and the composition of ore-forming fluids: Econ. Geol. vol. 60, 1101-1166.

Kouvo, O., Vuorelainen, Y., and Long, J. V. P., 1963, A tetragonal iron sulfide: Amer. Min., vol. 48, 511-524.

Kracek, F. C., 1946, Phase relations in the system sulfur-silver and the transitions in silver-sulfide: Trans. Amer. Geophys. Union, vol. 27, 364-374.

Kraft, R. W., 1967, Controlled eutectics: Scien. Amer., vol. 216, no. 2, 86-92.

Kullerud, G., 1953, The FeS-ZnS system: a geological thermometer: Norsk. Geol. Tidsskr., vol. 32, 61-147.

_____, 1961, Two-liquid field in the Fe-S system: Carnegie Inst. Wash. Year Book 60, 174-176.

_____, 1962, Method for mixing liquids at controlled temperatures: Carnegie Inst. Wash. Year Book 61, 160-161.

_____, 1963a, The Fe-Ni-S system: Carnegie Inst. Wash. Year Book 62, 175-189.

_____, 1963b, Thermal stability of pentlandite: Can. Min., vol. 7, 353-366.

_____, 1964, The Cu-Fe-S system: Carnegie Inst. Wash. Year Book 63, 200-202.

_____, 1967a, Sulfide studies in Researches in Geochemistry: Holt, Rinehart, and Winston, Inc., New York, 286-321.

_____, 1967b, The Fe-S-O-H- system: Carnegie Inst. Wash. Year Book 65, 352-354.

Kullerud, G., Doe, B. R., Buseck, P. R., and Troften, P. F., 1963, Heating experiments on monoclinic pyrrhotites: Carnegie Inst. Wash. Year Book 62, 210-213.

Kullerud, G., and Yoder, H. S., 1959, Pyrite stability relations in the Fe-S system: Econ. Geol., vol. 54, 533-572.

Lepp, H., 1956, Precision measurements of the cell edge of synthetic pyrite: Amer. Min., vol. 41, 347-349.

Lüder, E., 1924, Gleichgewichte zwischen Metallpaaren und Schwefel; Das ternare System Silber-Eisen-Schwefel: Metall u. Erz, 4, 65-69.

Meyer, B., 1965, Elemental Sulfur: Intersci. Publ., John Wiley and Sons, New York.

Meyer, F. H., Riggs, G. L., McGlasson, R. L., and Sudbury, J. D., 1957, Corrosion products of mild steel in hydrogen sulfide environments: Corrosion, vol. 14, 109t-115t.

Murdock, J., and Berry, L. G., 1954, X-ray measurements on argentopyrite: Am. Min., vol. 39, 475-484.

Ostwald, W., 1902, Lehrbuch der allgemeinen Chemie: Verlag. von W. Engelmann, Leipzig, vol. 2, pt. 2, 1188 p.

Palache, C., Berman, H., and Frondel, C., 1944, The System of Mineralogy, vol. 1: John Wiley and Sons, Inc., New York.

Parrish, W., 1953, X-ray reflection angle tables for several standards: Philips Lab., Res. Lab. Tech. Rept. 28.

Pavlyuchenko, M. M., and Samal, G. I., 1964, Kinetics and mechanism of the thermal decomposition of copper sulfide: Gelerogennye Reakts. i Reakts. Sposobnost, 85-94; Chem. Abst., vol. 64, 15048c.

Peacock, M. A., 1942, On sternbergite and frieseite (Abstract): Geol. Soc. Amer. Ann. Mtg., 229.

Petrenko, G. I., 1906, Uber die Legierungen des Silbers mit Thallium, Wismut, und Antimon: Zeit Anorg. Chem., vol. 50, 133-144.

Petruk, W., 1964, Mineralogy of the Pallaco tin ore from Empresa Minera Unificada de Potosi, Bolivia, for Prospection Ltd.: Can. Dept. Mines and Tech. Surv., IR 64-14, 1-6.

_____, 1966, Preliminary mineralogical study of the silver deposits in the Cobalt area, Ontario: Can. Dept. Mines and Tech. Surv., IC 179, 1-36.

Rahlfs, P., 1936, Uber die Rubischen Hochtemperurmodifikationen der Sulfide, Selenide, und Telluride des Silbers und des einwertigen Kupfers: Zeit. Physik. Chem., vol. B31, 157-194.

Ramdohr, P., 1950, Die Lagerstatte von Broken Hill in New South Wales: Heidel. Beit. zur Min. und Pet., bd. 2, 291-333.

Ramdohr, P., 1954, Uber metamorphose und sekundare Mobilisierung: Geol. Rund., vol. 42, 11-19.

_____, 1955, Die Erzmineralien und Ihre Verwachsungen: Akademie Verlag, Berlin.

_____, 1960, Die Erzmineralien und Ihre Verwachsungen (Second Edition): Akademie Verlag, Berlin.

Ramsdell, L. S., 1943, The crystallography of acanthite, Ag_2S: Amer. Min., vol. 28, 401-425.

Rassow, H., 1920, Einfache Methode zur Bestimmung von Schmeltzpunkten und kritischen Temperaturen: Zeit. anorg. und allgem. Chem., vol. 114, 117-150.

Ricci, J. E., 1951, The Phase Rule and Heterogeneous Equilibrium: D. Van Nostrand Co., New York.

Richardson, F. D., and Jeffes, J. H. E., 1952, The thermodynamics of substances of interest in iron and steel making, III. Sulfides: Jour. Iron and Steel Inst., vol. 171, 165-175.

Roberts, H. S., 1935, Polymorphism in the FeS-S solid solutions, I. Thermal study: Jour. Amer. Chem. Soc., vol. 57, 1034-1038.

Roland, G. W., 1966, Phase relations and geologic application of the system Ag-As-S: Unpubl. Ph.D. thesis, Lehigh Univ.

Rosenqvist, T., 1949, A thermodynamic investigation of the system silver-silver sulfide: Amer. Inst. Min. Metal. Engr. Trans., vol. 185, 451-460.

Sadanaga, R., and Sueno, S., 1967, X-ray study on the α-β transition of Ag_2S: Mineral. Jour., vol. 5, 124-148.

Samal, G. I., 1965, Kinetics of the thermal decomposition of iron disulfide: Geterogennye Khim. Reaktsic. Inst. Obshch. i. Neorgan. Khim. Akad. Nauk Belorussk. SSR, 93-99; Chem. Abst. vol. 64, 15048d.

Skinner, B. J., 1966, The system Cu-Ag-S: Econ. Geol., vol. 61, 1-26.

Skinner, B. J., Erd, R. C., and Grimaldi, F. S., 1964, Greigite, the thio-spinel of iron; a new mineral: Amer. Min., vol. 49, 543-555.

Skinner, B. J., Jambor, J. J., and Ross, M., 1966, Mckinstryite, a new copper-silver sulfide: Econ. Geol., vol. 61, 1383-1389.

Somanchi, S., and Clark, L. A., 1966, The occurrence of an Ag_6Sb phase at Cobalt, Ontario: Can. Min., vol. 8, 618-619.

Stanton, R. L., 1957, Studies of polished surfaces of pyrite, and some implications: Can. Min., vol. 6, 87-118.

Stillwell, F. L., 1953, Mineralogy of the Broken Hill Lode: Geol. of Aust. Ore Dep., Fifth Empire Mining and Metallurgical Congress, vol. 1, 601-626.

Straumanis, M. E., Amstutz, G. C., and Chan, S., 1964, Lattice parameters and expansion coefficients of FeS_2 (Natural and synthetic) and of CoS_2: Amer. Min., vol. 49, 206-211.

Streng, A., 1878, Ueber den Silberkies von Andreasberg: Neues Jahrb., 906-913.

Sutherland, J. K., 1967, The chemistry of some New Brunswick pyrites: Can. Min., vol. 9, 71-84.

Swanson, H. E., Cook, M. I., Isaacs, T., and Evans, E. H., 1960, Standard X-ray diffraction powder patterns: Nat. Bur. Stds. Circular 539, vol. 9.

Swanson, H. E., Fuyat, R. K., and Ugrinic, G. M., 1955a, Standard X-ray diffraction powder patterns: Nat. Bur. Stds. Circular 539, vol. 4.

Swanson, H. E., Gilfrich, N. Y., Ugrinic, G. M., 1955b, Standard X-ray diffraction powder patterns: Nat. Bur. Stds. Circular 539, vol. 5.

Swanson, H. E., and Tatge, E., 1953, Standard X-ray diffraction powder patterns: Nat. Bur. Stds. Circular 539, vol. 1.

Tammann, G., and Oelsen, W., 1930, Die Abhangigkeit der Konzentration gesattigter Mischkristalle von der Temperatur; Die Loslichkeit des Eisens in Blei, Silber, Wismut, und Cadmium: Zeit. anorg. Chem., vol. 186, 277-279.

Thompson, R., 1957, Cobalt camp in Structural Geology of Canadian Ore Deposits: Can. Inst. Min. Metal., Congress vol., 377-388.

Toulmin, P., and Barton, P. B., 1964, A thermodynamic study of pyrite and pyrrhotite: Geochim. Cosmochim. Acta, vol. 28, 641-671.

Tuller, W. N., 1954, Sulfur Data Book: McGraw-Hill Book Co., New York.

Wagner, C., 1953, Investigations on silver sulfide: Jour. Chem. Phys., vol. 21, 1819-1827.

Waltershausen, W. S., 1866, Einige nachtragliche Bemerkungen uber den Silberkies: Ges. Wiss. Gottingen, Nachr., 9, 66-68.

Weisbach, A., 1877, Ueber die Silberkiese: Neues Jahrb., 906-913.

West, J. R., 1950, Thermodynamic properties of sulfur: Ind. and Eng. Chem., vol. 42, 713-718.

Williamson, E. D., and Morey, G. W., 1918, The laws of chemical equilibrium: Jour. Am. Chem. Soc., vol. 40, 49-59.

Wuensch, B., 1963, On the superstructure of pyrrhotite: Min. Soc. Amer. Spec. Pap. 1, 157-162.

Vegard, L., 1916, The structure of silver crystals: Phil. Mag., vol. 31, 83.

VITA

Lawrence A. Taylor was born on September 14, 1938 in Paterson, New Jersey. He attended grade school in Port Jervis, New York, and was graduated from Port Jervis High School in 1956. After attending evening sessions at Orange County Community College, Middletown, New York, during the 1957-1958 academic year, he entered Indiana University in September, 1958, and received his B.S. in geology in August, 1961. As a graduate student at Indiana University, he was a Research Assistant in the Geochemistry Section of the Indiana Geological Survey and received his M.S. in geology in January 1963. After 18 months as an Instructor in the Department of Geology, University of Delaware and a geologist for the Delaware Geological Survey, he entered Lehigh University in September 1964. He was a Teaching Assistant at Lehigh in 1964-1965 and a National Aeronautics and Space Administration Fellow from July, 1965 to June, 1968. In August, 1960, he married Patricia Ann Ridley in Milford, Pennsylvania; the Taylors have two children, Jeffrey Andrew, born March 30, 1965 and Kelly Ann, born August 22, 1967.

Publications:

(1) Phase Equilibria in the system Ag-Fe-S (Abstract). Program, 1967 Annual Meetings of the Geological Society of America held in New Orleans, Louisiana.